HIGHER ALCOHOL SYNTHESIS ON MAGNESIUM/ALUMINUM

MIXED OXIDE SUPPORTED POTASSIUM CARBONATE

PROMOTED MOLYBDENUM SULFIDE

A Dissertation
Presented to
The Academic Faculty

by

Michael Robert Morrill

In Partial Fulfillment
of the Requirements for the Degree
Doctor of Philosophy in the
School of Chemical & Biomolecular Engineering

Georgia Institute of Technology
August 2013

HIGHER ALCOHOL SYNTHESIS ON MAGNESIUM/ALUMINUM MIXED OXIDE SUPPORTED POTASSIUM CARBONATE PROMOTED MOLYBDENUM SULFIDE

Approved by:

Dr. Christopher W. Jones, Co-Advisor
School of Chemical & Biomolecular
Engineering
Georgia Institute of Technology

Dr. David S. Sholl
School of Chemical & Biomolecular
Engineering
Georgia Institute of Technology

Dr. Faisal Alamgir
School of Materials Science and
Engineering
Georgia Institute of Technology

Dr. Pradeep K. Agrawal, Co-Advisor
School of Chemical & Biomolecular
Engineering
Georgia Institute of Technology

Dr. Dennis W. Hess
School of Chemical & Biomolecular
Engineering
Georgia Institute of Technology

Dr. Jake D. Soper
School of Chemistry and Biochemistry
Georgia Institute of Technology

Date Approved: July, 1st, 2013

ACKNOWLEDGMENTS

TABLE OF CONTENTS

LIST OF TABLES

LIST OF FIGURES

LIST OF SYMBOLS AND ABBREVIATIONS

AC	Activated Carbon
ASF	Anderson-Schultz-Flory
BET	Brunauer-Emmett-Teller
C_A	Surface concentration (mol/L)
CUS	Coordinatively Unsaturated Sites
D_{eff}	Effective Diffusivity (cm^2/s)
DFT	Density Functional Theory
DRS	Diffuse Reflectance Spectroscopy
EA	Elemental Analysis
EXAFS	X-Ray Absorption Near Edge Fine Structure
FID	Flame Ionization Detector
GC	Gas Chromatography
h	Heat Transfer Coefficient
HDS	Hydrodesulfurization
L	Particle Radius (cm)
MFC	Mass Flow Controller
MMO	Mixed Metal Oxide
P&ID	Plumbing and Instrumentation Diagram
R_{obs}	Observed rate of reaction (moles/ml cat/min)
STEM	Scanning Transmission Electron Microscopy
TCD	Thermal Conductivity Detector
TPD	Temperature Programmed Desorption

UV-vis	Ultra Violet – Visible Spectroscopy
VI	Virtual Instrument
subVI	Imbedded Virtual Instrument
WPN	Weisz-Prater Number
XRD	X-Ray Diffraction
XAS	X-Ray Absorption Spectroscopy
XANES	X-Ray Absorption Near Edge Spectroscopy

SUMMARY

Higher alcohols synthesized via CO hydrogenation reactions have been a topic of intense study both in industry and academia for over thirty years. A variety of transition metals and promoters have been used in catalysts for this reaction. MoS_2, in particular, is popular due to its low cost, resistance to sulfur poisoning, and ability to selectively produce higher alcohols over hydrocarbons.

The bulk material has a rich history in hydrodesulfurization reactions (HDS), and as such, a great deal is known about the material's structure and reactivity. However, even with this deep body of knowledge about the bulk catalyst, no one has yet been able to implement an industrially viable variation of the catalyst to make higher alcohols.

Supported MoS_2 has also been studied for the same purpose. Generally, supports are employed to improve catalyst productivity per gram of Mo by dispersing the metal and increasing the amount of catalytically active surface area. However, product selectivity may also be influenced by chemical properties of the supports. Specifically, gamma alumina has been shown to raise hydrocarbon formation due to intrinsic surface acidity.

In Chapter 2 of this thesis, the effects of basic supports on the CO hydrogenation reaction are reported. K promoted Mo is supported on two basic materials – commercial sepiolite ($Si_{12}Mg_8O_{30}(OH)_4$) and hydrotalcite-derived Mg/Al mixed metal oxides (MMO). The catalysts are reacted with syngas, and the resultant product selectivities are compared at isoconversions. Activated carbon supported Mo and bulk MoS_2 are also used

as controls. It is shown that MMO provides a unique promotional effect by suppressing methanol formation and favoring higher alcohols.

The specific role of MMO in the reaction is investigated in Chapter 3 by combining it in three different ways with Mo. 1) MMO is impregnated with Mo in the classic fashion. 2) Bare MMO or MMO/K is placed as a secondary bed downstream of the principle catalyst (K promoted Mo supported on MMO). 3) Bare MMO or MMO/K is mixed with the principle catalyst to make a homogeneous bed.

It is shown that MMO by itself is somewhat inert in the reaction while MMO/K has some higher alcohol forming activity. More importantly however, it is shown that the MMO:Mo ratio has far greater effects on selectivity than the morphology of MoS_2. There is evidence however that MoS_2 morphology can affect activity. It is hypothesized that a greater degree of stacking in MoS_2 domains leads to reduced activity.

The existence of coupling and homologation pathways are investigated in Chapter 4 by feeding methanol or ethanol into the syngas as it enters the catalyst bed. By comparing changes in the productivity of different higher alcohols with the liquid feed, it is shown that an MMO supported catalyst is much more reactive with methanol and somewhat more reactive with ethanol than its bulk MoS_2 counterpart. It is shown that for both the bulk and supported catalysts, the addition of a C_x alcohol results in the largest increase in C_{x+1} products, suggesting that alcohol homologation is in fact the most favored route to higher alcohols by these materials.

In Chapter 5 of this thesis, conclusions are reported and MMO is discussed as an interesting and potentially useful support for higher alcohol formation because it serves both to disperse Mo as do other metal oxides and also to promote methanol reactivity,

which results in lowered methanol selectivity and greater higher alcohol selectivities.

Future directions for research are also discussed.

CHAPTER 1: INTRODUCTION[a]

1-1 Syngas

Syngas[1-3] has been a popular topic of research since the mid 1900's. It is a combination of H_2, CO, and CO_2 and is typically derived from coal,[4,5] natural gas,[6,7] and biomass.[8,9] It was first used by Fischer and Tropsch[10] in the 1920's to make long chain hydrocarbons. Syngas conversion is currently being investigated for the purpose of making fuels and chemical feedstocks.[11-13]

Along with methanol, ethanol and C_{3+} alcohols such as 1-propanol and 1-butanol are the focus of many studies due to their increasing use as fuel additives and chemicals. Syngas conversion over solid catalysts based on a multitude of transition metals has been studied for this purpose, including Cu, Fe, Zn, Ru, Rh, Mn, and Mo-based compositions.[11,12,14-26]

1-2 MoS$_2$/K as selective catalyst for higher alcohols from syngas

Molybdenum sulfide based catalysts, when combined with an alkali metal such as potassium,[27-33] are of particular interest due to their low cost compared to noble metal catalysts, their high selectivity for C_{2+} alcohols, and their high resistance to sulfur poisoning. However, they also possess disadvantages such as lower activity than noble metal catalysts and the need for comparatively higher reaction pressures to achieve useful catalytic productivities.[13,18,34-38] To reduce this disadvantage, promoters such as cobalt[30,32,33,39-42] have been added to increase alcohol selectivity and nickel[43-45] has been used to improve catalytic activity.

Historically MoS_2 has been used in hydrodesulfurization (HDS) reactions to lower sulfur content in natural gas and fuels.[46-48] MoS_2 itself has a lamellar structure where

---

layers have triangular prismatic unit cells.[49-51] MoS_2 domains can have as few as one layer of S-Mo-S atoms but often have 5 layers or more. Additionally, the material can take on crystalline or poorly crystalline character depending on synthesis method.[52-54] Typically poorly crystalline MoS_2 is preferred for the purpose of catalytic reactions due to a higher abundance of edge sites, which are believed to be most active.[28,44,55]

In the context of using MoS_2 for higher alcohol synthesis the addition of a basic promoter such as potassium is vital[28,30,32,33,56,57]. Other group I metals such as rubidium have also been effectively used.[20] The role of alkali is believed to be several fold. First it serves to titrate hydrocarbon-forming Brønsted acid sites on the catalyst's surface. By deactivating such sites, selectivity for alcohols increases. Notably however, alcohol productivity is not improved by this phenomenon alone because the number of alcohol producing sites is left unchanged. Second, alkali is believed to partially inhibit CO dissociation, which better allows for CO species to be inserted into C_xH_y species and then form oxygenates.[28,58,59] Finally, alkali is believed to assist in the coupling of alcohols, which will be discussed later in the text.[33,60]

1-3 Supports for MoS_2/K

In addition to bulk MoS_2-based catalysts, supported MoS_2 catalysts have also been widely evaluated as a means to maximize higher alcohol selectivity and productivity. Early academic studies were performed by Concha et al. and Tatsumi et al. using SiO_2, TiO_2, MgO, Al_2O_3, CeO_2, and a variety of carbons as supports.[31,56,61,62] Concha studied MoS_2 with no alkali addition while Tatsumi studied reduced, oxidic Mo rather than MoS_2. The authors found activity to be the parameter most affected by the support, with activated carbon yielding the most active catalyst and MgO the least. Both groups concluded that the support surface area could not be well correlated with activity.

Tatsumi et al. followed up their initial work with studies of Mo supported on silica, where several olefins and alcohols were co-fed into the reactant syngas stream.[63,64]

2

They found added C_n olefins to yield higher amounts of C_{n+1} alcohols and concluded that CO insertion was the primary chain growth mechanism over these catalysts, rather than methanol homologation or aldol condensation of lower alcohols (Guerbet reaction). They concluded that KCl served to suppress hydrocarbon formation while promoting hydrogenation of alkenes and hydroformylation reactions to form alcohols. Additionally, they found that KCl promotion did not alter isomer distribution, which suggested that C_{3+} primary alcohols were all formed via similar pathways. Finally, they showed that (acid catalyzed) alcohol dehydration pathways could be inhibited if an adequate amount of alkali was loaded onto the catalyst.

Carbon supported MoS_2 has also been widely investigated. In addition to the work of Tatsumi and Concha, studies were performed over activated carbon by many other researchers[32,63-70] who further confirmed the ability of carbon supports to improve catalytic activity. Several other researchers studied MoS_2 catalysts supported on multi-walled carbon nanotubes (MWCNT).[71-83] The primary findings of these studies were that use of MWCNT as supports generally improved activity over traditional activated carbons. This result was attributed to high dispersion of MoS_2 domains that formed due to the nanotube structure. The authors quantified dispersion primarily via CO chemisorption but also used H_2 chemisorption, XRD, TPR, and TEM to support their claims. These studies showed that Mo impregnation over highly microporous supports led to comparatively large metal agglomerates, which were less active for higher alcohol synthesis. This insight correlates well the previous observations that support surface area alone cannot be readily correlated to catalytic activity. Finally, these studies on carbon supports showed that unless a promoter such as Rh was added to the catalyst, selectivity for methanol was the highest among the alcohols, regardless of alkali loading.

A series of studies was performed on γ-alumina supported MoS_2. Li et al. evaluated the effects of Pd and Rh addition, finding that the metals could also improve catalytic activity.[84,85] They hypothesized that the improvement was due to increased Mo dispersion

3

as shown by X-ray diffraction (XRD) and laser Raman spectroscopy (LRS). Additionally, they found that the addition of Rh, a metal that shows significant higher alcohol activity and selectivity in its own right, increased C_{2+} alcohol selectivity. Several other studies described the effects of the calcination temperature of the MoO_x/Al_2O_3 precursor on the activity and selectivity of the sulfided catalyst.[86,87] These studies, one of which included Co in the catalyst, found that activity and higher alcohol selectivity increased with calcination temperature until reaching a plateau between 500 – 800 °C, with these effects attributed to the formation of specific K-Mo-O structures. The study of the cobalt-free catalysts showed that the alcohol distribution changed slightly with calcination temperature, with the catalyst being more selective for methanol when the calcination treatment produced the optimal activity.

1-4 Importance of Mo-K interactions

Jiang et al. investigated Mo-K interactions on γ-alumina supported MoS_2.[86-88] They found that KCl served first to form "K-Mo-S" surface species, which favored alcohol formation. Second, they found that once the K:Mo ratio was high enough to saturate the Mo surface, additional KCl would aggregate and block hydrocarbon favoring, coordinatively unsaturated sites (CUS). While alkali metals are generally understood to inhibit hydrocarbon formation, the authors provided evidence that Mo-K interactions might specifically inhibit sulfidation and consequently lead to a less reduced catalyst.

1-5 Reaction pathways and Mo structural significance

Bian et al. investigated the reaction stability of a 13% Mo 4% K on a γ-alumina catalyst.[89] They showed that the space time yield of alcohols increased dramatically for the first 15 hours of reaction and then increased more slowly until the 200 hour point where the reaction reached a nearly steady state. Using EXAFS they found the primary

difference between the freshly sulfided catalyst and the post-reaction catalyst to be Mo-Mo and Mo-S coordination, both of which dropped over the course of the reaction. The authors concluded that the loss of sulfur from the catalyst surface resulted in the formation of "highly" CUS (Coordinatively Unsaturated Sites) that favored alcohol formation, observing that alcohol space time yield increased over time.

This finding seems to contrast with the previously mentioned works that hypothesized that CUS sites favored hydrocarbon formation over alcohols. However, the catalytic role of these sites in MoS_2 catalysts in hydrogenation reactions has not yet been fully elucidated. Jalowiecki et al. evaluated the hydrogenation of isoprene over alumina supported MoS_2 and showed that certain types of CUS sites favored isomerization while others favored hydrogenation.[90] In their work, the CUS site structure was suggested to be altered simply by changing the MoS_2 loading. In that study, Mo loadings between 3 and 16 % yielded MoS_2 slabs of different dimensions and number of stacked layers. These differences yielded varying amounts of low sulfur CUS sites located on edge planes.

Perhaps the two most important findings of the body of work on CO hydrogenation over supported MoS_2 are that dispersing MoS_2 domains greatly enhances catalytic activity and that the support itself can affect selectivity by facilitating other reaction pathways, some of which are undesired such as alcohol dehydration. With these findings in mind, we investigated[91] the use of mesoporous Mg/Al mixed metal oxide (MMO) derived from layered double hydroxides[92-94] as a support to create dispersed MoS_2 domains for higher alcohol synthesis. We hypothesized that a more basic support would promote alcohol forming reactions, unlike γ-alumina, which is acidic, and is known instead to promote alcohol dehydration. We found that the MMO support, when loaded with 5 wt. % Mo, showed strikingly lower methanol selectivity than other supported catalysts, deviating from a typical Anderson Schulz Flory distribution, while maintaining a high C_{2+} alcohol selectivity at 8 % CO conversion. In that report, [91] we postulated that the role of secondary reactions such as alcohol coupling could be a cause

of the unusual alcohol distribution significantly biased towards C_{2+} and other higher alcohols.

1-6 Significance of Mo loading

We chose to further investigate the Mo/K/MMO catalyst system by varying the Mo and K loadings while operating at low CO conversions. Indeed, it was expected that changes in reactivity would be observed, as the previously mentioned work on diene hydrogenation over γ-alumina supported MoS_2 showed that Mo loading itself had significant effects on the product distribution.[90] Additionally, several other studies have also investigated the hydrogenation activity of MoS_2-based catalysts and correlated the Mo domain size with reactivity.[50,95]

Several groups have investigated the effects of Mo loading specifically on CO hydrogenation reactions. Bian et al.[96] studied γ-alumina supported MoS_2/K and showed that higher alcohol selectivity and productivity increased with Mo loading. However, in that work, alkali metals were added to the material, and the K:Mo (0.8:1) ratio was conserved for each catalyst (loaded from 3 wt. % to 18 wt. % Mo). This conservation naturally led to decreasing support acidity with increasing Mo (and K) loading, due to the acid-neutralizing effects of the added K. Given that acidic γ-alumina has been shown to dehydrate alcohols by itself[97-99] or when used as a support with MoS_2,[100] this change in support acidity may overshadow reactivity differences caused by the variations in Mo CUS that result from different Mo loadings. Li et al. performed a similar study on activated carbon supported MoS_2-K (loaded from 15 wt. % to 37 wt. %).[67] They showed that increasing Mo loading led to a decreasing methanol to $C_{2+}OH$ ratio and an increasing catalytic activity up to a Mo loading of 27 %. They attributed these outcomes to "more complete" Mo-K interactions that came about as Mo-support interactions became proportionately less prominent.

1-7 Alcohol coupling

Based on past work,[60,67,101-103] alcohol coupling reactions, notable alternative pathways to higher alcohols over classic CO insertions,[33,60,101-103] may play an important role in the formation of higher alcohols over supported MoS_2 catalysts. Specifically, aldol condensations between adsorbed intermediates are believed to yield an additional pathway to higher alcohols. Christensen et al. recently investigated this phenomenon in a study whereby they co-fed ethanol with the syngas over alkali-promoted bulk MoS_2 catalysts.[33,60] Their results showed that a 5 mol % co-feed yielded greater increases in 1-butanol than in 1-propanol productivity – a result that contradicts the expectations of the classic CO insertion pathway that was suggested to operate in a number of reports.[33,60,63,64,104] They hypothesized that the higher alcohol formation pathway was in fact an aldol condensation of two ethanol molecules.

The coupling of two primary alcohols, one of which must have a beta carbon, via aldol intermediates is known as the Guerbet reaction, which has been shown to occur over Pd, Rh, Ni, and Cu catalysts.[105-112] Additionally, basic metal oxides have also proven to be useful catalysts or catalyst supports for this reaction. [101,103,113-116] Given this background, alkali-promoted, MMO-supported MoS_2 could form higher alcohols either by (i) a classical CO insertion into a growing hydrocarbon chain, as in the work of Tatsumi et al. [63,64] and/or by (ii) condensing adsorbed aldehyde-like species that may come from reaction intermediates or stable alcohols that were formed and readsorbed.[60] The present work addresses the role of the Mo and K loadings on the catalytic activity and selectivity of the Mo/K/MMO catalyst family and sheds new insights into the possible importance of the various pathways described above in yielding the unusual higher alcohol selectivities reported previously over these MMO-supported catalysts.[91]

1-8 Topics of this dissertation

The present work is aimed at addressing the use of MMO as a support for MoS_2. It first focuses on the comparative advantages of MMO over other supports for alcohol-forming CO hydrogenation reactions (Chapter 2). This first study is followed by a more detailed investigation of the functionality of MMO in the reaction and of the character of Mo domains on the support (Chapter 3). Finally, pathways to higher alcohols are elucidated by interpreting the results of methanol and ethanol co-feed experiments (Chapter 4). This thesis presents a comprehensive picture of both how MMO yields novel selectivity results and how this character may prove useful in the creation of catalysts in the future.

CHAPTER 2: INVESTIGATION OF BASIC SUPPORTS[b]

Mo is supported on commercial activated carbon, commercial sepiolite, and Mg/Al mixed metal oxide material (MMO) and then promoted with K_2CO_3 and sulfided in-situ. The catalysts are then used in CO hydrogenation reactions at 310 °C, 1500 psig, CO:H_2 1:1, 50 ppm H_2S, and a flow rate of 15 – 60 SLPM. The productivity and selectivities of these catalysts are compared to the reaction run on a lab-synthesized bulk MoS_2/K catalyst. The MMO-supported catalyst is shown to be substantially more selective for C_2 – C_4 linear alcohols than for methanol and offers good alcohol to hydrocarbon selectivity. Unlike the other three catalysts used in the study, methanol selectivity of the MMO supported material deviates greatly from the Anderson-Shultz-Flory (ASF) distribution.

2-1 Experimental details

2-1-1 Support preparation

Activated carbon and sepiolite were obtained from commercial sources (Aldrich and Tulsa respectively). The MMO support was synthesized using methods similar to those described in the literature.[91,117-119] In brief, three solutions were prepared – A, B, and C. Magnesium nitrate hexahydrate (Alfa Aesar, 98 – 102%), aluminum nitrate nonahydrate (Alfa Aesar, 98 – 102%), and distilled water were combined with an approximate Mg:Al molar ratio of 7:3 and 0.6 M in metal ions to make solution A. Solutions B and C were 1.2 M NaOH (EMD, 97.0%) and 0.15 M Na_2CO_3 (Aldrich, 99.5+%) respectively.

First, 100 ml of solution C was heated to 65 °C and stirred. 360 ml of solutions A and B were then added simultaneously to C at a constant flow rate of approximately 11

---

ml/min with constant stirring. The flow rate of solution B was varied to maintain a mixture pH of 9.5 +/- 0.05 measured with an Oakton 110 series pH meter. After the addition of solutions A and B, the resultant mixture was stirred for 24 hours at 65 °C, filtered at room temperature, washed with 2 L of distilled water, and dried overnight at 105 °C. Finally, the material was ground with a mortar and pestle and heated in a calcination oven to 450 °C at 5 °C/min in ambient air for 2 hours to convert it from hydrotalcite to MMO.

2-1-2 Molybdenum impregnation

Supported MoO_3 was synthesized on the various carriers by an identical incipient wetness impregnation procedure followed by a thermal treatment. To prevent hydrotalcite "memory" effects[117-121] which potentially reduce catalytic activity by increasing crystallite size and "burying" promoters, DMSO (Aldrich, 99.9+%) was used as the impregnation solvent. A more thorough treatment of this topic is found in Appendix A.

Targeting approximately 5% wt. Mo, an appropriate amount of ammonium molybdate tetrahydrate (AMT) (Aldrich, ACS Reagent) and DMSO were combined and stirred at room temperature until the AMT was dissolved. The solution was then added to the support and heated at 135 °C for 12 hours in open atmosphere. The resultant solid was then placed in a quartz tube and heated to 450 °C for 2 hours with a heating rate of 5 °C/min under 40 ml/min of flowing nitrogen. The sample was then cooled to room temperature and stored in a sealed vial and filled with argon. These samples consisted primarily of MoO_3 dispersed on the support.

Bulk molybdenum sulfide was prepared from methods described in the literature.[30,32,33,122] AMT and 20 % $(NH_4)_2S$ (Alfa Aesar, 20 – 24% aq.) were combined and stirred for 1 hour at 65 °C. A 25 wt. % acetic acid solution was then added to the mixture to precipitate the thiomolybdate. After allowing the mixture to cool, it was filtered and washed with distilled water. The compound was then decomposed by heating at 5 °C /min to 450 °C under 40 ml/min flowing nitrogen for two hours to form MoS_2.

Before use in catalytic reactions, K_2CO_3 (Sigma-Aldrich, 99%), previously treated at 105 °C, was added to the supported MoO_3 or unsupported MoS_2 and ground using a mortar and pestle for 15 minutes. The mixture was pressed into 10 mm pellets at 1000 psig, crushed, and sieved to 20 – 40 mesh. The catalyst was then loaded into a ¼" steel tube with a layer of SiC (Alfa-Aesar, 46 grit) at its base and flushed with nitrogen in a down-flow configuration. The oxide pre-catalysts were then characterized with a variety of techniques described in the following sections.

2-1-3 X-ray diffraction (XRD)

Powdered X-ray diffraction was employed to assess the bulk domains of the catalyst. Data was collected using a Philips X-pert diffractometer using CuKα radiation. Samples were first ground into a fine powder with a mortar and pestle, and approximately 300 mg was then loaded into an aluminum sample tray. The sample was then pressed into a flat wafer while still inside the tray and analyzed at 40 mV and 40 mA at a 2 θ from 10 – 90 °.

2-1-4 Nitrogen physisorption

Surface area and pore volume data were collected via nitrogen physisorption at 77 K using a Micromeritics Tristar II. Approximately 150 mg of sample was loaded into a custom 15 ml Micromeritics sample tube and heated to 200 °C under vacuum for 10 hours before analysis. Data was collected at partial pressures ranging from 0.001 to 1.00 – 35 points for the adsorption curve and 35 points for the desorption curve.

2-1-5 Raman spectroscopy (LRS)

Raman spectra were also used to assess Mo domain structure and composition. The data were obtained using a Witec confocal Raman microscope (Alpha 300R) with an Ar+ ion laser (λ = 514.5 nm) with 1 mW of intensity of the excitation source. The microscope magnification was set to 10x with a high resolution grating of 1800 dpi. Samples were scanned from 200 – 1500 nm.

2-1-6 Elemental Analysis (EA)

Elemental analysis was performed with a Perkin Elmer Optima 7300 DV equipped with an optical emission spectrometer. Aliquots of each catalyst were digested in an H_2O_2/HNO_3 solution and then analyzed in duplicate.

2-1-7 Temperature Programmed Desorption (TPD)

Basic sites were quantified via temperature-programmed desorption of CO_2 using a Micromeritics Autochem II. In these experiments, ca. 0.12 g of sample was loaded into a quartz sample tube. Helium (Airgas, UHP) was passed over the sample at 50 ml/min to pretreat each material as it was heated to 700 °C at 10 °C/min. The sample was then cooled to 50 °C and exposed to pure CO_2 (Airgas, research grade) at 50 ml/min for 2 hours. The tube was then flushed again with He at 50 ml/min for one hour. Finally the sample was heated (under flowing He) to 700 °C at 10 °C/min, and a TCD was used to quantify the desorbing gas.

Acid sites were quantified using the same instrument, but using 2% NH_3 in N_2 (Matheson-Trigas, 1.871% NH_3) as the probe molecule. The TPD procedure was identical to that of the CO_2 TPD, except that sample was heated only to 450 °C, cooled to 100 °C, then exposed to 0.2% NH_3/N_2, and heated again to 450 °C.

2-1-8 Reaction

Before reaction with syngas, 10% H_2S/H_2 (Matheson Tri-Gas, UHP) was passed over the catalyst at 40 ml/min. During the flow the bed was heated from 22 °C and 15 psig to 450 °C at 5 °C/min and held for 2 hours. While still under 40 ml/min H_2S/H_2 flow, the bed was allowed to cool to 310 °C. Finally, the reactor was flushed with syngas, 1:1 H_2(Airgas, UHP):CO (Airgas, UHP and 50 ppm H_2S, diluted from 5000 H_2S in He, Matheson Tri-Gas, UHP, purified with 5A molecular sieve carbonyl trap) at 100 ml/min for 5 minutes and then pressurized to 1500 psig. Reactions were carried out until activity and product selectivity stabilized, which took 2 to 4 days. A summary of these parameters is shown in **Table 2.1**. Several precautions had to be taken to keep syngas composition consistent over the course of reaction and to ensure reaction parameters such

as temperature and pressure were properly being controlled. These precautions are discussed in Appendices B and C respectively.

The Weisz-Prater criterion was used to ensure that the reaction was not mass transport limited. Additionally, the potential for hotspots on the catalyst surface was investigated by comparing approximate reaction enthalpy with the heat transfer coefficient for the MMO supported catalyst. The calculations indicated that the reaction would not cause catalyst particle surface temperature to climb more than 0.5 °C. These calculations are discussed further in Appendix D.

Table 2.1. Summary of reaction parameters

Parameter	Magnitude
Pretreatment	
Pressure (psig)	*15*
Temperature (°C)	450
Gas Flow (SLPM)	0.02
Heating Rate (°C/min)	5
H_2S Concentration (%)	10%
Time (hr)	2
Reaction	
Pressure (psig)	1500
Temperature (°C)	310
Syngas Flow (SLPM)	0.010 - 0.100
H_2S Concentration (ppm)	50
$CO:H_2$	1

CO conversion, product yields and selectivities were calculated from pseudo-steady-state data. The space velocity was adjusted by varying the syngas flow rate until a conversion of ca. 8% was reached. Following reaction, the reactor was depressurized and allowed to cool to room temperature (~23 °C). The catalysts were then passivated while

inside the reactor by passing 1% O_2 in He (Matheson Tri-gas, UHP) for 6 hours at room temperature and 40 ml/min through the reactor.

2-1-9 Product quantification via gas chromatography (GC)

An Agilent 7890 GC was used to quantify reaction products. Specifically, methane, ethane, propane, butane, ethylene, carbon dioxide, methanol, ethanol, 1-propanol, 2-propanol, 1-butanol, 2-methyl-1-propanol, methyl acetate, ethyl acetate, methyl formate, ethyl formate were quantified using single point calibration curves. The GC was equipped with two thermal conductivity detectors (TCD) and one flame ionization detector (FID). The reactor outlet was sampled online through 3 sample loops connected in series, which were later injected into the GC columns in parallel. The plumbing configuration of the GC columns and detectors along with their specification are shown in Figure 2.1.
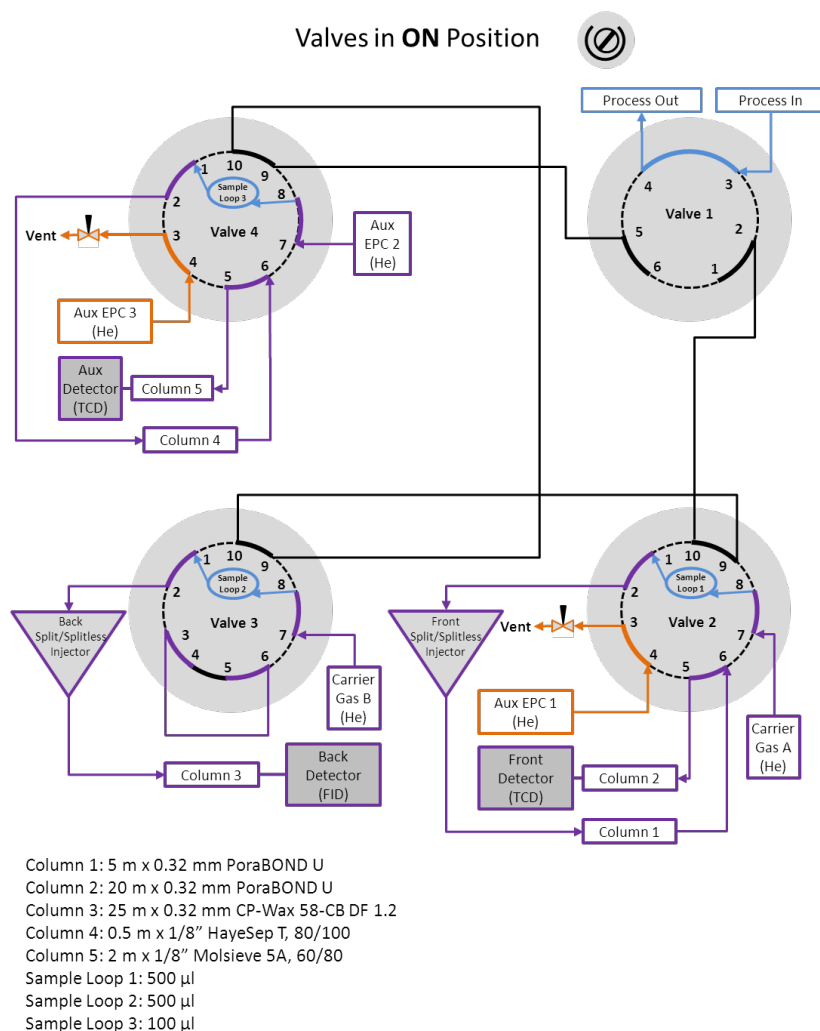
Figure 2.1. GC sample loop, column schematics, and plumbing diagram of the instrument used in study.

2-2 XRD measurements

XRD patterns of the synthesized materials are shown in Figure 2.2. The bulk MoS_2 pattern showed distinct 002, 100, 103, 105, and 110 MoS_2 planes. Peaks associated with the 100 and 110 planes could also be observed in the activated carbon and MMO supported samples, though they were substantially less intense, indicating smaller and/or less crystalline domains. Features associated with MoS_2 planes were not discernible on

the sepiolite supported sample, possibly because they overlapped with the pattern of the support itself.
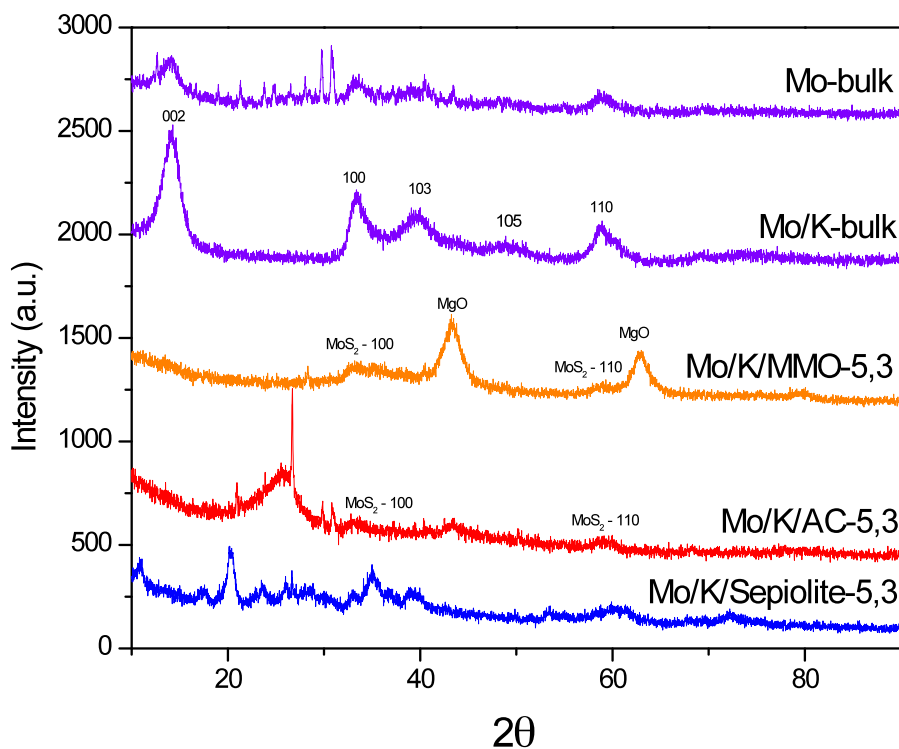
Figure 2.2. XRD of supported and unsupported K_2CO_3 promoted MoS_2. Supported samples were sulfided in-situ and reacted with syngas for 2-4 days.

2-3 Raman Spectroscopy

Raman spectroscopy also revealed the presence of MoS_2 domains as shown in Figure 2.3. In all but the activated carbon supported sample, characteristic[123] Mo-S stretching bands were readily observable at 380 and 408 cm^{-1}. The estimated resolution of the spectrometer is approximately 2 cm^{-1}, and as such, the observable bands are considered identical. The stretches were less apparent in the activated carbon sample most likely because the carbon support absorbed most of the light.

16
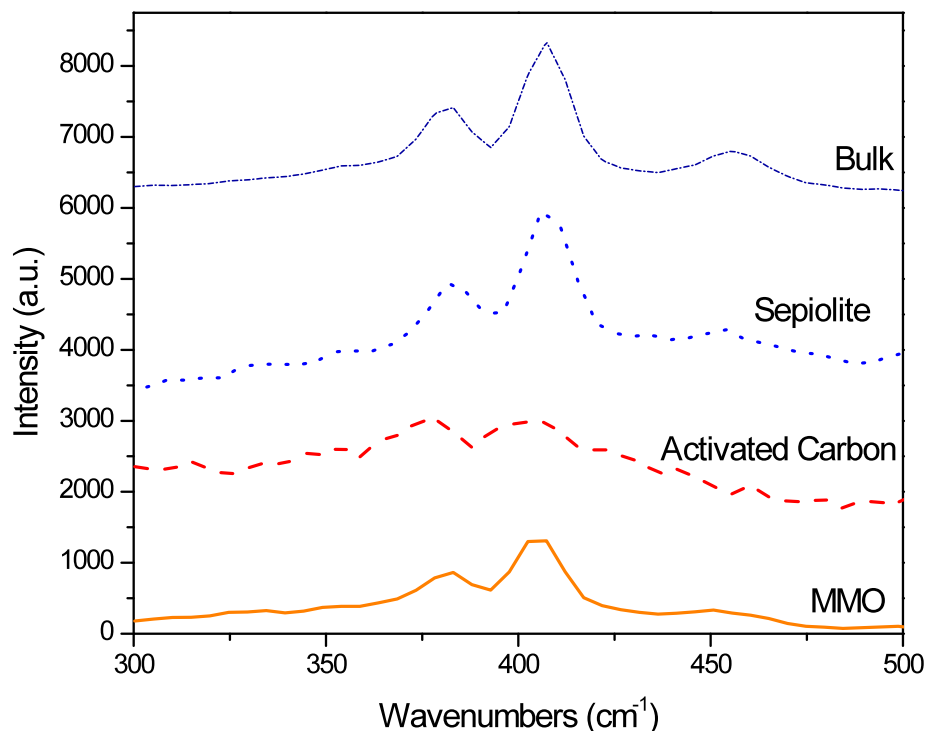
Figure 2.3. Raman spectroscopy of the reaction-aged, sulfided catalysts using a 1800 grating, 514 nm, 0.5 mW laser

2-4 Nitrogen Physisorption

The BET surface areas (reported in Table 2.2) computed from nitrogen physisorption data show that the activated carbon and sepiolite catalysts lost surface area over the course of sulfidation and reaction. This result may be a consequence of sintering or carbon/sulfur deposition. The MMO supported catalyst showed a slight increase in BET surface area, but the difference is considered to be within the error of the instrument. Strong metal-support interactions not found could reduce the potential for sintering. The catalysts all showed a lower post-reaction molybdenum content, which supports the hypothesis of carbon buildup on the catalyst surface. Pore blockage from hydrocarbon wax build up is also a possible cause for reduced surface areas. However

17

volatile product analysis reveals only low molecular weight hydrocarbon species and there were no waxes found in downstream traps.

The carbon-supported catalyst appears to lose a significant amount of Mo and K over the course of reaction. This outcome is most likely a result of carbon deposition from CO reacting on the catalyst surface, which is common for carbon supports that have some microporous character. [74,124,125]

Table 2.2. Pre-reaction/sulfidation catalyst and sulfided, reaction aged catalyst compositions and surface areas measured via ICP and nitrogen physisorption respectively.

	Oxide pre-reaction			Post-reaction sulfide catalyst		
Catalyst Support	*Mo (wt. %)*	*K (wt. %)*	*Surface Area (m^2/g)*	*Mo (wt. %)*	*K (wt. %)*	*Surface Area (m^2/g)*
Bulk	30.3	14.5	89	29.8	14.5	-
MMO	5.2	2.1	71	4.9	2.1	78
Carbon	4.3	1.8	331	2.2	0.9	175
Sepiolite	4.5	3.0	89	4.0	2.1	76

2-5 Reactivity Results

The results of the catalytic reactions are reported in Table 2. The bulk MoS_2 catalyst, showed high selectivity for both methanol and ethanol. This result is consistent with that found in other studies. [30,32,33,44,126,127]

Additionally, methane accounted for most of the hydrocarbons produced over this catalyst. The MMO-supported catalyst showed the greatest $C_{2+}OH$ selectivity overall at 55.5%, in addition to the highest 1-propanol and 1-butanol selectivities. Most notable was the low methanol selectivity, which was uncharacteristically substantially lower than

the ethanol, 1-propanol, and 1-butanol selectivities. By comparison, the methanol selectivity on the MMO supported catalyst was almost 8 times lower than that observed in the bulk MoS_2 catalyst. The MMO supported catalyst was less active than the activated carbon supported and bulk catalysts. Given the hypothesis that basic alkali blocks active sites, it is possible the MMO support interacts with the MoS_2 domains in a similar fashion.

Table 2.3. Reaction results of supported and unsupported MoS_2 Catalysts.

| Support | GHSV (ml/g/hr) | % Conv. | % Selectivity Organic Products by Carbon excluding CO_2 | | | | | | | C_{2+} OH Prod (g/g$_{Mo}$/hr) |
			MeOH	EtOH	1-PrOH	1-BuOH	CH_4	$C_{2+}OH$	Tot. HC	
Bulk	8004	8	34.1	32.9	5.5	0.9	19.6	39.3	22.2	0.23
MMO	1377	8	4.5	25.9	18.7	10.9	13.9	55.5	37.0	0.23
Carbon	3973	8	14.2	33.5	13.6	4.6	15.7	51.7	32.0	0.88
Sep	1937	8	2.7	5.0	2.3	1.0	20.3	8.3	88.5	0.06

When activities are normalized per gram of molybdenum, the activated carbon supported catalyst was the most productive for higher alcohols with an hourly productivity of 0.88 g-C_{2+}OH/g-Mo/hr. The MMO and bulk samples had roughly the same activity, at 0.23 g-C_{2+}OH/g-Mo/hr, and the sepiolite sample was the least active at 0.06 g-C_{2+}OH/g-Mo/hr. Of the supports used in this study, activated carbon was the least basic as shown by CO_2 TPD as shown in Table 2.4. While it is not fully established whether support basicity has a similar effect on catalytic activity and selectivity as alkali, it is noteworthy that the most neutral support, activated carbon, had the highest activity while the most basic support, MMO, had the lowest. While catalytic activity did appear to correlate with support basicity, other factors, such as differences in MoS_2 dispersion among the different catalysts may also influence the results. Counter to this hypothesis,

XRD shows that the supported catalysts are all highly dispersed, although future, more detailed investigations of the MoS_2 domains are needed.

Table 2.4. NH_3 and CO_2 TPD results for supports used in this study.

Supports	NH_3 Uptake (mmol/g)	CO_2 Uptake (mmol/g)
Sepiolite	0.29	0.08
MMO	0.20	0.21
Activated Carbon	0.01	0.02

The sepiolite supported catalyst was highly selective for hydrocarbons, most likely due to its high acid site content as shown by NH_3 TPD as shown in Table 2.4. A similar result was observed when syngas was reacted over acidic alumina and silica supported MoS_2.[44,59,100,126,128] While CO_2 TPD shows the catalyst does possess some basic sites, we hypothesize that the acid sites are not adequately neutralized at the potassium levels used here, and hence hydrocarbon formation is more highly favored in the reaction of syngas over this catalyst under these conditions.

Interestingly, the methanol selectivity was lower for both the carbon and MMO supported catalyst than for the bulk catalyst. However, the MMO supported catalyst yielded selectivities that were much more strongly biased towards C_{3+} alcohols than any of the other catalysts.

The Anderson-Shultz-Flory distribution of the alcohols reported in Figure 2.4a. shows that the MMO supported catalyst deviates substantially from the trend shown for ethanol, 1-propanol, and 1-butanol. Additionally, the chain growth parameter, α, is the largest for the MMO supported sample among the catalysts studied, indicating a higher probability for longer chains than the unsupported catalyst and the two other supported ones.

The ASF distribution shown in Figure 2.4b for hydrocarbons reveals that the MMO supported catalyst possessed a greater chain growth probability than the activated carbon and bulk catalysts. There are a multitude of possible explanations for this observation. These include hydrogenation of methanol to form methane. However, methane selectivity seems to follow the ASF trend. Alternatively, some form of metal-oxide promoted alcohol coupling could contribute to the ASF distribution of alcohols on the MMO catalyst. This phenomenon has been observed on transition metal free $Mg_xAl_xO_x$[103] and on a Cu/ZnO catalyst.[34,35] In addition, Christensen et. al.[60] showed that alcohol coupling was possible over CoMoS when an ethanol co-feed was used in conjunction with syngas. In that work, reactions showed increased 1-butanol and 1-propanol selectivity in addition to higher selectivities for higher hydrocarbons. Although these findings are not directly analogous to syngas reactions over MMO supported MoS_2, they suggest that there are multiple potential pathways that may contribute to the unique product distributions observed in this work beyond traditional CO homologation.[33,60]
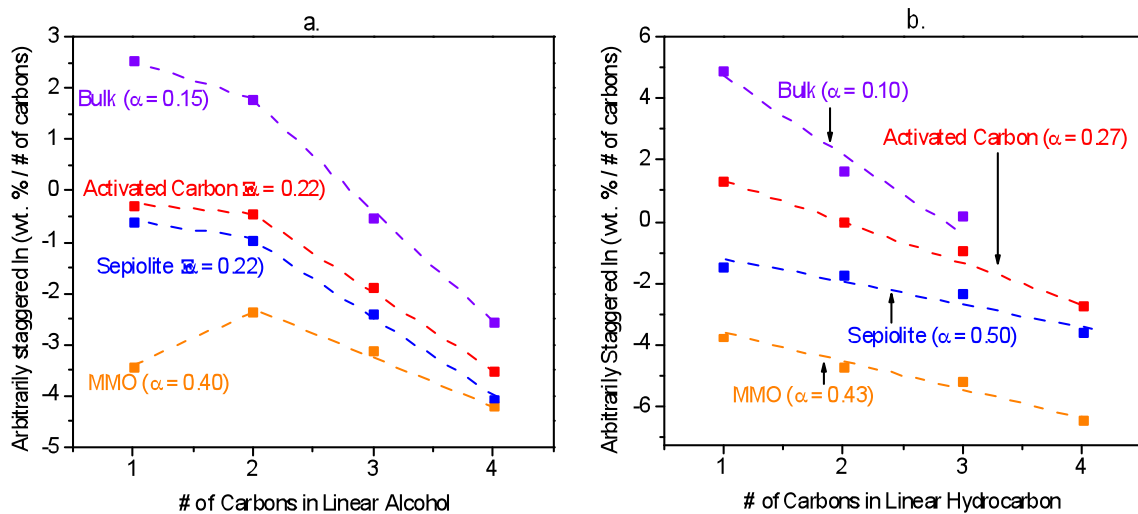
Figure 2.4. The ASF distribution of alcohols (a) and hydrocarbons (b) on various supported and unsupported potassium promoted MoS_2 catalysts. The α values (chain growth parameters) were computed for $C_2 - C_4$ linear alcohols and for $C_1 - C_4$ linear hydrocarbons.

Another possibly complementary explanation of the uncharacteristically low methanol selectivity observed on the potassium promoted, MMO supported MoS_2 catalyst may be associated with the capacity of metal oxides, MgO in particular, to decompose methanol to H_2, CO, and CO_2.[33,129,130] Goodarznia et. al.[131] showed that C_2 oxygenates such as methyl formate and ethanol could be formed from methanol alone when MgO was combined with potassium and copper. MMO supported MoS_2 may possess a similar capacity.

Finally, low methanol selectivity may possibly be explained as an artifact of basicity – whether it comes from the support or from an alkali promoter. Several studies that investigated the impact of potassium loading found that the methanol to ethanol ratio reached a minimum around the level that potassium loading was optimal for higher alcohol productivity.[58,88,132,133] Ultimately, additional investigation is needed to better understand the nature of higher alcohol formation on the MMO supported MoS_2 catalyst.

2-6 Summary

It has been demonstrated that MMO supported K/MoS_2 materials bring unique aspects to catalytic mixed alcohol synthesis from syngas. First, the catalyst allows for lower methanol selectivity, well below the values predicted by the ASF distribution. Second, the catalyst increases alcohol chain growth, yielding high selectivities for 1-propanol and 1-butanol. The relative and possibly complementary effects of the alkali promoter and MMO support as well as the mechanism(s) leading to the unique product selectivity will be investigated in the following chapter.

CHAPTER 3: ROLE OF MMO IN ALCOHOL FORMING REACTIONS[c]

A series of MoS_2 catalysts supported on Mg/Al hydrotalcite-derived mixed-metal oxide (MMO) supports promoted with K_2CO_3 is used for alcohol synthesis via CO hydrogenation. Alcohol selectivities are found to vary greatly when the Mo is loaded on the support at 5 wt. % compared with 15 wt. % Mo samples, all with a Mo:K atomic ratio of 1:1. The most striking difference between the catalysts is the comparatively low methanol and high C_{3+} alcohol selectivities and productivities achieved with the 5 % Mo catalyst. This catalyst also produces more ethane than the 15 % Mo catalyst, which is shown to be associated with ethanol dehydration and hydrogenation over residual acid sites on this catalyst with lower K content.

A series of catalysts with a nominal composition of 5 % Mo and 3 % K supported on MMO prepared in different manners all yield similar catalytic selectivities, thus showing that selectivity is predominately controlled by the MMO to Mo ratio, rather than the synthetic method. When the Mo loading is the same, catalytic higher alcohol productivity may be correlated to the degree of stacking of the MoS_2 layers, as assessed via X-ray diffraction and scanning transmission electron microscopy. Control reactions where K loading is increased or the positioning of the MMO in the catalyst bed is changed via creation of multiple or mixed catalyst beds show that Mo/K/MMO domains play a significant role in alcohol forming reactions.

Higher alcohol forming pathways are proposed to occur via CO homologation pathways or via coupling of adsorbed reaction intermediates at or near MoS_2 domains. No evidence is observed for significant alcohol coupling pathways by adsorption of alcohols over downstream, bare MMO supports, although some coupling may occur over

---

[c] Material from this section has been published.. Morrill, M. R. et al. *ACS Catal*. **2013**, *3*, 1665–1675.

K-promoted MMO supports. Nitrogen physisorption, XRD, Raman, UV-vis DRS, STEM, and XANES are used to characterize the catalysts, demonstrating that the degree of stacking of the MoS_2 domains differs significantly between the low (5 % Mo) and high (15 % Mo) loading catalysts.

3-1 Experimental details

3-1-1 Catalyst Preparation

MMO supported catalysts with approximate Mo loadings of 5 and 15 wt. % were synthesized and combined with K_2CO_3 (Sigma-Aldrich, 99 %) in a manner similar to our previous study.[91] For this paper, the samples are referred to as Mo/K/MMO-5,3 (the first number, 5, denoting nominal Mo weight loading and the second number, 3, denoting K weight loading) and Mo/K/MMO-15,9 respectively. In brief, MMO was made via co-precipitation of a magnesium nitrate hexahydrate (Alfa Aesar, 98–102 %) and aluminum nitrate nonahydrate (Alfa Aesar, 98–102 %) aqueous solution (Mg:Al molar ratio of 7:3 and 0.6 M in metal ions) and with 1.2 M NaOH (EMD, 97.0 %) and 0.15 M Na_2CO_3 (Aldrich, 99.5+ %) at 65 °C and a pH of 9.5. The solution was then stirred for 48 hours, filtered, washed with deionized water, dried at 105 °C, then calcined at 450 °C for 2 h. Ammonium molybdate tetrahydrate (AMT) (Aldrich, ACS Reagent) was dissolved in DMSO (Aldrich, 99.9+ %) and added to MMO at room temperature via incipient wetness impregnation. As previously mentioned, DMSO was used as an impregnation solvent rather than water to prevent the partial reformation of the original hydrotalcite structure.

The material was then dried in open atmosphere at 135 °C for 12 hours, loaded into a quartz tube, and decomposed via heating to 450 °C for 2 h with a heating rate of 5 °C/min under 40 ml/min of flowing nitrogen, which was used rather than air to maintain consistency with the previous study which included carbon as a support.

Due to the low solubility of AMT in DMSO, the incipient wetness impregnation step was repeated multiple times to load adequate AMT onto the MMO support for

Mo/K/MMO-15,9. After each impregnation, the sample was heated to 135 °C in open atmosphere for approximately 12 hours, then cooled to room temperature again. After the decomposition step (heating to 450 °C for 2 h), the resultant MoO_x/MMO samples were physically ground for 15 minutes with K_2CO_3 (Sigma-Aldrich, 99 %, stored in an oven at 105 °C), pressed into 10 mm pellets at 1500 psig, crushed, and sieved to 20 – 40 mesh.

For catalytic reactions, sieved particles accounting for approximately 50 mg Mo (1.0 g of a 5 % Mo catalyst and 0.33 g of a 15 % Mo catalyst) were loaded into a ¼" steel tube and pretreated with 10 % H_2S/H_2 (Matheson Tri-Gas, UHP) as described in our previous study.[91] Reaction parameters are summarized in Table 2.1. Namely syngas composed of 45 % H_2 (Airgas, UHP), 45 % CO (Airgas, UHP, purified with 5A molecular sieve carbonyl trap), 10 % N_2 (Airgas UHP) as an internal standard, and 50 ppm H_2S (from 5000 ppm H_2S in He, Matheson Tri-Gas, UHP) was fed over a packed bed of catalyst at 310 °C and 1500 psig at flow rates from approximately 10 – 100 standard ml/min (700 – 17000 ml syngas/g catalyst/hr). Reactions were carried out until activity and product selectivity stabilized, which took approximately 4 days. Conversions were then changed as needed by changing syngas flow rate through the reactor. Please note that studies of toxic (CO, H_2S) and flammable (H_2, CO, H_2S) gases under high pressure requires significant safety precautions.

3-1-2 XRD and N_2 physisorption

XRD and N_2 physisorption were performed identically to what was performed in the previous chapter.

3-1-3 Raman and UV-visible diffuse internal reflectance spectroscopy (UV-vis)

Raman spectra were obtained for both the oxide and sulfide samples using a Witec confocal Raman microscope (Alpha 300R) with an Ar^+ ion laser ($\lambda = 514.5$ nm) with 1 mW (for MoS_2) and 3 mW (for MoO_x) excitation source intensity. UV-Vis spectra were obtained on a Cary UV-Vis 500 with an internal diffuse reflectance cell. Pure MMO was used as a background.

3-1-4 Scanning Transmission Electron Microscopy (STEM)

Several of the sulfided samples were analyzed with STEM. Samples for STEM were prepared by dispersing the materials in 2-propanol, sonicating the dispersion, and dropping small aliquots of the suspension on a TEM grid. Images were collected on a JEOL 2200FS-AC STEM operating at 200 keV at Oak Ridge National Laboratory. Each sample was scanned in three to 5 different locations with the user zooming in on regions that contained layered MoS_2 structures.

3-1-5 X-ray absorption spectroscopy (XAS)

XAS was performed at beam lines X18B and X23A2 of the National Synchrotron Light Source (NSLS), Brookhaven National Laboratory. The storage ring was typically operated at 2.8 GeV with a ring current of about 300 mA. The XAS data were obtained in the transmission mode at the Mo K edge (20 keV) with a spot size of 0.5mm × 5mm. The Mo K edge spectra were measured at room temperature in air with Mo foil (0.015 mm, 99.9%, Goodfellow) as energy references. Supported Mo samples were ground with boron nitride (99%, Aldrich) to obtain an absorption thickness of 1 inside a 5/32" ID Pyrex tube. Three scans from 19700 eV to 21220 eV were collected for each sample. The XAS data were processed using the Athena[134] software for background removal, post-edge normalization, and X-ray absorption near-edge structure (XANES) analysis. Standard bulk MoS_2 (Acros, 98.5%) was used to determine the amplitude reduction factors (S_0^2) for Mo−S and Mo−Mo. The interatomic distances (r), coordination numbers (CN), Debye−Waller factors (σ^2), and energy shifts (ΔE_0) were derived from fitting the results in the Artemis software package.[134] The extended X-Ray absorption fine structure (EXAFS) results were fitted in R-space using two shells (Mo–S & Mo–Mo) generated theoretically using FEFF 6.0.[134,135]

3-2 XRD

XRD patterns of the synthesized materials are shown in Figure 3.1. Diffraction lines that are characteristic of the MgO component of MMO at 44° and 64° were readily apparent on all supported samples. The lines are smaller on Mo/K/MMO-15,9 mostly likely due to disruption of MMO crystallinity on account of larger concentrations Mo and K. A single diffraction line at 27° that corresponds to the (021) plane in MoO_3[136] is observed only on the oxide precatalyst form of Mo/K/MMO-15,9. The Mo/K/MMO-5,3 counterpart does not show this diffraction line because the MMO support contains comparably smaller Mo domains. This difference is also reflected in the Raman and UV-vis spectra, which are discussed later in the text.

Both the oxide precatalyst forms of Mo/K/MMO-5,3 and Mo/K/MMO-15,9 show small peaks around 32° that are characteristic of potassium molybdate structures. Small peaks for the MoS_2 [100] (33°) and [110] (58°) planes were observed on both supported, sulfide samples. An interesting difference between the sulfide catalysts is observed for the [002] plane of sulfide domains at 14°, which is prominent for the bulk MoS_2 sample, apparent for the Mo/K/MMO-15,9 catalyst, and absent for the Mo/K/MMO-5,3 catalyst. The presence of the line could be indicative of greater Mo-S stacking in the sulfided domains,[52,136] or because Mo loadings are different for the two catalysts, the peak's absence in Mo/K/MMO-5,3 could be attributed to the lower Mo loading.
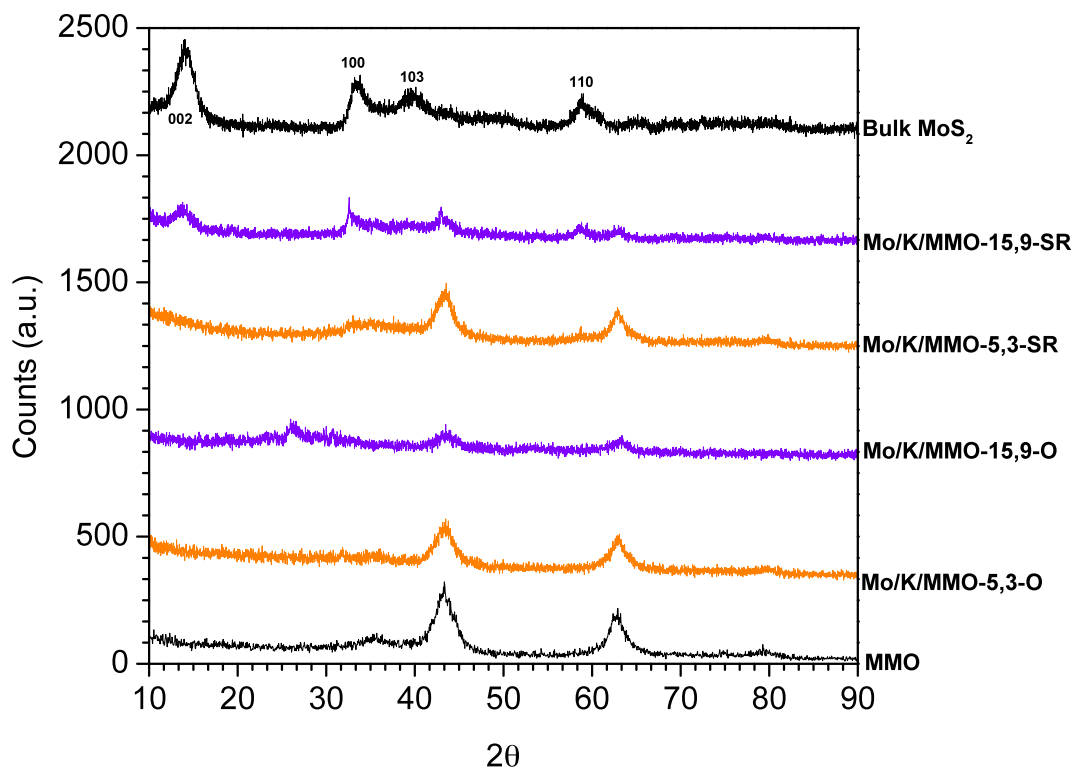
Figure 3.1. XRD data of supported and unsupported K_2CO_3 promoted MoS_2. Supported samples were sulfided in-situ and reacted with syngas for 2-4 days.

3-3 N$_2$ Physisorption

The BET surface areas shown in Table 1 are calculated from nitrogen physisorption data and show a small drop when the MMO support was impregnated with 5 % Mo and 3 % K and a large drop in surface area when the support was impregnated with 15 % Mo and 9 % K presumably due to higher surface coverage from multiple impregnation steps. Additionally, the Mo/K/MMO-5,3 sample lost much more surface area than Mo/K/MMO-15,9 after sulfidation and reaction. This effect may be due a bigger impact of carbon deposition or sintering on the highly porous, exposed MMO surface of Mo/K/MMO-5,3 compared to the higher loading Mo/K/MMO-15,9 sample.

Table 3.1. BET surface area derived from nitrogen physisorption data for the materials used in this study.

Sample	BET Surface Area (m^2/g)
MMO support	209
Mo/K/MMO-5,3 – oxide precatalyst	151
Mo/K/MMO-5,3 – sulfided, reacted	69
Mo/K/MMO-15,9 – oxide precatalyst	26
Mo/K/MMO-15,9 – sulfided, reacted	24

3-4 Raman spectroscopy

The Raman spectra of the oxide precatalysts are shown in Figure 3.2a The spectra of the oxide precatalysts were collected before the addition of K_2CO_3 to emphasize only the differences in the Mo domains. The 15 % and 5 % loaded Mo, alkali free counterparts are denoted as Mo/MMO-15 and Mo/MMO-5, respectively. The Mo/MMO-15 spectrum showed bands at 957, 847, and 370 cm^{-1}. These bands are characteristic of $Mo_7O_{24}^{4-}$ domains that become increasingly prevalent when Mo loading rises.[137-139] Raman bands at bands 902 and 321 cm^{-1} are readily apparent for Mo/K/MMO-5 and are characteristic of MoO_4^{2-} domains. The band at 902 cm^{-1} is also present in the Mo/MMO-15 spectra indicating that at high Mo loadings, a multitude of oxide domains will form.

Bands representing crystalline MoO_3 are absent from Mo/MMO-15, which has a Mo loading well above the monolayer surface coverage threshold. Notably, the sample itself was dark brown in color. These color centers have potential to scatter light and in turn mask characteristic bands. The sample's color is likely caused by a small amount of autoreduced Mo that formed during the decomposition of AMT. A second Raman spectrum was taken after treating Mo/MMO-5 and Mo/MMO-15 in a calcination oven in air at 450 °C for 2 hours (Mo/MMO-5-Air and Mo/MMO-15-Air respectively). The

resultant spectrum shown in Figure 3.2b contains similar molybdate bands as Mo/MMO-15 and additional MoO_3 bands, as was originally expected. The autoreduced Mo likely existed in very small proportions given the absence of MoO_2 character in both the XRD and XANES data. Specifically, the XRD pattern shows no MoO_2 diffraction lines, which implies that either crystalline MoO_2 is not present in the sample at all or that the domains are too small to be detected. The XANES spectrum, which will be discussed in more detail later, shows a K-edge that correlates almost perfectly with MoO_3. Additionally, the band at 550 cm^{-1} on Mo/MMO-5, which correlates with neither MoO_2 nor MoO_3 disappeared on Mo/MMO-5-Air, indicating that it is not a likely component of the MoO_x structures.
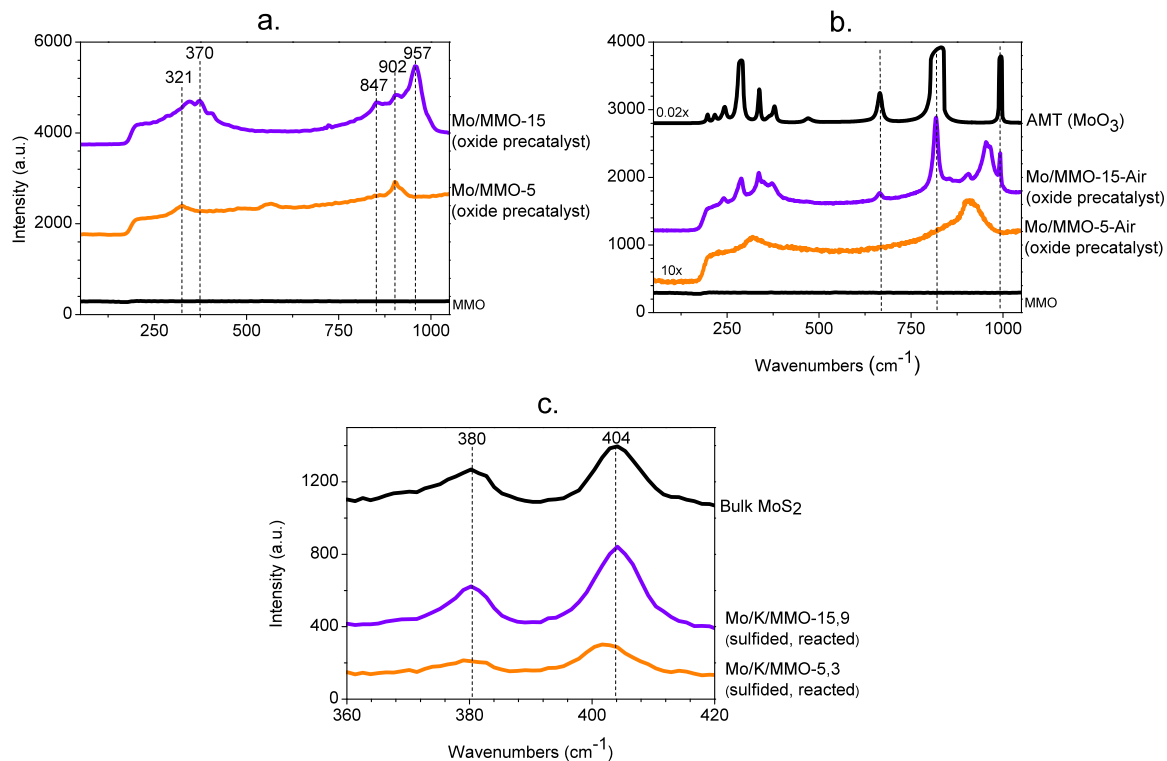
Figure 3.2. Raman spectra of the MMO supported Mo/K materials precatalysts pretreated in nitrogen (a) and air (b) both analyzed with a 1.5 mW 514 nm laser. The sulfided, reacted catalyst (c) was analyzed with a 0.5 mW 514 nm laser.

Unlike in the case of the oxide precatalysts, the Raman spectra of the sulfided, catalysts after reaction, shown in Figure 3.2c do not show dramatic differences between the samples with different Mo loadings. Bands at 380 and 404 cm^{-1}, which are characteristic of Mo-S vibrations, were present in the two sulfide samples.[123] The implications of the Raman spectra of the sulfide samples are simply that the two catalysts possess similar Mo-S bonds that are not influenced differently by support interactions and that the peaks for the Mo-O vibrations have disappeared.

3-5 UV-vis DRS

Additional information about the supported MoO_3 domains is obtained from UV-vis DRS data.[139,140] The absorption edge energies of the various samples in this study were determined by plotting $[F(R_\infty)h\nu]^2$ vs. $h\nu$ and then finding the x-intercept of the line fitted to the low-energy rise of each spectrum in the dataset. This rise represents a ligand to metal charge transfer, whose energy is represented by the x-intercept of the fit line.[137,139-141] Generally, lower energies are associated with larger aggregates. The UV-vis data in Figure 3.3a are complementary to the Raman spectra, yielding useful insights into the molybdenum domain sizes of the oxide precatalysts. The highest edge energy band of Mo/K/MMO-15 is between that of crystalline $Mo_7O_{24}^{6-}$ and $Mo_2O_7^{2-}$ standards from literature while the edge energy for bulk MoO_3 is between that of MoO_3 and $Mo_7O_{24}^{6-}$.[137,139-141]

Finally the edge energy of Mo/K/MMO-5 is close to that of crystalline MoO_4^{2-}. The spectra for Mo/MMO-15 has a second, less intense edge at approximately 2.2 eV, which is absent from the UV-vis of Mo/MMO-15-Air shown in Figure 3.3b. Consequently, this edge is considered a mathematical artifact due to the dark color of the sample and extremely low reflectance.
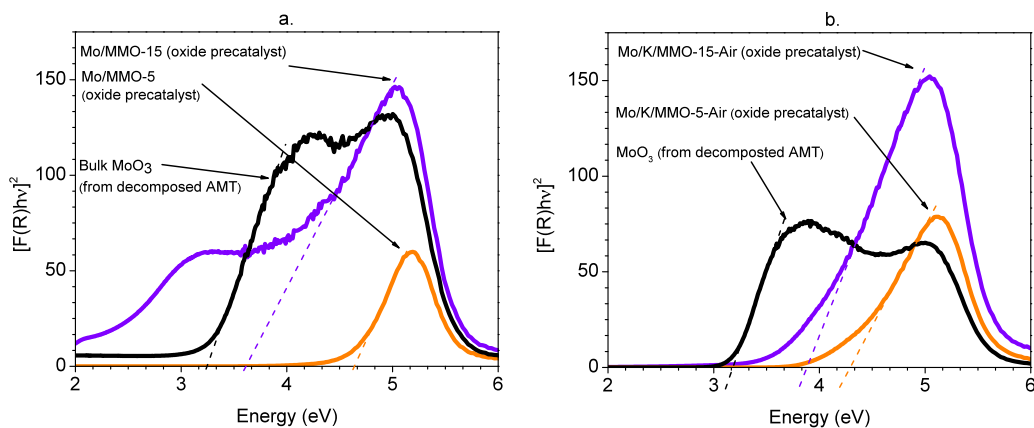
Figure 3.3. UV-vis DRS spectra for bulk MoO_3 (from decomposed AMT), Mo/MMO-15, and Mo/MMO-5. Samples in (a) were pretreated at 450 °C in nitrogen while samples in (b) were pretreated in air at the same temperature.

3-6 STEM

The differences in the supported MoS_2 domains observed with XRD were clarified with STEM. Images of Mo/K/MMO-15,9 and Mo/K/MMO-5,3 are shown in Figure 3.4a-d. Both samples have long, thin MoS_2 domains, but the structures in Mo/K/MMO-15,9 have approximately five stacked Mo-S layers while Mo/K/MMO-5,3 has about two. Additionally, both of these samples have notably different domains from those observed in a bulk MoS_2 standard (shown in Figure 3.4e-f), which is made up of short, wide sheets with six or more Mo-S layers. The different morphologies seen in the MMO supported samples likely occur as a result of the differing initial Mo_yO_x domains, which according to the Raman and UV-vis spectra are (relatively) small on Mo/MMO-5 and larger on Mo/MMO-15.

33
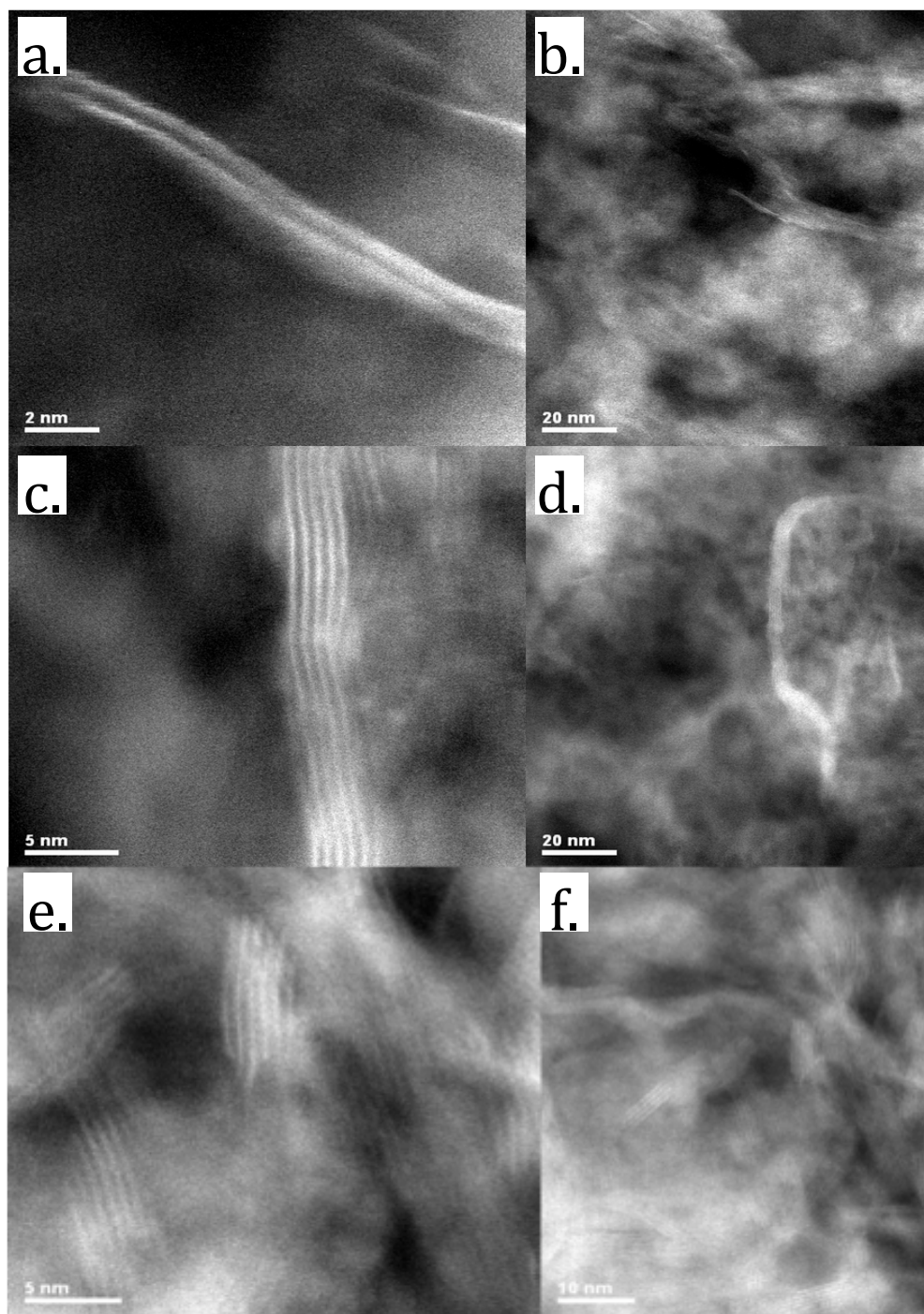
Figure 3.4. STEM images of Mo/K/MMO-5,3 (a) and (b) and Mo/K/MMO-15,9 (c) and (d) after sulfidation and reaction with syngas. Unreacted bulk MoS_2 is shown in (e) and (f) for reference.

3-7 XAS

The electronic and geometric structure of the molybdenum domains in the Mo/K/MMO-15,9 and Mo/K/MMO-5,3 samples are further characterized by the XANES spectra shown in Figure 3.5. XANES has been used to provide insights into oxidation states and coordination environment.[25,142-146] This technique is specifically useful for assessing the state of Mo in the samples, as it may exist in catalysts and precatalysts in the form of MoO_2, MoO_3, and MoS_2, with each type of domain known to facilitate different reactions. [46,147,148] MoO_2 domains may exist as a product of incomplete sulfidation, which sometimes occurs when supports and promoters are added to a catalyst.[67] Previously, we have used XANES spectroscopy to characterize the state of the Mo species in supported catalysts, demonstrating that the XANES edge energy is correlated with the electronic structure of the molybdenum.[20]

In the case of the catalysts investigated in this study, three important observations are made from the XANES data. First, the two catalysts (Mo/K/MMO-5,3 and Mo/K/MMO-15,9) as oxides or sulfides closely resemble their bulk counterparts, which indicates high levels of oxidation or sulfidation respectively, as opposed to significant oxysulfide content. Second, the two catalysts have indistinguishable edge energies when in the oxide form. As sulfides, they are also indistinguishable from one another. This outcome suggests that the average electronic structure of the Mo species is not affected by small differences in Mo domain structure. Finally, both the pre-edge and post-edge features in the XANES spectra of the catalysts, as oxides or as sulfides, are also nearly identical. This outcome is slightly unexpected in the case of the oxide precatalysts given the differences revealed by UV-vis and Raman data. Specifically, one might expect the greater Mo-support interactions on Mo/K/MMO-5,3 than on Mo/K/MMO-15,9 in addition to the fundamentally different oxide domains (MoO_4^{2-} and $Mo_7O_{24}^{6-}$) to affect the K-edge. The most probable explanation for this observation is that the Mo^{VI}-O bonds are

all similar in structure in these materials, regardless of whether the bonding oxygen atom comes from the oxide support or the Mo domain itself.
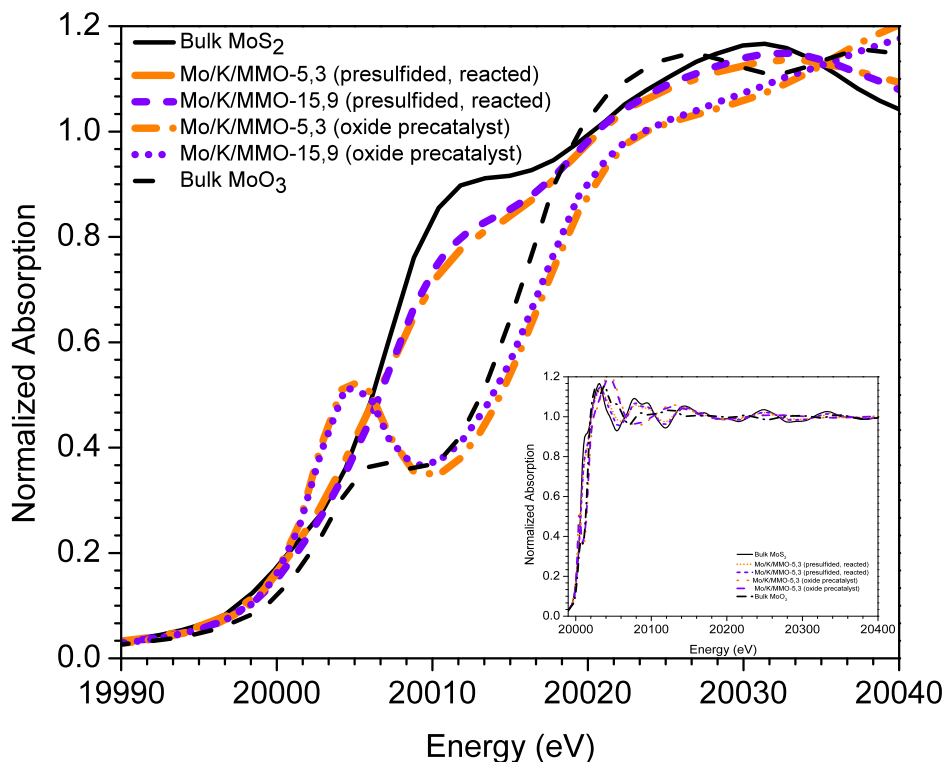
Figure 3.5. XANES Mo K-edge spectra of the 5 % and 15 % Mo supported MMO samples after combination with K_2CO_3, presulfidation, and reaction with CO.

The Fourier transforms (FT) of k^3-weighted extended X-ray absorption fine structure (EXAFS) at the Mo K edge of bulk MoS_2 and the Mo/K/MMO samples after sulfidation and reaction are shown in Figure 3.6 and the structural parameters derived from the corresponding curve fits are presented in Table 3.2. Example curve fits associated with these results are compared to the experimental EXAFS associated with Mo/K/MMO-15,9 (sulfided and reacted) are shown in Figure 3.7. All of the R-factors of the fits are less than 0.04, indicating good agreement between the experimental EXAFS and the corresponding curve fits. The Mo–S and Mo–Mo interatomic distances in the supported MoS_2 samples (Mo/K/MMO-5,3 and Mo/K/MMO-15,9) matched that of bulk

MoS$_2$ standard within experimental error, indicating that the supported Mo oxides were effectively sulfided in the supported samples, which is consistent with the XANES results. However, both of the supported sulfides presented a significantly lower Mo–Mo coordination number (~4) than that in bulk MoS$_2$ (6), and a greater Mo–Mo Debye-Waller factor ($\geq 3 \times 10^{-3}$ Å^2) than the corresponding value in bulk MoS$_2$ (1.9×10^{-3} Å^2), which indicates a high dispersion of Mo in the supported Mo sulfides.

The two dimensional structure of a single MoS$_2$ layer has structural regularity consistent with a Mo–Mo coordination number of six within the layer. A reduced Mo–Mo coordination number of about four in the supported MoS$_2$ (Table 3.2) suggests that a single MoS$_2$ layer is truncated in one dimension and may be as small as two Mo atoms wide. Since the coordination number of Mo–Mo did not change upon increasing the Mo loading from 5 wt. % to 15 wt. % the overall structure of the truncated layers must be quite similar. Because an increase in the number of stacked layers of a supported MoS$_2$ material is not expected to increase the coordination of the first Mo-Mo shell, it is unsurprising that the increase in number of MoS$_2$ "sheets" for Mo/K/MMO-5,3 and Mo/K/MMO-15,9 as was observed in STEM (**Figure 3.4**) had little effect on the Mo-Mo coordination numbers of the corresponding curve fits.
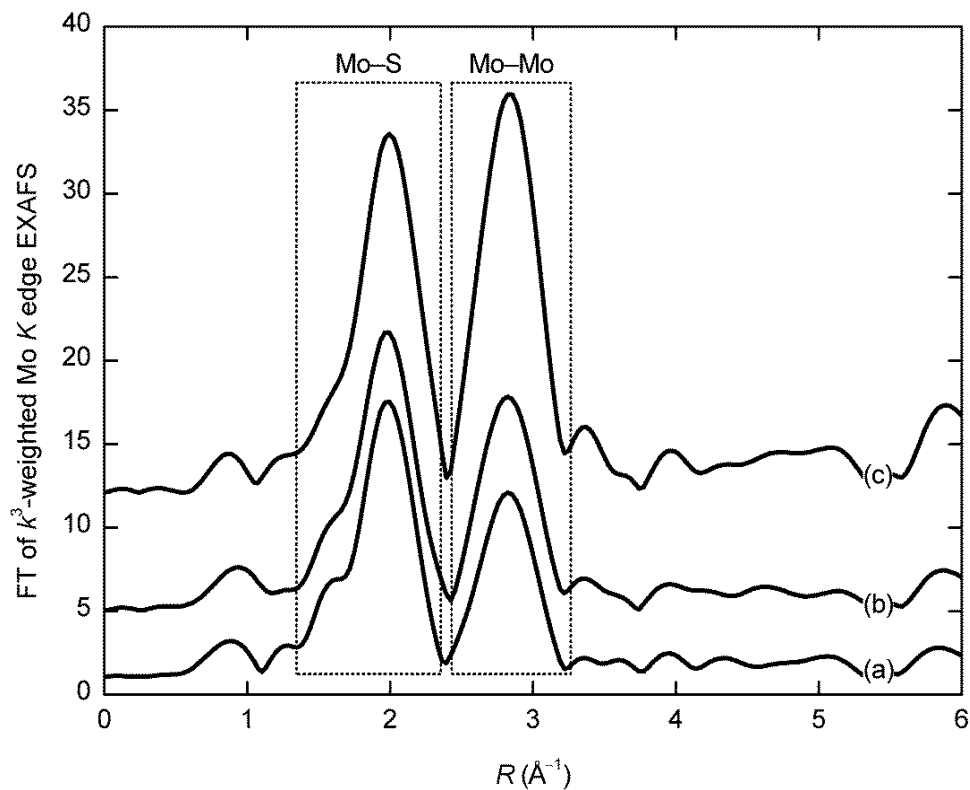
Figure 3.6. Fourier transform (not corrected for phase shifts) of k^3-weighted Mo K edge EXAFS of: (a) Mo/K/MMO-5,3, sulfided and reacted; (b) Mo/K/MMO-15,9, sulfided and reacted; (c) bulk MoS_2 standard. Spectra are offset for clarity. (Figure created by University of Virginia collaborator Dr. Heng Shou.)

Table 3.2. Results from the analysis of Mo K edge EXAFS

Sample	Shell	CN	r (Å)	$\Delta\sigma^2$ (10^{-3} Å^2)	ΔE_0 (eV)	R factor
Bulk MoS$_2$	Mo–S	6[a]	2.40 ± 0.01	2.3 ± 1.1	2.4 ± 1.0	0.028
	Mo–Mo	6[a]	3.14 ± 0.01	1.9 ± 1.2	−5.7 ± 1.6	
Mo/K/MMO-5,3, sulfided	Mo–S	5.2 ± 0.5	2.40 ± 0.01	3.0 ± 1.1	1.8 ± 1.0	0.033
and reacted	Mo–Mo	3.8 ± 1.5	3.13 ± 0.01	3.6 ± 2.0	−8.6 ± 2.3	
Mo/K/MMO-15,9,	Mo–S	4.9 ± 0.4	2.41 ± 0.01	2.6 ± 0.9	4.0 ± 0.9	0.031
sulfided and reacted	Mo–Mo	3.9 ± 1.2	3.13 ± 0.01	3.0 ± 1.4	−6.9 ± 1.9	

Fitting parameters: Fourier transform range, Δk, 2−14.5 Å^{-1}; fitting range, ΔR, 1−3.2 Å; weighting, k^1 & k^3; S_0^2(Mo−S) = 0.84, S_0^2(Mo−Mo) = 0.79

[a] Value was assigned in curving-fitting on the basis of standard structure.

(Table created by University of Virginia collaborator Dr. Heng Shou.)
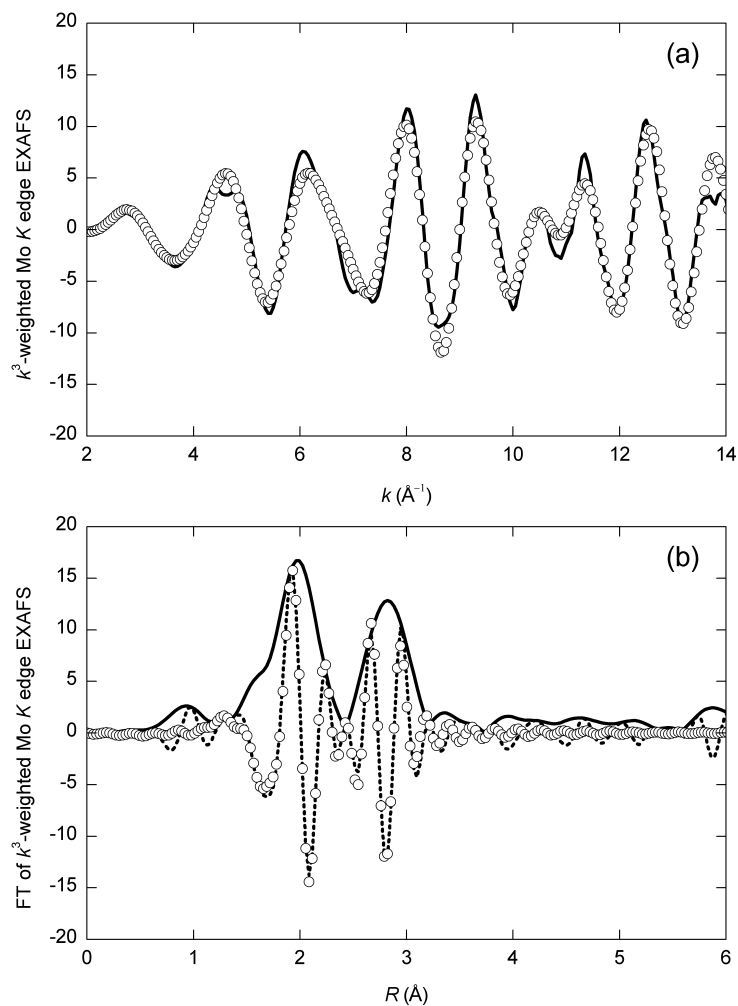
Figure 3.7. Comparison of the curve fit to experimental Mo K edge EXAFS of Mo/K/MMO-15,9 (sulfided and reacted): (a) k^3-Weighted Mo K edge EXAFS (solid line) and the result from curve fit (circles); (b) magnitude (solid line) and the imaginary part (dashed line) of the Fourier transform of EXAFS compared with the result from the curve fit (circles). (Figure created by University of Virginia collaborator Dr. Heng Shou.)

3-8 Reaction Results and Discussion

3-8-1 Effect of Mo and K Loading on Catalysis

Mo/K/MMO-5,3 and Mo/K/MMO-15,9 were synthesized and reacted with syngas (H_2:CO 1:1) at 310 °C and 1500 psig operating at 3-15% CO conversion. Linear alcohol and hydrocarbon selectivities for these catalysts are shown in Figure 3.8 and Table 3.3 (the latter contains data for reactions to be discussed later in the text). These selectivities are presented on a CO_2-free basis for clarity, but it should be noted that MoS_2-based catalysts efficiently catalyze the water-gas shift reaction, [42,149-152] so CO_2 selectivities are high (see Table 3.3). Two replicate batches for these catalysts were also synthesized and reacted to ensure consistency. Average selectivity data with error bars representing one standard deviation are shown in Figure 3.9.

Additionally, a multitude of catalysts were run as controls to verify the qualitative effects of several parameters. Specifically MMO-supported K-promoted Mo-free and MMO-supported K-fee Mo were tested along with aliquots of Mo/K/MMO5,3 that were presulfided at 310 °C or not presulfided at all. The results of these experiments are reported and discussed in Appendix E.

The most relevant of these controls was an aliquot of Mo/K/MMO-5,3 that was loaded with additional K such that the total K loading was the same as for Mo/K/MMO-15,9. Product selectivities for the resultant catalyst, Mo/K/MMO-5,9, are also shown in Figure 3.9 and Table 3.3.

Total selectivity for non-alcohol oxygenates (acetaldehyde, propionaldehyde, methyl formate, methyl acetate, and ethyl acetate) are relatively small for all three catalysts, with selectivities at 1.9 – 2.3 % for Mo/K/MMO-5,3, 1.8 – 3.1 % for Mo/K/MMO-5,9, and 2.8-3.7 % for Mo/K/MMO-15,9, indicating that oxygenate formation for these catalysts are chiefly linear, primary alcohols. With respect to linear hydrocarbons and alcohols, the two Mo/K/MMO-5,x catalysts show strikingly different selectivity trends from Mo/K/MMO-15,9. Specifically, methanol selectivities for

Mo/K/MMO-5,x are substantially less than for Mo/K/MMO-15,9 at all conversions. Ethanol selectivity decreases with increasing conversion for Mo/K/MMO-5,x samples but increases with conversion for Mo/K/MMO-15,9. These outcomes suggest the selectivity differences are not related to K loading alone but are instead related to differences seen in the characterization data (i.e. differently sized MoS_2 domains) and/or high MMO:Mo ratios.

Ethane selectivity over these catalysts also emphasizes an important difference. There was little ethane production over the Mo/K/MMO-x,9 catalysts while it was comparatively high over Mo/K/MMO-5,3. In addition to being a product of Fischer-Tropsch type CO insertions, ethane may also be a product of the dehydration of ethanol followed by hydrogenation of the produced olefin. The dehydration of alcohols is known to occur over acidic sites such as those found on alumina, which is also a component of the MMO support. In a reducing environment dehydration can be followed by hydrogenation and thus methanol is converted to dimethyl ether, ethanol to ethane, and 1-propanol to propane. Because smaller alcohols or their respective intermediates must first be formed for dehydration to take place, the reaction is likely secondary and should take place preferentially at higher conversions.

Indeed, ethane selectivity for Mo/K/MMO-5,3, as shown in Figure 3.8 and Table 3.3 (and propane selectivity, included with "Total HC" in Table 3.3) follow the expectation of increasing ethane selectivity with conversion. The Mo/K/MMO-x,9 catalysts, on the other hand, do not. Instead these catalysts produce almost negligible amounts of C_{2+} hydrocarbons. This result is expected given their high K content which should neutralize acidic sites. Methanol is not likely involved in similar dehydration pathways given the absence of dimethyl either, which was produced in quantities that were too small to be relevant. Ethylene was also notably absent from reaction products for all the catalysts, so assuming it is formed during ethanol dehydration, it must be quickly hydrogenated to ethane.

C$_{3+}$ alcohol selectivity on Mo/K/MMO-5,9 surpasses that of Mo/K/MMO-5,3, which is expected and consistent with several studies that have quantified the effects of increasing K loadings on MoS$_2$ catalysts.[42,51,74,88,153,154] The interpretations of these studies (titration of acid sites and partial suppression of CO dissociation) do not however explain why the C$_{3+}$ alcohol selectivity of Mo/K/MMO-5,3 is greater than that of Mo/K/MMO-15,9. In having a greater K loading and the same Mo:K ratio, the latter catalyst should have a more basic surface and therefore more highly favor alcohol formation. The Mo/K/MMO-5,x catalyst must then have a character not directly related to K loading that also favors linear, primary alcohol formation over the formation of other oxygenates.

C$_{3+}$ alcohol productivity (g OH/g Mo/hr) is reported in Table 3.3 and shows a decrease with increasing CO conversion for the Mo/K/MMO-5,x catalysts but remains relatively constant for Mo/K/MMO-15,9. Additionally, C$_{3+}$ alcohol productivity for the Mo/K/MMO-5,x catalysts is more than twice that over Mo/K/MMO-15,9 at low conversions. These outcomes again suggest a fundamental difference in character between the catalysts that cannot be explained by differences in K loading alone. Rather, this character is likely related to two key differences in catalyst structure: (i) variations in the proportion of surface-exposed MMO, Mo, and K and (ii) differences in MoS$_2$ structure such as the stacking of the MoS$_2$ domains as reflected in XRD and STEM. Based on the data presented above, it is unknown what changes in selectivity either of these cases could bring about. Therefore, additional experiments were undertaken.

Case (i) would result if the MMO support served to promote different reaction pathways than K over a sulfide catalyst. Several papers in the literature show that MMO or MgO, a component in MMO, can couple alcohols in conjunction with other metals[102,103,114,115] effectively making 1-propanol from methanol and ethanol, 1-butanol from 2 ethanol molecules, and 2-methyl-propanol from 1-propanol and methanol. With that functionality, MMO could potentially perform a similar reaction over supported MoS$_2$ catalysts with or without the promotion of K. Alternatively, the interface of the

MoS$_2$ domains with the MMO support could be important in the spillover and coupling of reactive intermediates between the various domains. Simply put, if MMO or MMO/Mo/K surfaces favor coupling of alcohols compared to MoS$_2$/K domains, a high MMO:Mo ratio would result in a bias towards C$_{3+}$ alcohols not observed in the reaction of more conventional bulk MoS$_2$/K, and in parallel, a supported catalyst with high Mo content as well.

Potential effects of case (ii) are more ambiguous. Several theoretical and experimental studies have linked differing edge geometries and coordinatively unsaturated site (CUS) numbers and spacings of the MoS$_2$ to active sites for CO and/or H$_2$ adsorption on MoS$_2$.[95,155-160] Thus, in addition to different CUS structures, it is possible that different size MoS$_2$ domains could yield different active site concentrations that then lead to modified selectivities for higher alcohols. However, the precise effect of these different structures in the context of CO hydrogenation over supported MoS$_2$ is yet unknown. The following section provides an experimental pathway for deconvoluting case (i) and case (ii).
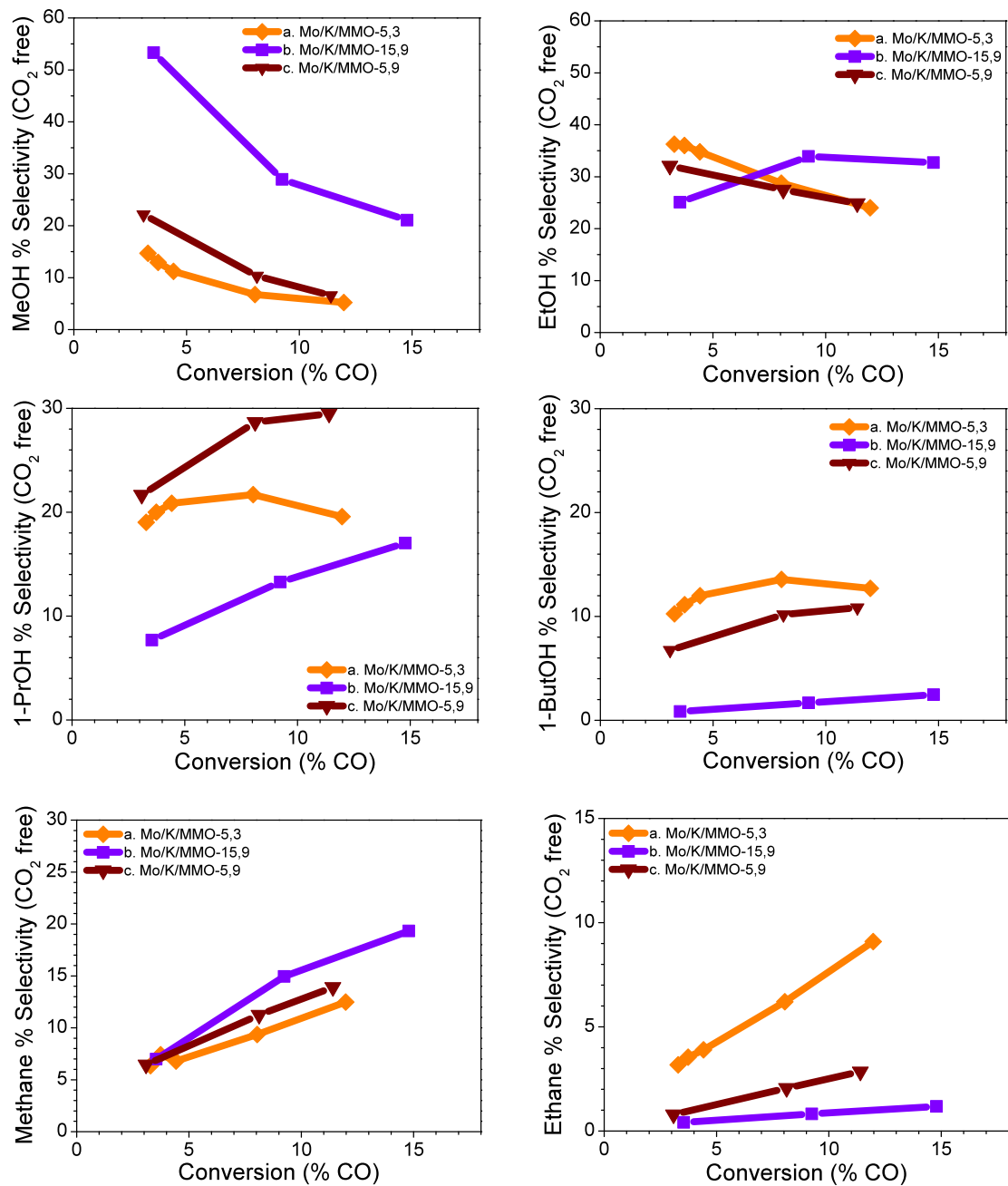
Figure 3.8. Alcohol and hydrocarbon selectivity (CO_2-free) vs. CO conversion for C_1 to C_4 alcohols over MMO supported catalysts, Mo/K/MMO-5,3, Mo/K/MMO-15,9, and Mo/K/MMO-5,9.

Table 3.3. Reactivity results for samples used in study.

ID	WHSV (ml/g/hr)	Conv. (% CO)	CO₂ Sel. (% CO)	MeOH	EtOH	1-PrOH	1-ButOH	i-ButOH	CH₄	C₂H₆	Total OH	Total HC	C₅₊ OH Prod (g$_{OH}$/g$_{Mo}$/hr)
Mo/K/MMO-5,3	4610	3.3	29.3	14.7	36.3	19.0	10.2	1.9	6.4	3.2	82.7	15.0	0.25
Mo/K/MMO-5,3	1366	8.0	39.4	6.7	28.7	21.7	13.6	2.3	9.4	6.2	73.7	24.2	0.18
Mo/K/MMO-5,3	796	12.0	43.8	5.2	24.0	19.6	12.7	2.4	12.5	9.1	64.4	33.7	0.13
Mo/K/MMO-5,9	5113	3.1	32.6	22.1	32.1	21.7	6.8	3.8	6.4	0.8	86.7	10.5	0.25
Mo/K/MMO-5,9	1278	8.1	39.6	10.3	27.5	28.7	10.2	4.9	11.2	2.1	81.8	16.4	0.20
Mo/K/MMO-5,9	721	11.4	42.4	6.6	24.9	29.5	10.8	5.4	13.9	2.9	77.5	20.6	0.16
Mo/K/MMO-15,9	16465	3.5	21.1	53.3	25.1	7.7	0.8	1.2	7.0	0.4	88.2	9.1	0.10
Mo/K/MMO-15,9	4180	9.2	32.3	28.9	33.9	13.3	1.7	1.5	14.9	0.8	79.5	16.8	0.10
Mo/K/MMO-15,9	2259	14.8	35.4	21.1	32.7	17.0	2.5	1.7	19.3	1.2	75.2	21.6	0.11
Mo/K/MMO-15,9-MMOs	5127	2.7	25.0	46.5	27.3	8.2	1.3	1.8	8.5	0.6	85.3	11.3	0.09
Mo/K/MMO-15,9-MMOs	1357	7.7	37.0	21.3	36.2	15.3	2.8	1.9	16.3	1.3	77.8	19.1	0.10
Mo/K/MMO-15,9-MMOs	745	11.8	40.5	14.2	32.9	17.8	3.6	2.1	22.6	2.0	71.1	26.7	0.09
Mo/K/MMO-15,9-MMOg	3237	2.9	26.6	18.5	32.9	21.4	10.6	4.0	2.7	2.1	87.9	9.7	0.17
Mo/K/MMO-15,9-MMOg	1293	5.6	33.9	12.2	30.6	21.3	12.1	4.7	6.6	3.6	81.3	16.0	0.13
Mo/K/MMO-15,9-MMOg	754	8.0	39.3	7.5	28.3	22.0	13.5	4.8	7.4	5.2	76.6	20.4	0.10
Mo/K-bulk-MMOg	3123	2.7	26.8	25.6	30.4	17.9	9.6	4.6	4.1	1.1	88.6	8.6	0.18
Mo/K-bulk-MMOg	1280	5.5	34.2	15.3	32.3	19.5	10.1	5.2	7.3	2.2	82.9	14.1	0.14
Mo/K-bulk-MMOg	732	8.0	38.0	10.7	30.1	21.2	12.0	5.6	7.6	2.8	80.2	16.8	0.13

46
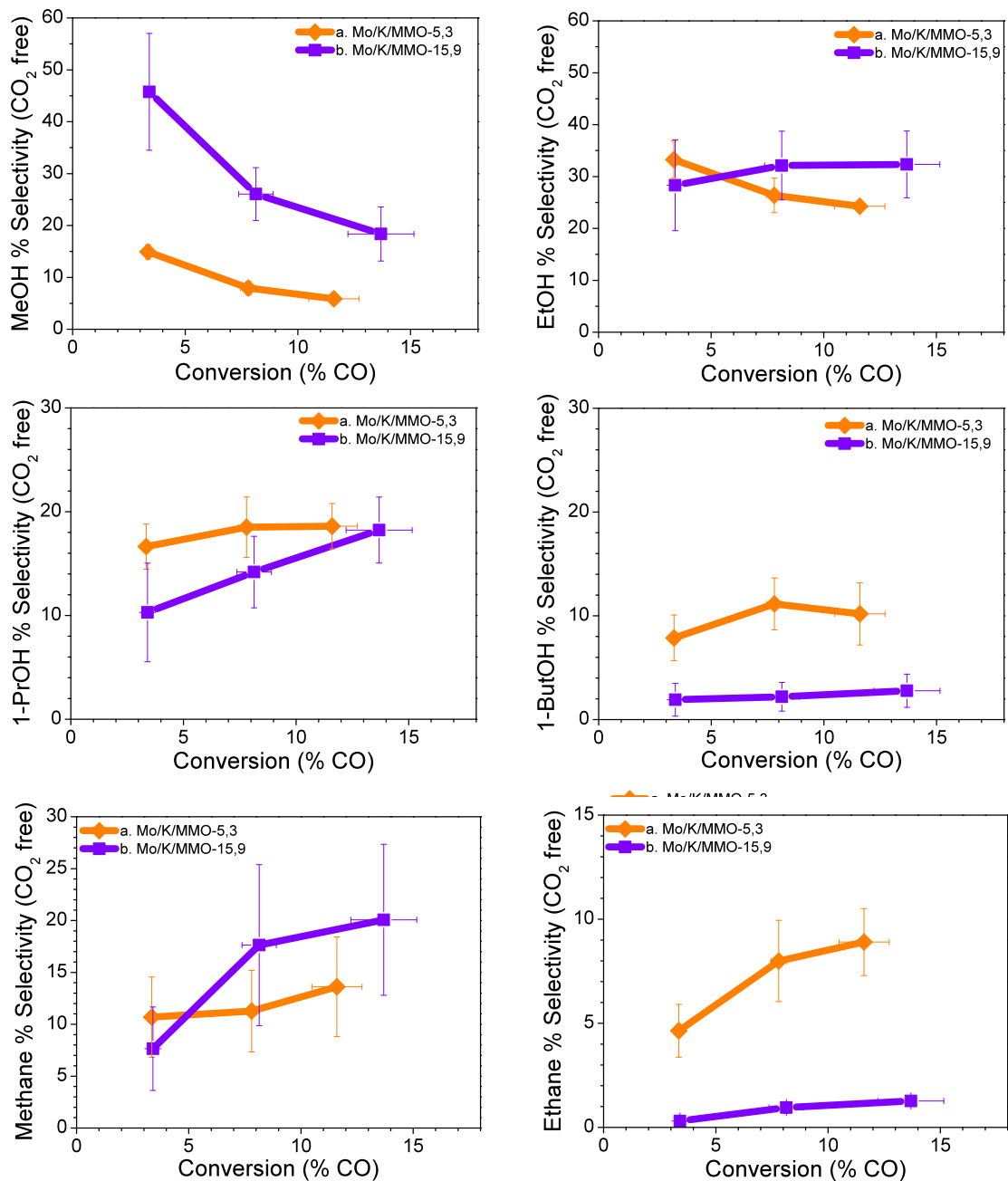
Figure 3.9. Average alcohol and hydrocarbon selectivity (CO_2-free) vs. CO conversion over three replicate batches for methane and ethane over the two MMO supported catalysts, Mo/K/MMO-5,3 and Mo/K/MMO-15,9 with error bars representing 1 standard deviation.

3-8-2 Role of MMO in Catalysis

To gain insight into case (i) (variations in the proportion of surface-exposed MMO, Mo, and K), namely the functionality of MMO, bare MMO was combined with Mo in three different fashions for follow-up experiments. In the first experiment, sieved Mo/K/MMO-15,9 particles were placed upstream of a separate bed of identically sized bare MMO particles such that the total Mo, K, and MMO amounts were the same as in Mo/K/MMO-5,3 reaction (but with differing size and distribution of Mo and K domains). This reaction is referred to as Mo/K/MMO-15,9-MMOs. Figure 3.10 shows a schematic description of the catalyst bed for this experiment in addition to several others that will be discussed next.

For the second experiment, a mortar and pestle was used to grind the oxide precatalyst Mo/K/MMO-15,9 with bare MMO such that the total elemental composition of the resultant catalyst also matched that of Mo/K/MMO-5,3. This catalyst is referred to as Mo/K/MMO-15,9-MMOg (Figure 3.10e). The XRD patterns and BET surface area data of the oxide precatalyst and sulfided, reacted materials for these two cases are shown in Figure 3.11 and **Table 3.3** respectively. Notably, the XRD pattern for the Mo/K/MMO-15,9-MMOg precatalyst contained diffraction lines characteristic of molybdenum (VI) oxide and potassium molybdate at 27 ° and 32 ° respectively, which were similar in magnitude to those of Mo/K/MMO-15,9.

However, once sulfided and reacted, Mo/K/MMO-15,9-MMOg then showed XRD lines more similar to those of Mo/K/MMO-5,3 – a short broad peak (MoS_2) at 33 ° and two peaks (MgO) of much greater magnitude at 44 ° and 64 °. This result suggests that initial oxide domain size does not in fact greatly affect sulfide domain size once the catalyst is sulfided. In other words, under sulfidation conditions, the Mo species can migrate around the support to a significant extent, to the point where the Mo/K/MMO-15,9-MMOg catalyst appears to have sulfide domains that are similar to the Mo/K/MMO-5,3 catalyst by XRD despite very different preparation conditions. An extremely small

peak at 14 ° correlating with the MoS_2 [002] plane can also be observed, indicating slightly more order in the stacking structure than in Mo/K/MMO-5,3. The overall Mo to MMO ratio in the precatalyst seems to play a dominant role in establishing the size of the MoS_2 domains.

Bulk MoS_2 (synthesized as described in Chapter 2) was ground with bare MMO and K_2CO_3 to make the catalyst for the third and final experiment exploring the role of MMO, denoted as Mo/K-bulk-MMOg (Figure 3.10f). Despite the different Mo precursor, this catalyst had the same composition as the previous two – 85 % MMO, 5 % Mo, and 3 % K. The XRD pattern for this catalyst shown in Figure 3.11 is similar to that of the sulfide form of Mo/K/MMO-15,9-MMOg, differing primarily in the magnitude of the peak at 14 °, indicating a level of Mo-S stacking more closely resembling that of the original bulk (unsupported) catalyst.
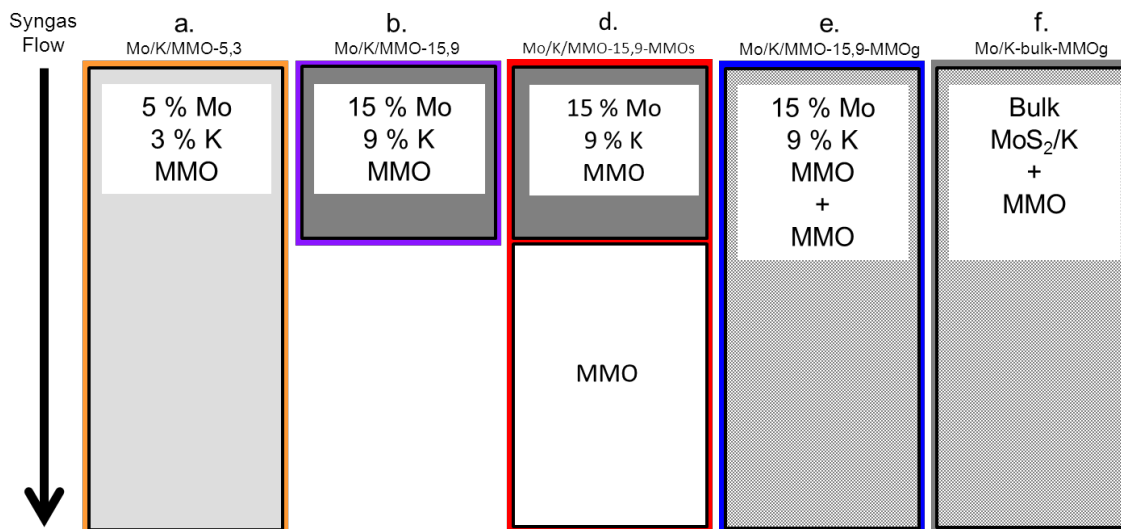
Figure 3.10. Catalyst bed schematics showing the various combinations of Mo, K, and MMO used in reaction. Cases a. and b. represent the base cases for the study. Case c. (not shown) represents the same catalyst as case a. but with a higher K content. Case d. is the combination of catalyst b. and bare MMO in series such that the final overall bed composition is the same as case a. Case e. represents the same materials as case d. but ground into a homogeneous phase. Case f. was prepared similarly to e. but bulk MoS_2 was used as the Mo source instead of Mo/K/MMO-15,9. Cases a., d., e., and f. represent catalyst beds with the same total amounts of MoS_2, K_2CO_3, and MMO in the bed.
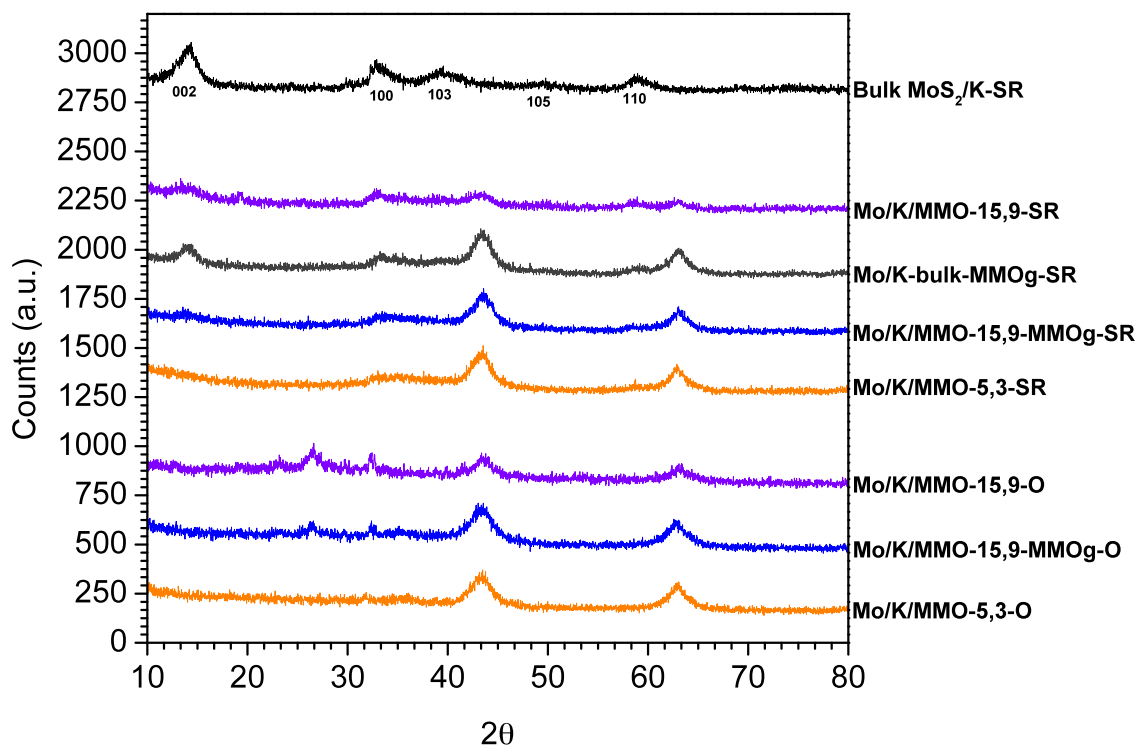
Figure 3.11. XRD patterns of Mo/K/MMO catalysts and precatalyst along with bulk MoS$_2$ references. Mo/K/MMO-15,9-MMOg-O has similar oxide domains to Mo/K/MMO-15,9-O while Mo/K/MMO-15,9-MMOg-SR has similar sulfide domains to Mo/K/MMO-5,3-SR. The notation "-SR" denotes a catalyst that has been sulfided and used in reaction. The notation "-O" denotes a catalyst that in its oxide precatalyst form.

Table 3.4.BET surface area and elemental analysis results for samples used in study.

Sample	BET Surface Area (m²/g)	Mo	K	S	Mg	Al
Bare MMO	209	0.0	0.0	0.0	30.2	13.8
Mo/K/MMO-5,3 – oxide precatalyst	151	5.0	2.4	0.1	26.9	12.3
Mo/K/MMO-5,3 – sulfided, reacted	69	5.1	2.7	4.2	26.7	12.2
Mo/K/MMO-5,9 – oxide precatalyst	N/A	4.5	7.9	0.1	23.4	11.0
Mo/K/MMO-5,9 – sulfided, reacted	N/A	4.3	7.5	3.4	23.0	10.5
Mo/K/MMO-15,9 – oxide precatalyst	26	16.4	7.2	0.5	17.6	8.4
Mo/K/MMO-15,9 – sulfided, reacted	24	14.7	5.8	11.0	16.4	7.8
Mo/K/MMO-15,9-MMOg–oxide precatalyst	83	5.2	2.8	0.2	23.2	10.5
Mo/K/MMO-15,9-MMOg – sulfided, reacted	84	6.4	2.7	3.9	N/A	N/A
Mo/K-bulk-MMOg – sulfide, reacted	113	4.0	2.0	3.3	N/A	N/A

Reactivity results for Mo/K/MMO-15,9-MMOs, Mo/K/MMO-15,9-MMOg, and Mo/K-bulk-MMOg are combined with those from Mo/K/MMO-5,3 and Mo/K/MMO-15,9 and shown in Figure 3.14 along with Table 3.3. The trends of increasing methane and lowered methanol with increasing conversion is observed for all five cases, which further strengthens the conclusions that methanol is a primary product of the reaction and is consumed via secondary reactions.[91]

The selectivity trends for the catalysts Mo/K/MMO-5,3, Mo/K/MMO-15,9-MMOg, and Mo/K-bulk-MMOg are shown to be virtually identical, despite the fact that the catalysts were generated via different synthesis routes (Mo/K/MMO-5,3 from a homogeneous mix of MMO, Mo, and K_2CO_3 with small MoO_x domains (Figure 9a); Mo/K/MMO-15,9-MMOg from the grinding of Mo/K/MMO-15,9, which has large MoO_x domains, and bare MMO (Figure 9e); and bulk MoS_2, K_2CO_3, and bare MMO (Figure 9f)). Specifically, the unusual trends associated with Mo/K/MMO-5,3 of lowered ethanol selectivity with increasing conversion and relatively high ethane selectivity were observed for Mo/K/MMO-15,9-MMOg and Mo/K-bulk-MMOg, but not for Mo/K/MMO-15,9-MMOs.

The fact that the low methanol selectivity observed over Mo/K/MMO-5,3[91] was not replicated by the Mo/K/MMO-15,9-MMOs experiment (with a downstream bare MMO bed) shows that the low methanol and high $C_{3+}OH$ selectivity are not simply due to

secondary reactions independently facilitated by bare MMO. If the low methanol and elevated higher alcohol selectivities over Mo/K/MMO-5,3 were associated with secondary reactions, they were likely not associated with conversion of stable products such as methanol into higher alcohols via alcohol coupling pathways (e.g. methanol + ethanol to give 1-propanol) over the bare, K-free support. These selectivity phenomena are likely instead related to reactions that occur only at an MMO-Mo-K interface or on MMO/K domains; both possibilities could result in adsorbed intermediates reacting to give the observed product distributions.

Thus, all the catalysts with an overall composition similar to Mo/K/MMO-5,3 gave similar catalytic selectivities regardless of how they were prepared. Interestingly, however, the catalysts displayed different higher alcohol productivities. Specifically, of the three catalysts, Mo/K/MMO-5,3 showed the highest C_{3+} OH productivity (0.18 g OH/g Mo/hr) at 8% CO conversion, whereas the two catalysts prepared via grinding (Mo/K-bulk-MMOg and Mo/K/MMO-15,9-MMOg) showed lower productivities (0.13 g OH/g Mo/hr and 0.12 g OH/g Mo/hr respectively). The higher alcohol productivities (Table 3.3) appear qualitatively to correlate inversely with the extent of [002] peak at 14 ° two theta in the XRD patterns (i. e. a smaller peak correlates to greater higher alcohol productivity). While the peaks are too small to be used in a line broadening analysis,[52] at similar Mo loadings a larger peak implies a higher level of orientation or MoS_2 slab stacking, as is observed in the STEM images in Figure 3.4 where the bulk MoS_2 has the largest amount of stacking and Mo/K/MMO-5,3 the least.

The effect of MMO on the reaction can perhaps most directly be observed by comparing C_4 alcohol selectivity for Mo/K/MMO-15,9 and Mo/K/MMO-15,9-MMOg. The addition of bare MMO to the former catalyst by dry impregnation resulted in over a 5-fold increase in 1-butanol selectivity and 3-fold increase in 2-methyl-1-propanol selectivity at 8% CO conversion. While 1-butanol is a product of homologation or coupling, 2-methyl-1-propanol is primarily hypothesized to be a product only of alcohol

coupling. As such, relatively high 2-methyl-1-propanol selectivities provide a strong indicator of alcohol coupling pathways operating over some catalysts.

It should be noted that the ethylene selectivity was low for all the reactions in this work (< 1%). This outcome is especially significant for the Mo/K/MMO-15,9-MMOs experiment, which was designed to probe the role of the MMO support in catalyzing secondary reactions. If the MMO support dehydrated ethanol to produce ethylene over the Mo/K/MMO-5,3 catalyst, before olefin hydrogenation to yield ethane (as observed over this catalyst), it would be expected that the Mo/K/MMO-15,9-MMOs experiment would produce greater amounts of ethylene in the absence of a hydrogenating function in the second catalyst bed. The absence of ethylene in the Mo/K/MMO-15,9-MMOs product stream indicates that, similar to the discussion of the alcohol coupling pathways, bare MMO does not serve to dehydrate ethanol, producing ethylene and then ethane. Rather, dehydration, which is hypothesized to be the principal ethane formation pathway, must occur over acidic MoS_2 or MMO-Mo interface sites.
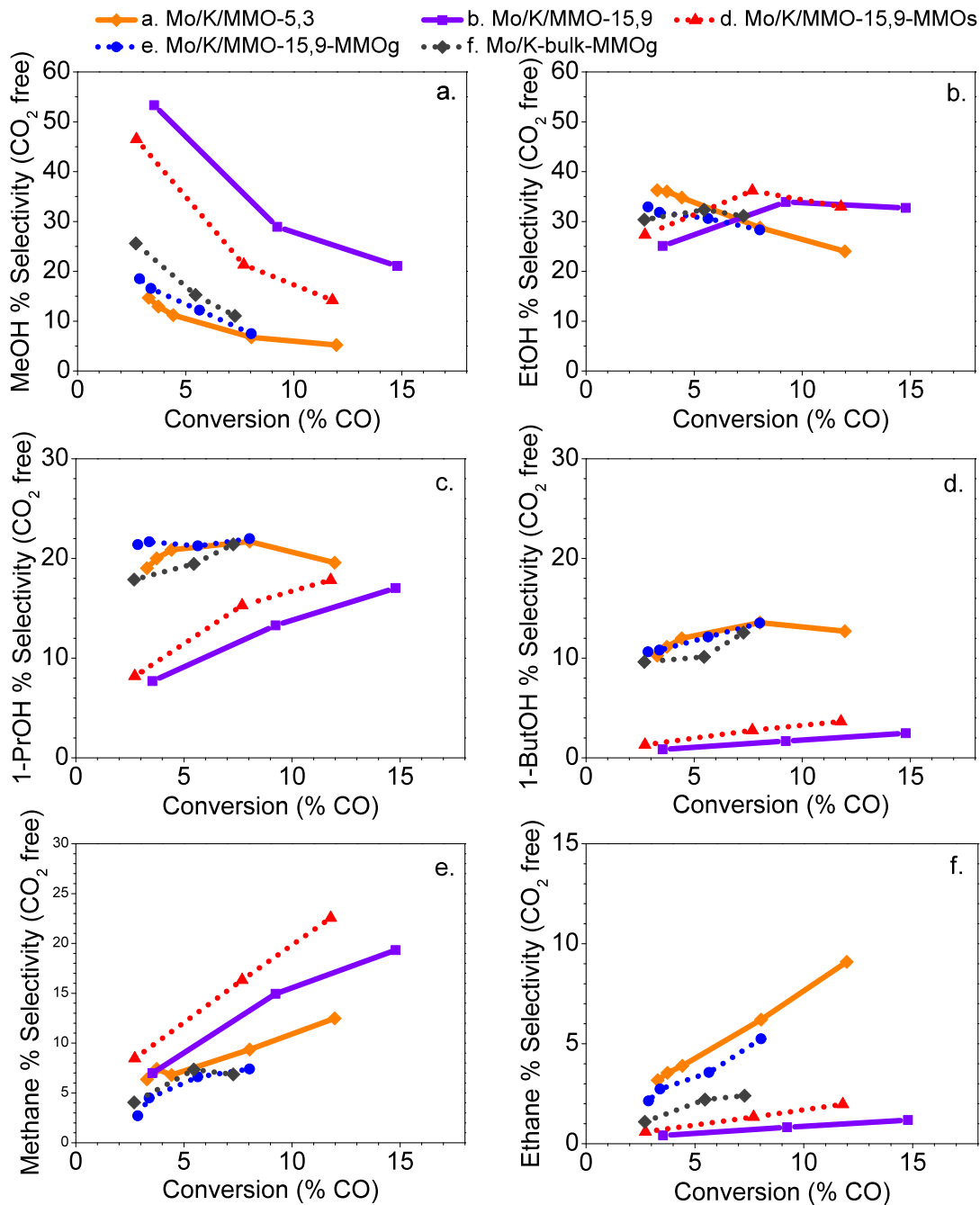
Figure 3.12. Alcohol and hydrocarbon selectivity (CO_2-free) vs. CO conversion for C_1 to C_4 alcohols over MMO supported catalysts, Mo/K/MMO-5,3, Mo/K/MMO-15,9, Mo/K/MMO-15,9-MMOs, Mo/K/MMO-15,9-MMOg, and Mo/K-bulk-MMOg.

3-8-3　Role of MMO-K in Catalysis

To investigate the possibility that stable alcohols, once formed over MoS_2/K, are desorbed, readsorbed, and coupled to produce higher alcohols by MMO-K type sites rather than bare MMO sites, three further reactions were run. For the first two experiments, bare MMO was mixed with K_2CO_3 with the same loading as Mo/K/MMO-5,3 (3 wt. % K) and formed into 20–40 mesh particles. These particles were placed in a bed downstream of a Mo/K/MMO-15,9 bed Figure 3.13f. or loosely combined with Mo/K/MMO-15,9 particles to make a single mixed bed Figure 3.13g.).

Reactivity results for the Mo/K/MMO-15,9-MMO/Ks and Mo/K/MMO-15,9-MMO/Km experiments are shown in Figure 3.14 and Table 3.3. The $C_{3+}OH$ selectivity for these two experiments was somewhat higher than for the Mo/K/MMO-15,9 and Mo/K/MMO-15,9-MMOs catalysts, which supports the possibility that MMO/K may serve to couple alcohols after their initial formation. Ethane and ethanol selectivities however did not mirror the trends observed for Mo/K/MMO-5,3. This outcome lends further support to the hypothesis that the dehydration/hydrogenation of ethanol occurs on acidic sites associated with small MoS_2 domains or $MMO\text{-}MoS_2$ interfaces, rather than via desorption of a stable alcohol followed by readsorption and dehydration on bare acidic MMO domains.
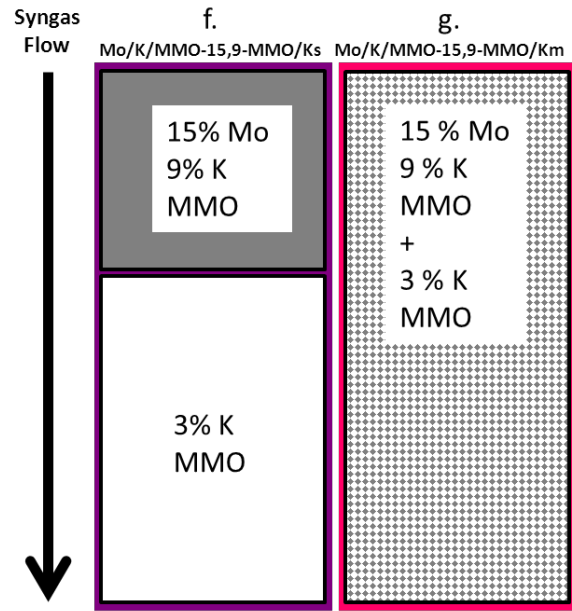
Figure 3.13. Catalyst bed schematics for reactions with added MMO/K showing MMO/K combined with Mo/K/MMO-15,9 in series – Mo/K/MMO-15,9-MMO/Ks (f), or mixed as particles – Mo/K/MMO-15,9-MMO/Km (g).
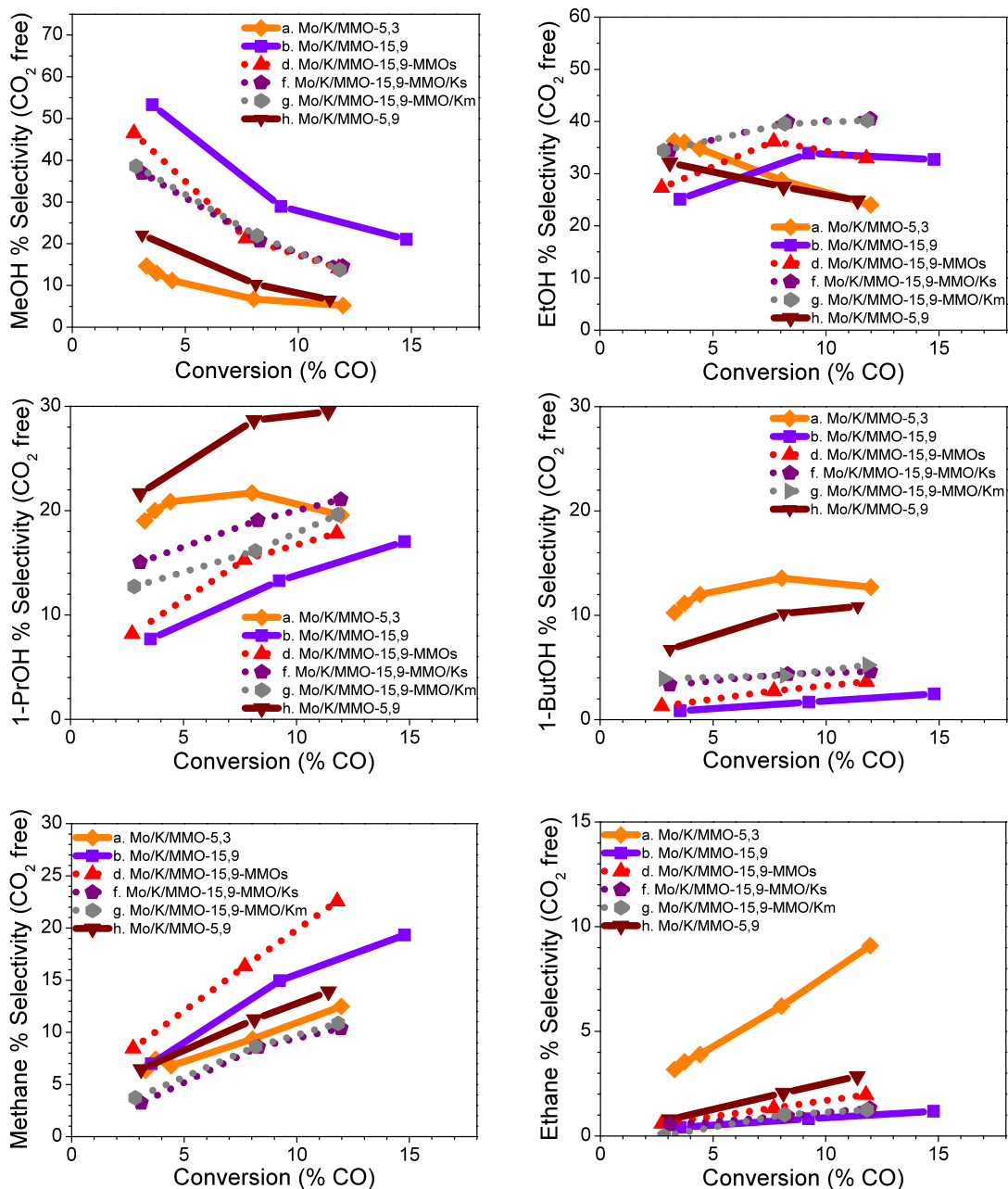
Figure 3.14. Alcohol and hydrocarbon selectivity (CO_2-free) vs. CO conversion for C_1 to C_4 alcohols over MMO supported catalysts combined with MMO/K – Mo/K/MMO-15,9-MMO/Ks and Mo/K/MMO-15,9-MMO/Ks. Mo/K/MMO-5,3, Mo/K/MMO-5,9, Mo/K/MMO-15,9, and Mo/K/MMO-15,9-MMOs shown for reference.

58

3-9 Summary

Two MMO-supported MoS_2 catalysts (Mo/K/MMO-5,3 and Mo/K/MMO-15,9) were used in CO hydrogenation to produce higher alcohols. The catalysts with low Mo loadings had MoS_2 domains containing the fewest layers and produced significantly higher amounts of C_{3+} alcohols and less methanol than the catalyst with the higher Mo loading. The catalyst with the lowest K loading (Mo/K/MMO-5,3) retained some residual acidity associated with the Mo/K/MMO domains that lead to significant ethane selectivity via ethanol dehydration and hydrogenation, whereas all other catalysts produced only small amounts of higher hydrocarbons, including ethane. Additional experiments using the Mo/K/MMO-15,9 catalyst followed by a second catalyst bed comprised of MMO demonstrated that the perturbed alcohol selectivities over the low Mo loading catalysts were associated primarily with reaction over the Mo domains over those catalysts, rather than via secondary reactions of readsorbed alcohols on MMO. Similar experiments involving the addition of MMO/K rather than bare MMO showed some indication of additional higher alcohol formation, but those additions were relatively minor in comparison to differences seen between the original "5,3" and "15,9" catalysts.

Finally, a series of catalysts prepared with a common composition (akin to and Mo/K/MMO-5,3) but with different forms of Mo in the precatalyst (MoO_3, MoO_4^{2-}, $Mo_7O_{24}^{6-}$, MoS_2) all yielded similar catalytic selectivities, suggesting that the ratio of MMO to Mo determined the catalytic selectivity in the final sulfide catalysts. Catalytic productivity, on the other hand, appeared to be correlated with the degree of stacking of the MoS_2 domains, as evidenced by the intensity of the [002] reflection in XRD measurements and the observed degree of layer stacking from STEM images. Higher alcohol synthesis over these catalysts is associated with both CO homologation and oxygenate coupling reactions occurring with adsorbed intermediates on or near K/MoS_2 domains. Higher alcohol distributions suggest that some oxygenate coupling pathways may contribute to the observed products, especially at higher K loadings.

CHAPTER 4: ALCOHOL CO-FEEDS AND COUPLING

It has been shown that MMO when combined with MoS_2/K yields selectivities favoring C_{3+} alcohols. The pathways involved in this outcome however are not yet well understood. In this chapter, homologation and coupling pathways are probed by co-feeding ethanol or methanol with syngas into a packed bed reactor containing a supported, bulk, or Mo-free catalyst. An investigation of changes in product distribution provides insights into this issue.

4-1 Experimental setup

The reactor used in Chapters 2 and 3 was modified by inserting a "tee" at the reactor inlet. A simplified schematic of the modifications is shown in Figure 4.1. In brief, an Isco 500G syringe pump with manual control was connected to the reactor inlet with a 1/16" 316 stainless steel line and a 1/8" needle valve. A soft seat check valve was placed just downstream of the pump to prevent contamination and damage from back flow. The line upstream of the valve was insulated and heated to 200 °C,

During reaction the alcohol feed was adjusted between 0.000 and 0.003 ml/min. When mixed with syngas flowing at 20 ml/min the molar concentration were 0-8 % methanol and 0-6 % ethanol.
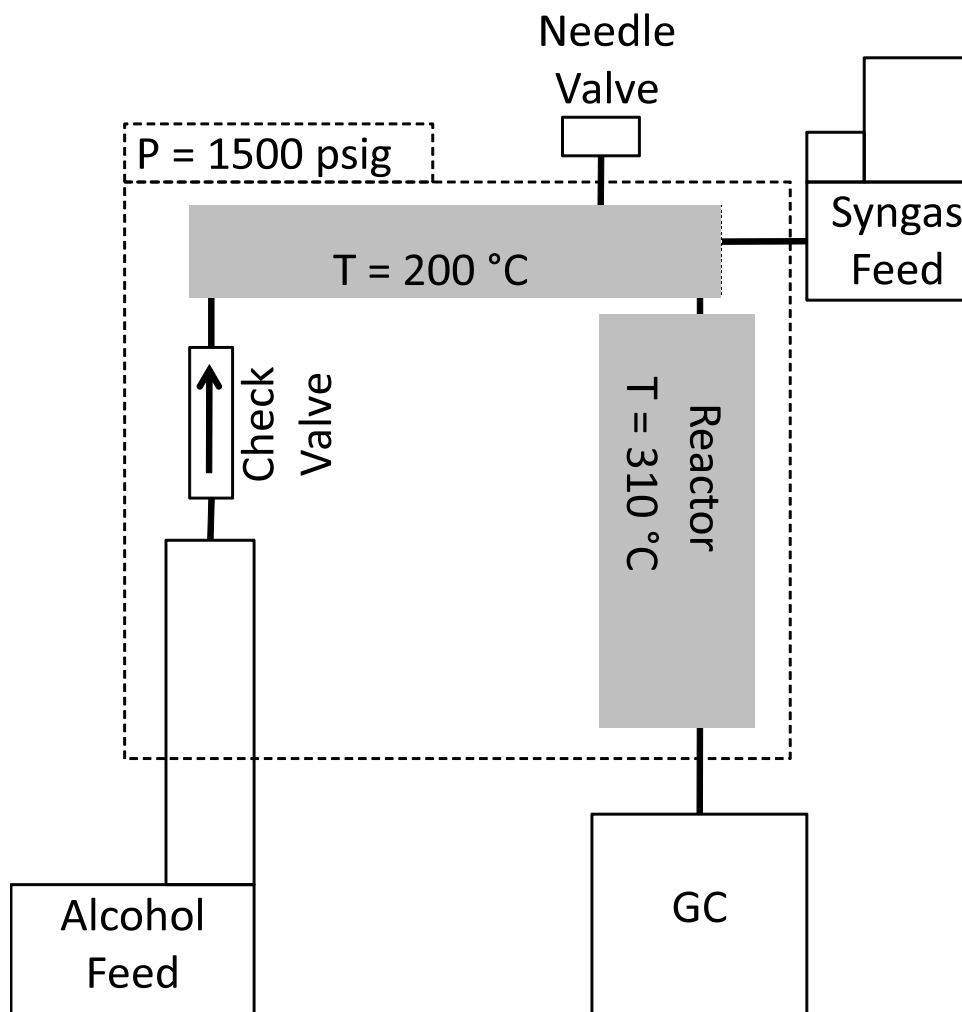
Figure 4.1. Simplified schematic of reactor retrofitted with an Isco syringe pump. The back pressure regulator between the GC and the reactor was removed from the schematic for simplicity.

GC was again used for product quantification. The plumbing configuration was left unchanged, but acetone, methyl propionate, ethyl propionate, and propionaldehyde were added to the list of components quantified by the chromatogram produced in the FID.

For reaction with syngas and Mo/K/MMO-5,3, the reactor was charged with 1 g of catalyst under the same operating and pretreatment conditions described in previous

chapters (reaction parameters summarized on Table 2.1). Once the reaction reached a pseudo steady-state after several days, the flow rate was adjusted such that CO conversion reached 8 %. Ethanol (Aldrich, anhydrous 99.5 %) was then fed into the reactor at a rate of 0.001 ml/min. Once the reaction again reached a pseudo steady-state (changes in selectivity and conversion < 3 % over a period of 12 hours), alcohol flow was changed to 0.003 ml/min. After the reaction reached pseudo steady-state a third time, the alcohol flow was shut off and the reaction was allowed to continue until product selectivity return to its "original" state at 0.00 ml/min ethanol flow. The pump was then flushed and refilled with methanol (Aldrich, anhydrous 99.8 %), and the process of injecting at 0.001 ml/min and 0.003 ml/min was repeated.

To highlight the effects of MMO on the reaction, bulk MoS_2/K synthesized as described in Chapter 2 was also reacted in a similar fashion as Mo/K/MMO-5,3. The reaction differed only in the amount of catalyst used in the reactor (0.11 g). This amount was chosen because it yielded a conversion similar to Mo/K/MMO-5,3 (8 %) when reacted with 20 ml/min syngas.

Finally MMO ground together with K_2CO_3 (3 % K, MMO/K-3) using a mortar and pestle was reacted to test for reactivity of the support and promoter alone with methanol. The reactor was charged with 0.9 g of the catalyst, which was an equivalent amount of MMO and K_2CO_3 used in the Mo/K/MMO-5,3 reaction. The catalyst was exposed to the same pretreatment and reaction conditions as the other two catalysts used in this study. The parameters are summarized in Table 2.1.

4-2 Results and Discussion

4-2-1 Carbon Balances

Carbon distributions for the major groups of components for the methanol and ethanol co-feed experiments are shown in Figure 4.2 and Figure 4.3 respectively and tabulated in Table 4.1. The vertical axis in the figures is written in terms of moles carbon

per g of Mo in the reactor per hour. These units were chosen because they allow for the most direct means to compare various reaction components as they are consumed or produced by the catalysts used in this study.

The "reacted CO" category shown in the first column of the figures was computed by calculating CO conversion from the internal standard and then normalizing it with syngas flow and the Mo in the reactor. Effectively the inlet carbon is divided into four groups – CO that reacts, CO that does not react, methanol, and ethanol. While these values cannot be directly measured during the course of a reaction, they are estimated by extrapolating approximate feed rates from previously obtained calibration curves and instrument setpoints. It must be noted, however, that this estimation is somewhat imprecise given that both the MFC controlling the syngas flow and the syringe pump controlling the alcohol feed rate are operated at below 10 % of their maximum set points. Outlet carbon was quantified purely from GC data.

Because these reactions are run at fairly low conversions (~8%), unreacted CO was omitted from the balance to better emphasize the effect of the alcohol feeds on reaction products. Additionally, adding the unreacted CO to the balance would greatly attenuate discrepancies between the alcohol-based carbon fed into the reactor and carbon-based products which exit the reactor outlet. The carbon from the alcohols fed into the reaction inlet is summed with the reacted CO in the fourth category ("Inlet ROH + Reacting CO) in Figure 4.2 and Figure 4.3. The sum of all carbon exiting the reactor not including the unreacted CO is reported in the fifth category in Figure 4.2 and Figure 4.3 ("Outlet C w/o CO). If the carbon entering and exiting the reactor was balanced perfectly the magnitude of the columns in the fourth and fifth categories of the figures would match.

The last column provides the balance in terms of a percentage. Most balances have less than 10 % error. The balance on Mo/K/MMO-5,3 with the ethanol feed is consistently below 90 %, which may be a result of C_{5+} alcohol production, which is not

among the products quantified by the GC. One noteworthy difference between the Mo/K/MMO-5,3 and Mo/K-bulk catalysts is the substantial increase in CO_2 and hydrocarbon production on the supported material. This increase appears correlated to an increase in CO conversion, which will be discussed later in the text. Numerical values for the balances (i.e. the columns labeled "Inlet + Reacting CO" and "Outlet C w/o CO") are reported in Table 4.1.
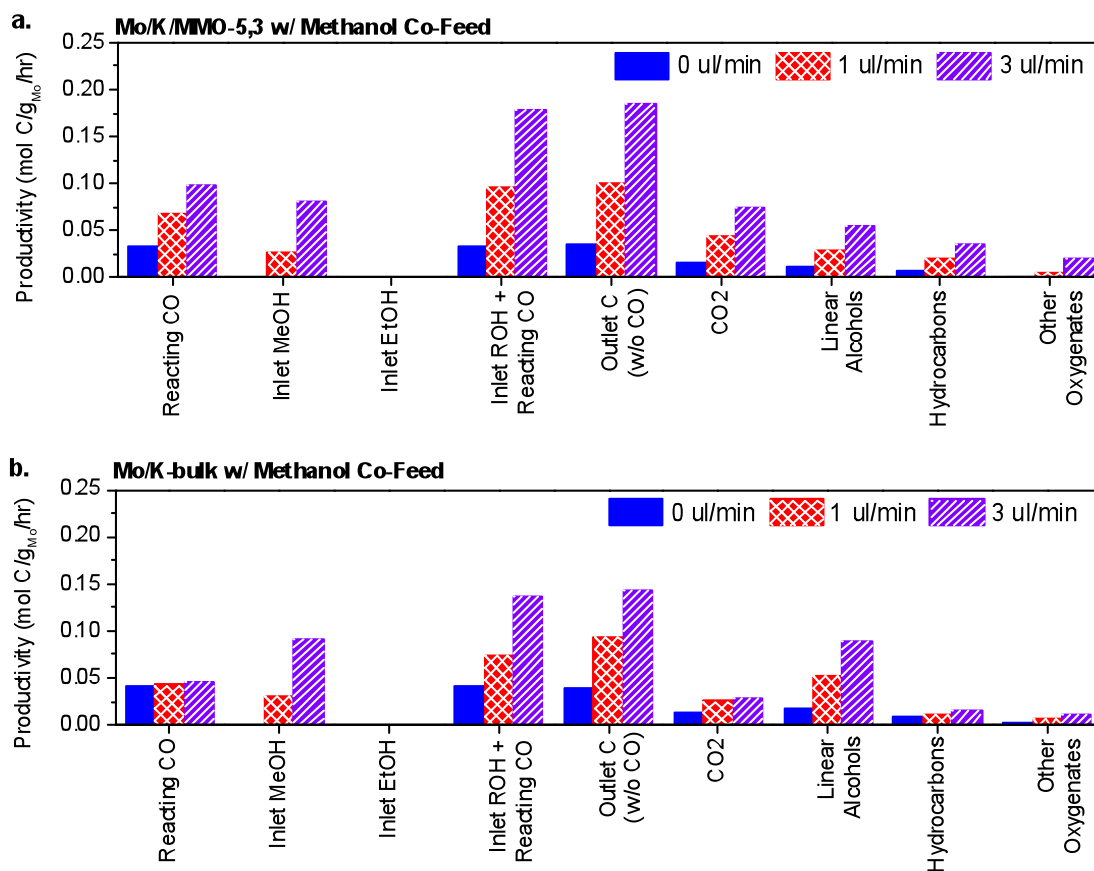
Figure 4.2. Carbon balance and lumped product distributions for methanol feed experiments over Mo/K/MMO-5,3 (a) and Mo/K-bulk (b).
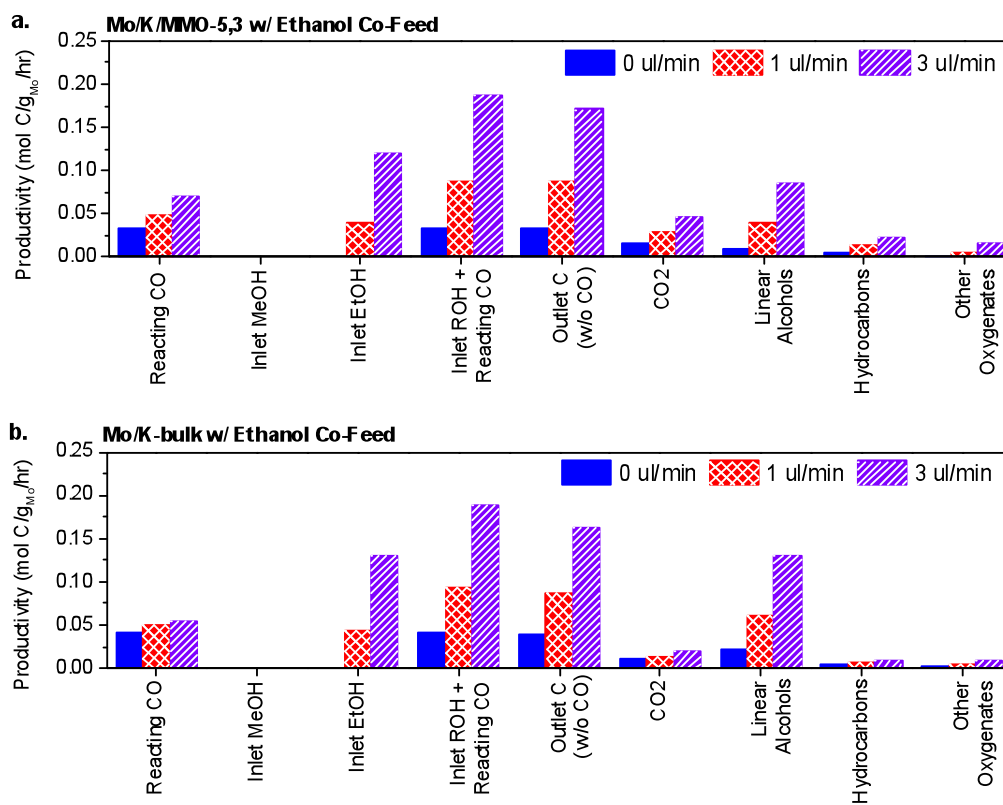
Figure 4.3. Carbon balance and lumped product distributions for ethanol feed experiments over Mo/K/MMO-5,3 (a) and Mo/K-bulk (b).

Table 4.1. Carbon balances for methanol and ethanol co-feed experiments

Catalyst	MeOH Feed (µL/min)	EtOH Feed (µL/min)	Productivity (mol$_C$/g$_{Mo}$/hr)		% Balance (Outlet/Inlet)
			Inlet C (w/o unreacted CO)	Outlet C (w/o CO)	
Mo/K/MMO-5,3	0	0	0.03	0.04	110.1
Mo/K/MMO-5,3	1	0	0.10	0.10	105.1
Mo/K/MMO-5,3	3	0	0.18	0.19	104.0
Mo/K/MMO-5,3	0	0	0.03	0.03	102.2
Mo/K/MMO-5,3	0	1	0.09	0.09	99.0
Mo/K/MMO-5,3	0	3	0.19	0.17	91.1
Mo/K-bulk	1	0	0.04	0.04	98.1
Mo/K-bulk	3	0	0.07	0.09	128.4
Mo/K-bulk	0	0	0.14	0.14	104.0
Mo/K-bulk	0	0	0.04	0.04	99.0
Mo/K-bulk	0	1	0.09	0.09	91.3
Mo/K-bulk	0	3	0.19	0.16	86.4
MMO/K-3	0	0	0.00	0.00	103.9
MMO/K-3	2	0	0.07	0.07	100.6
MMO/K-3	3	0	0.09	0.10	115.9

4-2-2 MeOH Feed

The results of the methanol feed for the major products are shown in Figure 4.4. They are reported in moles of carbon per g Mo per hour from a specific species denoted in the horizontal axis. The first column shows CO conversion as computed with the internal standard (note that the magnitude of the bars in the figures have been scaled such that they can be plotted on the same axis as the rest of the data). The supported catalyst shows a much more significant increase of CO conversion with increasing alcohol co-feed than the bulk catalyst. It appears that a significant amount of methanol also reacts, as the methanol concentration at the outlet is far lower than the inlet. In contrast, the bulk catalyst shows only minor increases in CO conversion (that are within the bounds of experimental error in the internal standard) while the outlet methanol concentration represents a substantial proportion of the inlet methanol.

C_{2+} alcohols also increase significantly with the methanol feed over the MMO supported catalyst. Because the alcohols are produced in decreasing amounts as the carbon chain increases, homologation pathways are almost certainly the dominant routes to higher alcohols rather than coupling pathways. A Fischer-Tropsch-like CO insertion, which is technically a homologation pathway, could be the primary pathway in this case but an olefin co-feed is required to verify this hypothesis. Methane is also observed to substantially increase, implying that the inlet methanol is reduced by hydrogen and that the corresponding water formed is converted to CO_2 via the WGS reaction.

Higher hydrocarbons are also seen to increase with the methanol feed concentration but in a lower proportion to their alcohol counterparts. Most likely these reactions are formed by the same secondary dehydration/hydrogenation reactions discussed in Chapter 3. Ethylene, an intermediate in this reaction, is observed in small quantities compared to other products. The low concentration suggests that the species, if it is truly an intermediate formed in significant quantities, is quickly consumed by hydrogenation reactions. Propylene likely follows a similar trend, but it cannot be distinguished from propane in the chromatogram. As such, its relative increase cannot be ascertained.

The bulk MoS_2 catalyst does not show such dramatic results under alcohol co-feeding conditions. While the methanol feed does result in increased higher alcohols at the reactor outlet, their concentrations are all a fraction of that observed on the supported catalyst. Methane productivity does not increase as dramatically on the bulk catalyst, which is consistent with the hypothesis that the bulk material is less reactive with methanol than the supported counterpart.
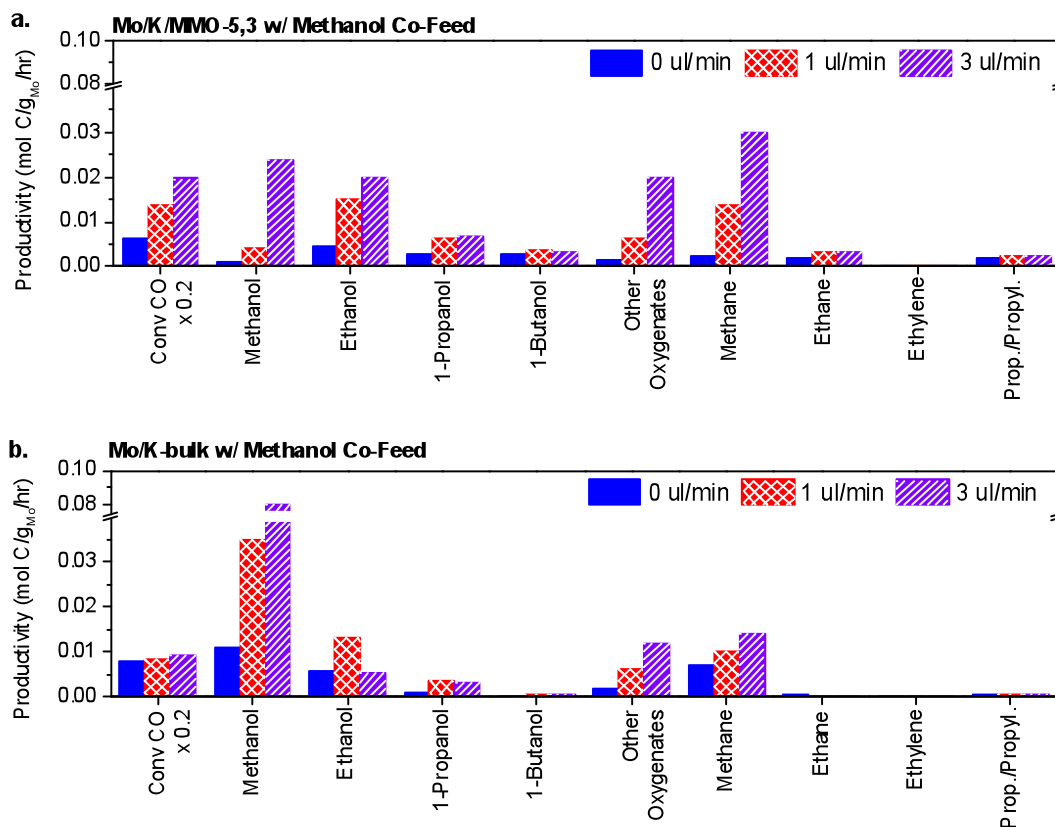
Figure 4.4. Major product distributions of the methanol feed over Mo/K/MMO-5,3 (a) and Mo/K-bulk (b).

The distribution of other oxygenates is reported in Figure 4.5. With the exception of methyl acetate, their magnitude is considerably less than observed for the linear alcohol and hydrocarbon products. Several observations may nevertheless be made. First, both catalysts formed significant amounts of methyl acetate and small but significant amounts of methyl propionate when the methanol concentration was high. This outcome suggests that methanol itself is a building block for the two species. While esters cannot be formed by the coupling of two alcohols, they are formed via Fischer esterification,[161] which uses an acid catalyst to combine a carboxylic acid and an alcohol to make an ester. The required carboxylic acids for this reaction could be formed via the carbonylation of an alcohol or olefin to make the corresponding C_{+1} alcohol[162-164] or via direct synthesis

from CO and H2.[165] The presence of esters also opens an alternate pathway to higher alcohols – reduction/hydrogenation of the ester to form two smaller alcohols.[166,167]

While these proposed pathways are reasonable, they are nevertheless hypothetical and must be considered with several caveats in mind. First, alcohol carbonylation reactions between an alcohol and CO are known to occur over Rh catalysts.[165,168] This reaction however has not yet been verified using Mo or metal oxide catalysts. Second, the presence of acids cannot be directly quantified or verified using the columns employed in this study as they form extremely broad peaks in the chromatograms that cannot be deconvoluted from other oxygenate species produced in the reaction. Consequently, further work is essential if carboxylic acids to esters or esters to alcohol routes are to be confirmed.

The increase in ethyl acetate observed for Mo/K/MMO-5,3 is likely a result of the increase in ethanol that then forms the acetate via a similar pathway as methyl acetate. Finally, 2-methyl-1-propanol increases significantly more on the bulk than the supported catalyst at a high methanol concentration. As 2-methyl-1-propanol is believed to be primarily a product of a Guerbet coupling, [109,114,115] this observation provides evidence that the bulk catalyst can facilitate this reaction in the presence of adequately high methanol concentrations, which is consistent with the findings of Christensen et al.[60] Additionally, it appears that MMO indeed does not significantly aid in the facilitation of coupling reactions when supporting MoS_2 as was previously hypothesized.
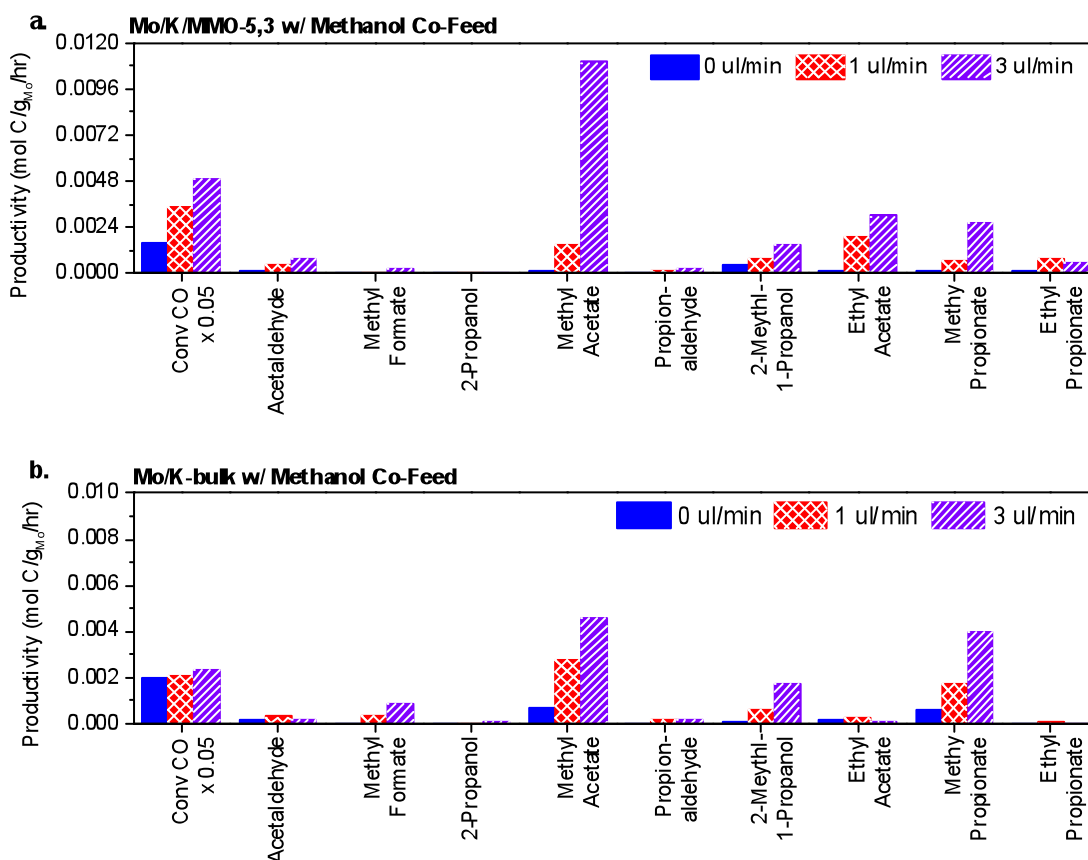
Figure 4.5. Minor product distributions of oxygenates other than linear alcohols for the methanol feed over Mo/K/MMO-5,3 (a) and Mo/K-bulk (b).

MMO/K-3 was also used as a catalyst in a methanol co-feed experiment as a control. The primary objective of its use was to discern if the high reactivity of methanol on Mo/K/MMO-5,3 was a result of MMO/K facilitating reactions independently of Mo or if that reactivity required all three species. The results are summarized in Figure 4.6 below.

The carbon balance for this catalyst, shown in Figure 4.6a, demonstrates that CO conversion is largely unaffected by the introduction of methanol. In Chapter 3 it was shown that bare MMO and MMO/K have fairly small effects on reactivity when provided as a separate catalyst bed. Here a similar observation is made. The increase in CO_2

productivity with the alcohol feed is likely a result of the small increases in CO conversion.

The product distributions of major species are shown in Figure 4.6b. However, all products quantified are produced in negligible amounts. Consequently, there is little evidence for significant alcohol homologation or coupling over this catalyst. Small amounts of the methanol appear to be hydrogenated to methane or partially hydrogenated to form oxygenates.
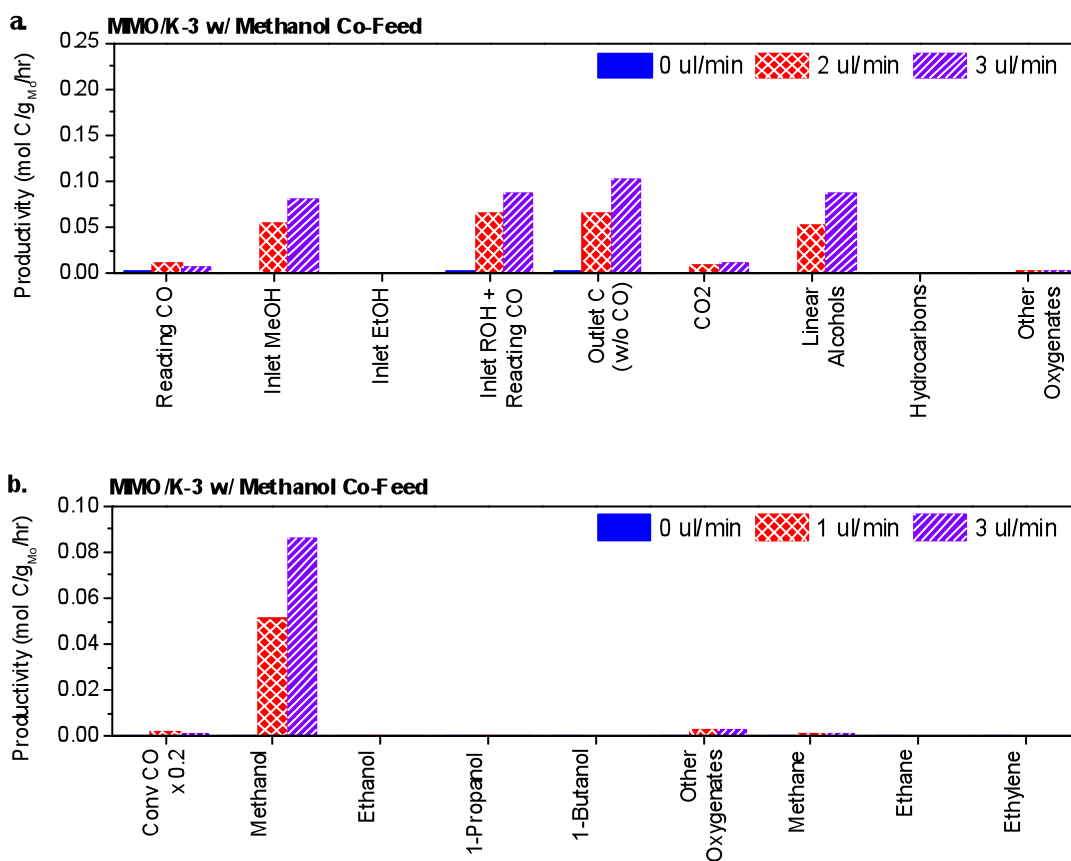
Figure 4.6. Carbon balance (a) and major product distributions (b) for syngas and methanol fed over MMO/K-3.

4-2-3 Ethanol Feed

The results of the ethanol co-feed over the two catalysts are not as dramatic as was observed for the methanol feed. However, several of the main trends are consistent between the two alcohol co-feed cases. Namely, more significant increases in higher alcohol production were observed for the MMO supported catalyst and for the bulk Mo/K catalyst. Similar to the methanol co-feed case, 1-propanol increases most dramatically, followed by 1-butanol on the MMO supported catalyst, which again suggests that CO homologation pathways primarily account for higher alcohol formation. Additionally, ethylene production increases over Mo/K/MMO-5,3, albeit at a fraction of the magnitude observed for methane when methanol was fed into the reactor.

Though not as dramatically as was observed for the methanol feed experiments, both catalysts showed increases in CO conversion with increasing ethanol feed. Again, higher alcohol production increased the most dramatically over Mo/K/MMO-5,3. Unsurprisingly, methanol production appears unaffected by the ethanol feed for both catalysts.
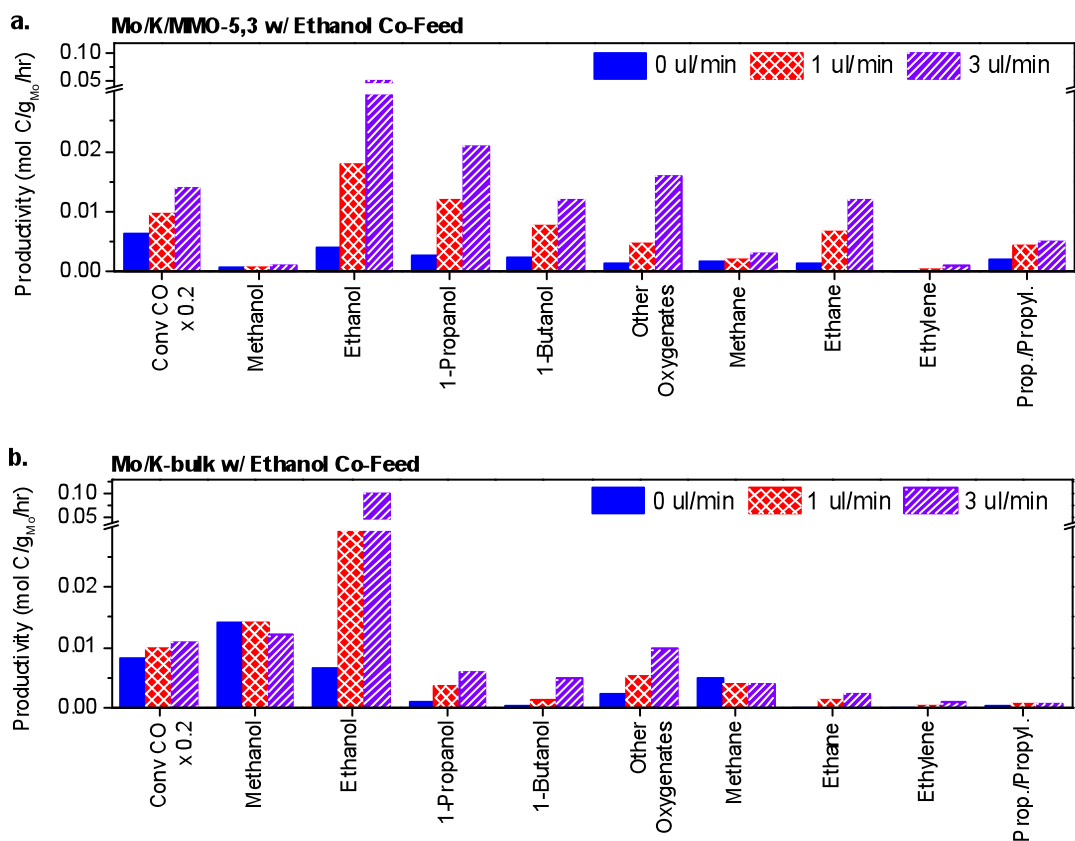
Figure 4.7. Reactivity results for major products of the ethanol feed over Mo/K/MMO-5,3 (a) and Mo/K-bulk (b).

Productivities for other oxygenates are shown in Figure 4.8. Most of the products that are quantified are relatively unaffected by the ethanol feed on both catalysts. However ethyl acetate and ethyl propionate changed most significantly. These increases are likely analogous to those observed in the methanol feed portion of the experiments, whereby methanol is proposed to be converted to acetic acid and then used in esterification reactions with methanol or ethanol to form methyl acetate or ethyl acetate respectively. Additionally, ethanol is likely converted to propanoic acid and used in an esterification with methanol and ethanol to make methyl propionate and ethyl propionate respectively – that later of which is produced insubstantial quantities on Mo/K/MMO-5,3.

The lack of methyl acetate production on Mo/K/MMO-5,3 with an ethanol co-feed provides strong support to the hypothesis that the product is made from methanol that has been converted to acetic acid. Because the catalyst produces so little methanol or because methanol exists in such low concentrations on the catalyst surface, minimal acetic acid must be made and the principle pathway to methyl acetate is effectively shut down. However the increase in ethyl acetate contradicts this hypothesis. Following the same formation pathway as methyl acetate, ethyl acetate also requires acetic acid. The increase in acetaldehyde production with ethanol feed concentration suggests the possibility that ethanol is converted first to an aldehyde and then to acetic acid. Alternatively, the substantial increases in ethane production suggest the formation of ethylene in equal quantities as an intermediate. A small portion of that ethylene could instead be oxidized and converted to acetic acid. As a future experiment, an olefin co-feed would be helpful in confirming this pathway.

Unlike the methanol feed case, 2-methyl-1-propanol does not increase significantly with increasing ethanol feed on the bulk catalyst. This outcome is consistent with the hypothesis that this species is formed by the Guerbet reaction, which requires methanol and 1-propanol. Instead 1-butanol, the product of the Guerbet coupling of two ethanol molecules, is observed to increase with the ethanol feed. Notably, 1-butanol was almost completely absent from the methanol feed experiment on the bulk catalyst. However, 1-butanol production is still much lower over the bulk than over the supported catalyst, which again suggests that though both catalysts primarily employ homologation pathways to form higher alcohols, the MMO supported catalyst does so much more effectively.
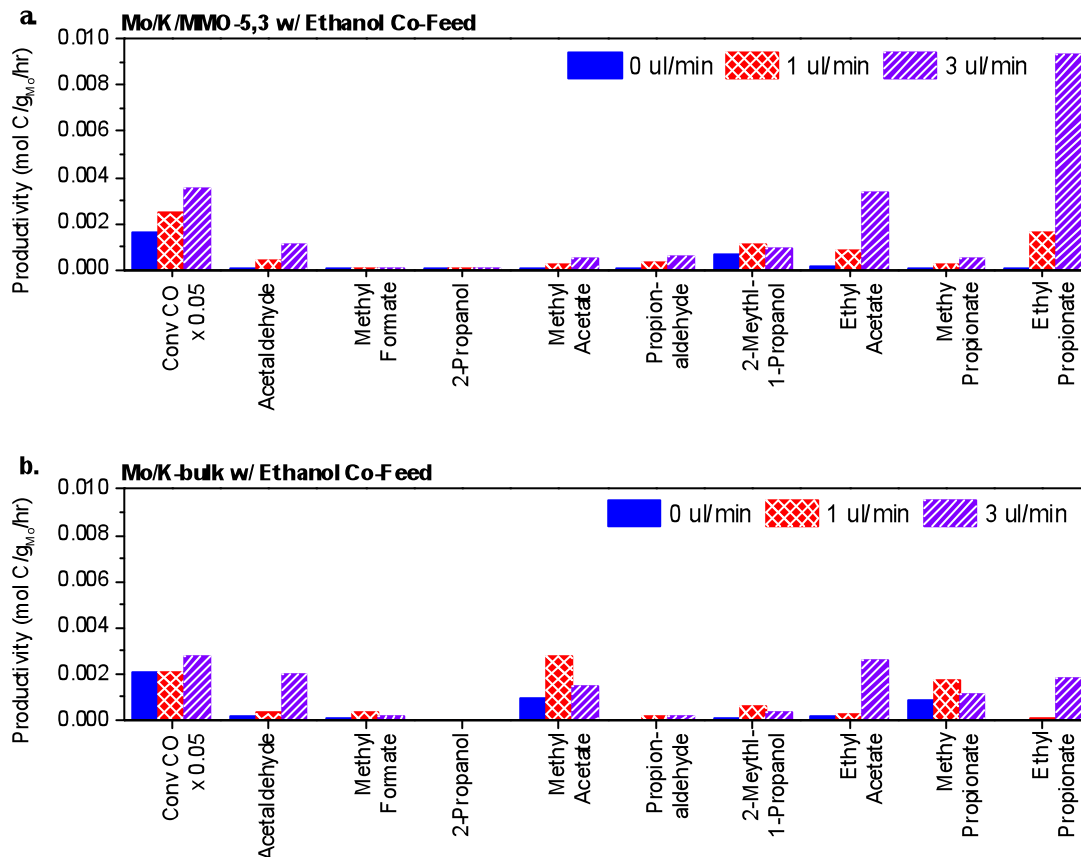
**Figure 4.8**. Product distributions of oxygenates other than linear alcohols for the ethanol feed over Mo/K/MMO-5,3 and Mo/K-bulk

4-3 Conclusions

The co-feeding of methanol and ethanol over Mo/K/MMO-5,3 and Mo/K-bulk highlights several important differences between the two catalysts. First, the supported catalyst is substantially more reactive with methanol than the bulk counterpart. While this increased reactivity yields greater amounts of higher alcohols, it also yields substantial increases in CO_2 and hydrocarbon production. The precise nature of the active sites that account for this reactivity is not yet known though the experiment with MMO/K-3 indicated that the support by itself could not facilitate these reactions and that Mo/K/MMO domains are in fact required for the enhanced reactivity.

The second major finding of this study is associated with the reaction pathways leading to higher alcohol formation. It was previously believed that alcohol coupling reactions could be occurring on the MMO supported catalyst and that a methanol feed would yield significant amounts of 2-methyl-1-propanol while an ethanol feed would yield similar amounts of 1-butanol. However while the reactivity data for the methanol feed did show an increase in 2-methyl-1-propanol, that increase paled in comparison to the increases in linear alcohol and ester production.

In terms of linear, primary alcohols, the methanol feed yielded the greatest increases in ethanol production followed by 1-propanol and 1-butanol. Similarly an ethanol feed yielded greatest increases in 1-propanol followed by 1-butanol. As such, it is concluded that alcohol homologation pathways are the most favored or most important pathways for higher alcohol formation over the MMO supported catalyst. These pathways also exist on the bulk catalyst, but appear to be much less significant, as this catalyst produces more methanol and fewer higher alcohols in general.

Finally reactivity data for the alcohol co-feeds showed that high concentrations of alcohols altered the "minor" product distributions (i.e. oxygenates that were not linear alcohols). Specifically high ethanol feeds yielded dramatic increases in ethyl acetate and ethyl propionate while high methanol feeds yielded high increases in methyl acetate and methyl propionate. These results were most dramatic for the Mo/K/MMO-5,3 catalyst, but they were also apparent on the bulk catalyst. Ultimately, this outcome suggests that MoS_2/K possess the capacity to employ carbonylation reactions to convert alcohols to carboxylic acids, to esterify those acids with other alcohols, and potentially reduce the resultant ester back to alcohols – one of which has one carbon more in its chain than the original reactant alcohol. Confirmation of these pathways nevertheless requires further investigation which will be discussed in the following chapter.

CHAPTER 5: CONCLUSIONS AND OUTLOOK

The work contained in this thesis focuses on various aspects of MMO as a support for K promoted MoS_2. These aspects include structural properties of the catalyst as well as reactivity both with syngas and with alcohols in a heated, pressurized environment. The key findings in this work are:

1. MMO is a unique support for potassium promoted MoS_2. The support possesses a major advantage over a conventional carbon support and bulk MoS_2 in that it yields a catalyst with low methanol selectivity but high higher alcohol selectivities. The support also possesses several disadvantages. Namely it yields higher C_{2+} hydrocarbon selectivities and lower activity than more traditional carbon supported K/MoS_2 catalysts.

2. Bare MMO does not facilitate reactions independently of Mo. By itself, MMO is several orders of magnitude less active for higher alcohol synthesis than a 5 % Mo, 3 % K on MMO counterpart even when heated and pressurized to typical reaction conditions.

3. MMO when combined with K is slightly reactive with syngas and alcohols, though without Mo, that reactivity is fairly inconsequential.

4. MMO when combined in large proportion with K promoted MoS_2 yields novel selectivities that cannot be mirrored by changing K loading alone. This result was unexpected, as alcohol selectivity is generally believed to be a result of catalyst basicity (in the context of MoS_2 catalysts).

5. The ratio of MMO:Mo has substantially greater effects on selectivity than the catalyst preparation method, Mo precursor structure, and MoS_2 domain structure. The latter characteristics may, however, affect catalytic activity.

6. CO homologation pathways are more active than coupling pathways on MMO supported MoS_2.

7. Co-feed experiments involving bulk or MMO supported MoS_2/K produced significant amounts of esters such as methyl acetate, ethyl acetate, methyl propionate, and ethyl propionate. The most likely pathway to these products is the carbonylation of alcohols to carboxylic acids that are then esterified with other alcohols. This pathway however cannot be verified with the presence of carboxylic acid in product streams, as they cannot be deconvoluted from other reaction products in the chromatogram.

8. In the context of CO hydrogenation, differences between MMO supported MoS_2 and bulk MoS_2 are most apparent when methanol is co-fed into the syngas. In that environment, the supported material shows substantially higher reactivity with the alcohol. Both CO conversion and higher alcohol production are enhanced. Additionally, alcohols co-fed with syngas over the supported catalyst yield high amounts of hydrocarbons and CO_2 in comparison to the bulk analog.

This research provides a solid foundation for future work centered both on creating an industrially viable catalyst for higher alcohol synthesis and fundamentally understanding reaction pathways. Potential thrusts for such work are as follows:

1. <u>Addition of olefins rather than alcohols to syngas feed.</u>

   Reactivity data gathered from such experiments would be helpful in verifying the pathways driving hydrocarbon formation on MMO supported catalysts. Reactivity data strongly suggests the prominence of alcohol dehydration/hydrogenation pathways, but experiments are needed to verify them more fully. Additionally it is not understood if this pathway is the primary source of C_{2+} hydrocarbons or if that pathway is instead more classical FT insertions that result after CO has been dissociatively adsorbed.

2. <u>Syngas free reaction of alcohols and Mo/K/MMO.</u>

   Methanol and ethanol were shown to be reactive with Mo/K/MMO in Chapter 4. However the synergistic effects of reacting syngas and alcohols are not well understood. Further experiments involving alcohols co-fed with an inert gas would prove useful in understanding this relationship.

3. <u>Elucidation of reaction mechanism via ^{13}C labeled reactants.</u>

   Although feeding alcohols and olefins into syngas is helpful in differentiating major reaction pathways, reactivity data is insufficient for elucidating the precise role of various reactants. Additionally, the source of carbon (i.e. from CO or from an alcohol or olefin) in a specific product cannot be determined. By feeding labeled alcohols and/or olefins into the syngas feed and analyzing reaction products via GC/MS, this information could be obtained.

4. <u>Use of MMO as a promoter rather than a support.</u>

   It has been shown that dispersion of Mo on MMO yields a catalyst less active than an activated carbon analog. Additionally, it has been shown that MMO can be mixed with bulk MoS_2 to yield similar selectivity and only slightly lower

activity to a MMO impregnated equivalent. As such, a carbon supported catalyst promoted with MMO and K together may in fact incorporate the selectivity advantages of MMO without the substantial sacrifice in activity normally observed in metal oxide supported MoS_2 catalysts.

5. Use of Mo k-edge XAS to quantify CUS (coordinatively unsaturated sites) on MoS_2.

Several studies have correlated activity and selectivity with CUS, but this character is extraordinarily difficult to quantify. Because a supported MoS_2 catalyst has relatively small domains, the presence of CUS might be more apparent in curve-fit EXAFS models. If CUS can be quantified using this method and correlations between CUS content and catalyst preparation method may be found, new routes to catalyst optimization may be investigated.

6. Mo dispersion analysis on supported materials.

The main focus of this work has been to understand the effect MMO on the CO hydrogenation reaction on K promoted MoS_2. However, most the catalysts prepared in the study were done so identically. Consequently, it is yet unknown if Mo dispersion was optimized for these materials. Because high levels of dispersion could potentially yield a more active catalyst, this topic merits further investigation. Specifically, carbon supported catalysts could benefit from a dispersion-focused study as support-metal interactions are generally assumed to yield a low metal dispersions.

APPENDIX A: MMO IMPREGNATION

The most common procedure for supporting Mo on a material is to dissolve a soluble form of Mo such as ammonium molybdate tetrahydrate in a solvent and then impregnating a desired material with the resulting Mo solution. While water is the most common solvent for Mo impregnations, its use creates complications when used to impregnate MMO.

Initially, that material is in the hydrotalcite form with Mg^{+2}/Al^{+3} metal ion layers separated by water/CO_3^{2-} ion layers. When the material is heated to 450 °C in air, the carbonate ions and water molecules are lost leaving behind a mixture of MgO and Al_2O_3. or mixed metal oxide (MMO). However, if the material is exposed to water, the layered hydrotalcite structure can partially reform. This phenomenon is known as a "memory" effect. [117-121]

In the context of Mo impregnation, this outcome results in inconsistent surface areas (25 – 180 m_2/g) between batches and potential trapping of promoter ions, which can lower catalytic activity and potentially alter selectivity. There are six steps involved in using hydrotalcites to make an MMO supported K_2CO_3 promoted Mo_xO catalyst using via aqueous solution impregnation.

1. Synthesize hydrotalcite.

2. Decompose hydrotalcite in ambient air in a calcination oven at 450 °C at 5 °C/min for 2 hours – MMO.

3. Impregnate resulting MMO is with an aqueous AMT solution and dried at 135 °C overnight – AMT/MMO.

4. Load material into in a quartz tube and heat under flowing N_2 to 450 °C at 5 °C/min for 2 hours – MoO_x/MMO.

5. Impregnate MoO_x/MMO with an aqueous solution of potassium carbonate and in an oven overnight at 135 °C.

6. Load MoO_x/K_2CO_3/MMO into a quartz tube and heat under flowing N_2 to 450 °C at 5 °C/min for 2 hours.

The memory effects mentioned in Chapters 2 and 3 are easily observed in XRD as shown in Figure A.1. Virtually all of the diffraction lines associated with hydrotalcite are observable in steps 3 and 5, they are however greatly attenuated. This outcome is expected due to the absence of carbonate ions in the impregnation solution and lack of exposure time of the MMO to water.
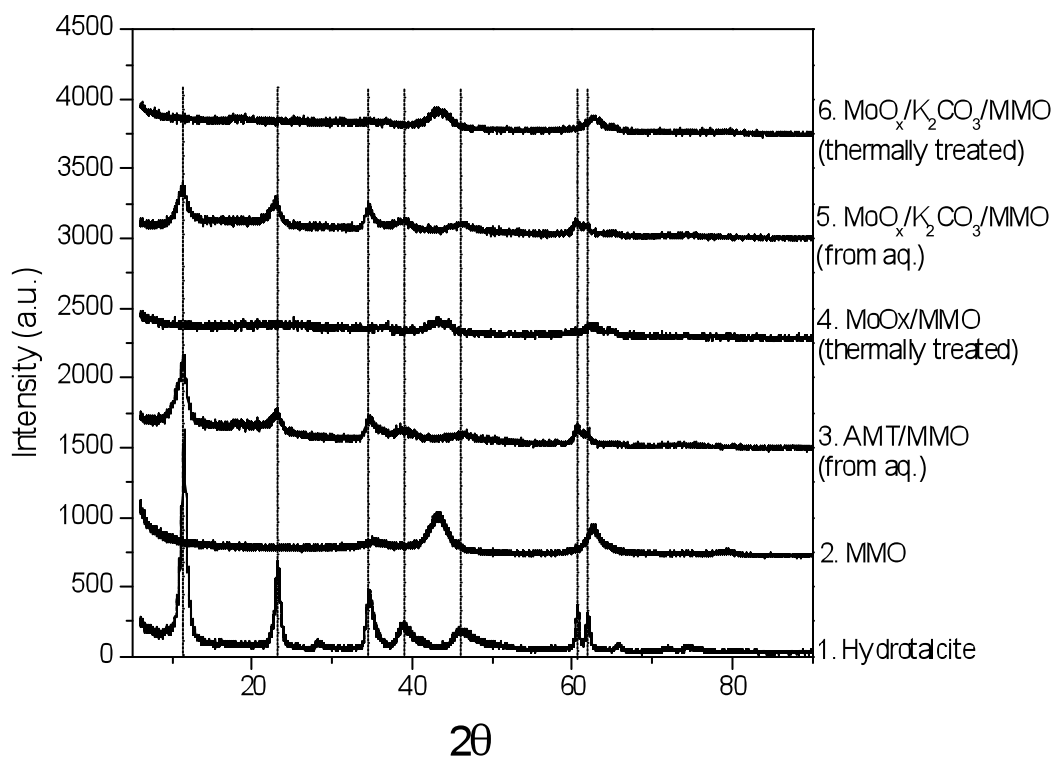
Figure A.1 XRD patterns of MMO impregnated with aqueous solutions of AMT and K_2CO_3.

On account of the structural and catalytic inconsistencies created by aqueous solution impregnation, a variety of organic solvents were tested as potential impregnation solvents to water such as methanol, ethanol, 2-propanol, acetonitrile, acetone, and DMSO. However AMT was found to be soluble only in DMSO albeit at approximately 10 % of its solubility in water. Fortunately at a 5 % Mo loading, AMT solubility in DMSO was still high enough to require only a single impregnation step. Additionally, K_2CO_3 was added to the catalyst via dry grinding. The procedure and resulting XRD (Figure A.2) are shown below.

1. Synthesize hydrotalcite.

2. Decompose hydrotalcite in ambient air in a calcination oven at 450 °C at 5 °C/min for 2 hours – MMO.

3. Impregnate resulting MMO is with an solution of DMSO and AMT and dried at 135 °C overnight – AMT/MMO.

4. Load material into in a quartz tube and heat under flowing N_2 to 450 °C at 5 °C/min for 2 hours – MoO_x/MMO.

5. Add K_2CO_3 to MoO_x/MMO via dry grinding with a mortar and pestle for 20 minutes.
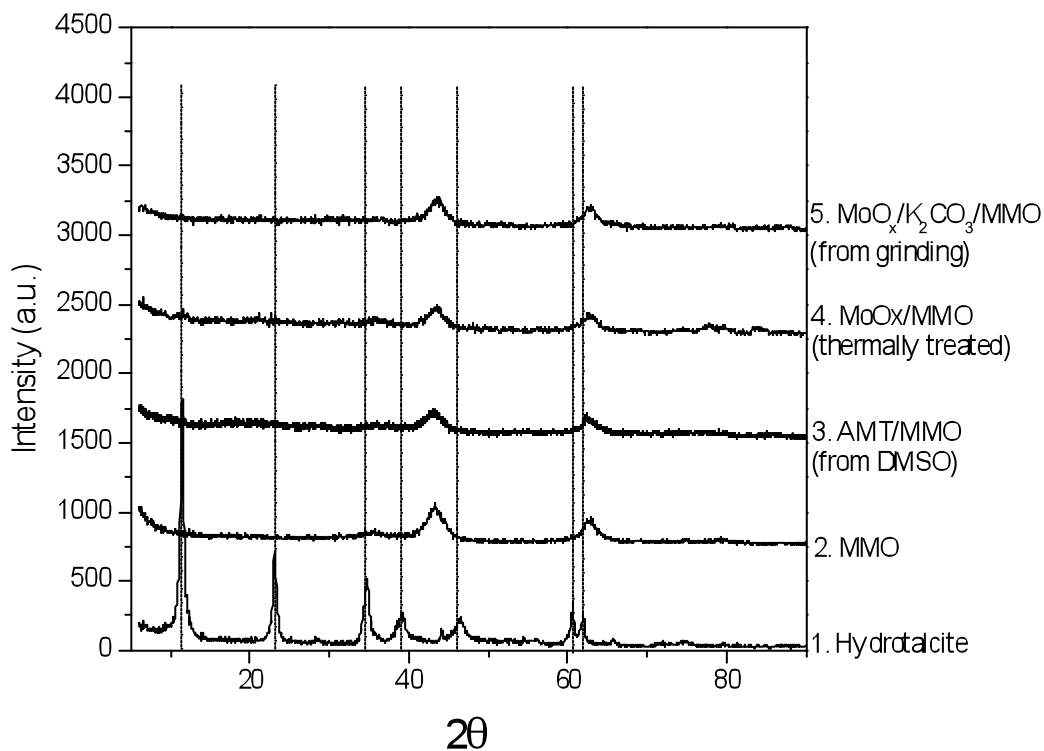
Figure A.2 XRD patterns of MMO impregnated with DMSO solution of AMT and ground with dry K_2CO_3.

Unlike the aqueous impregnation procedure, the DMSO/dry grinding procedure yields a catalyst that does not have the hydrotalcite structure after the initial decomposition (Step 2). Steps 3 and 5 show no evidence of hydrotalcite diffraction lines. Additionally, surface areas of different batches of catalysts prepared in this manner are in the range of 150 – 200 m_2/g.

APPENDIX B: CONTROLLING SYNGAS COMPOSITION

Forming higher alcohols from syngas by reacting it over MoS_2 requires high pressures to sustain reasonable rates of reaction. Because that pressure (1000 – 2500 psig) is on the upper end of the maximum pressure of a compressed cylinder of H_2, CO, and N_2, simulated syngas must be pre-compressed before being fed into the packed bed to make the most use of the gas in the cylinders. Using this method allows the compressed gas tanks to be used until their pressure drops to 500 psig rather than the operating pressure of the reaction, which is invariably much higher.

The syngas used in this thesis is created by combining gas from four different tanks – CO, H_2, N_2, 5000 ppm H_2S in He. These gases are mixed to a desired composition by fixing the flow rate of each gas through a valve or controller and feeding the streams into a common tank with a 1.5 L volume as shown in the "Pressurizing Zone" portion of **Figure** B.1. The gas in this tank is assumed to mix via turbulence and diffusion and typically has a pressure of 150 to 250 psig. The outlet of this tank is connected to a MaxPro DLE 15-1 compressor where it is compressed to pressures as high as 3500 psig in a 500 ml tank connected to the compressor outlet, which is shown in **Figure** B.1.
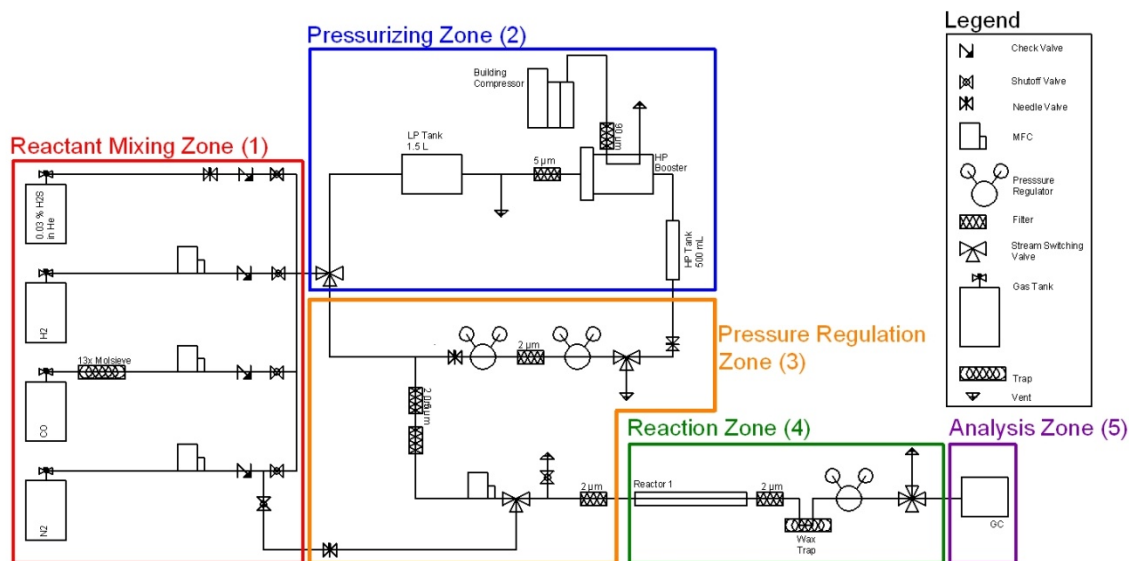
Figure B.1 A simplified plumbing and instrumentation diagram (P&ID) of the packed bed reactor system.

The outlet pressures of the regulators on the four component tanks are set to 500 psig. Flow of CO, H_2, and N_2 is controlled by Brooks MFC's (SLA5850S), which are somewhat insensitive to changes in inlet pressure. Flow from the H_2S/He tank however is controlled by a simple needle valve. This design choice was originally made to save cost. In order to maintain constant flow out of a needle valve, flow must be in the "choked" regime or it becomes outlet pressure dependent. Essentially, choked flow results from a fluid's velocity reaching sonic speeds. At this threshold increases in inlet pressure or decreases in outlet pressure cannot force higher speeds, so flow becomes effectively pressure independent. A more thorough treatment of the matter may be found in most chemical engineering texts such as Perry's Chemical Engineer's Handbook.[169]

This phenomenon is essential for the pressurizing of the primary syngas tank because its pressure slowly increases with time as it is pressurized. If the pressure of that tank becomes too high, the flow out of the needle valve would reduce and in turn lower the H_2S concentration of the syngas. For a tank of pure He, choked flow requires an inlet/outlet pressure quotient of approximately 2.05. Most other gases require a ratio

between 1.7 and 1.9.[169] As such the pressure of the primary syngas tank must not exceed

236 psig when the inlet pressure is 500 psig.

APPENDIX C: SYSTEM CONTROL AND DESIGN CONSIDERATIONS

National Instrument's LabView® software is used to operate and monitor most of the reaction parameters on the reactor used in this thesis – namely pressures, flows, and temperatures. While a full discussion of the interface and design choices used in the software cannot be fully addressed in this thesis, several specific characteristics merit treatment.

First, analog communication (0 – 10 VDC) was chosen over digital (RS-485) in the case of MFC communication. While digital input/output is generally more stable and more accurate than analog, analog communication was chosen because it is compatible with the DAQ hardware which was used to read analog signals from the pressure transducers and thermocouples used in the reactor. Analog input/output communication is also simpler to program in LabView®.

Second the LabView® user interface is known as a "VI" or "Virtual Instrument." The VI contains the programming code that collects and process data from the reactor hardware. It employs a variety of "sub VI's" to carry out specific functions within the main VI. One particularly important VI is inputs pressure, temperature, and flow data into an array of 43,200 points at 0.07 Hz and then overwrites the oldest points once the array is filled. From this array metadata is plotted on the computer screen with a refresh rate of 10 Hz. This design gives the user access to approximately one week of past data and the freedom to focus the plot on any group of data points within that period. The sub VI for writing to the array is shown in **Figure C.1**. The portion of the VI that plots the metadata is shown in **Figure** C.2.
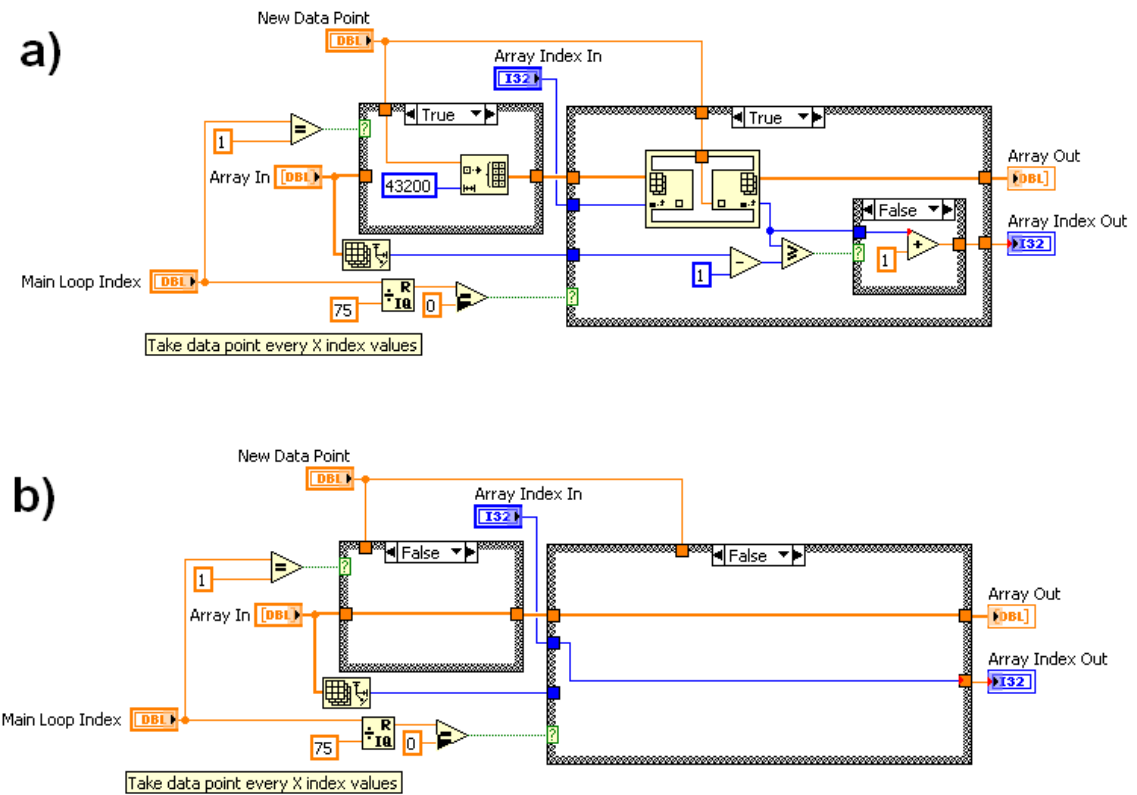
Figure C.1. The LabView® subVI that writes pressure, temperature, and flow meta data to an array of 43,200 points and overwrites the oldest points once the array has been filled.
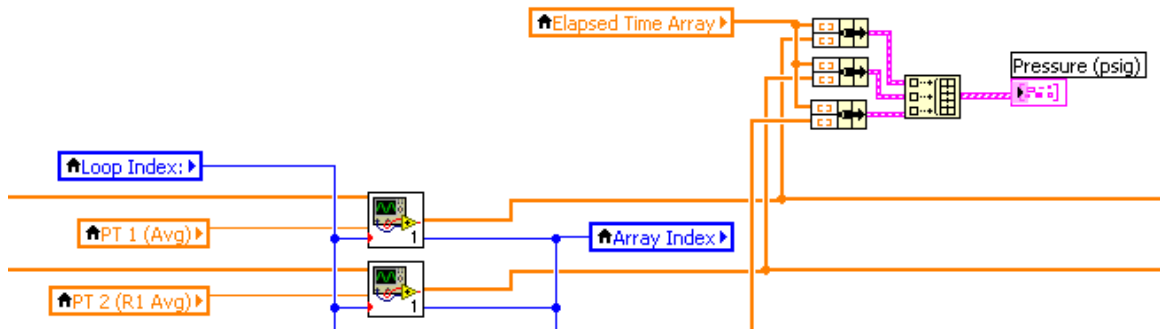
Figure C.2. The portion of the main LabView® VI that plots pressure, temperature, and flow metadata. It functions by combining information from the metadata arrays into clusters, combining the clusters into a array of clusters, and finally plotting the array.

Finally, LabView® 2010 lacks digital PID functionality. However, analog PID functionality can be modified such that it performs similar to a PID with digital logic. The modification to the analog PID is shown in **Figure C.3**. Essentially the analog PID outputs a value between zero and one. The subVI generates a random number and compares it to PID's output. If the random number is greater than the PID's output, the subVI outputs a "false" value to the main VI. Otherwise, it outputs a "true" value. By this method, if the PID outputs a value of 0.9, the subVI outputs "true" 90 % of the time, which is approximately what an equivalent digital PID controller would do.
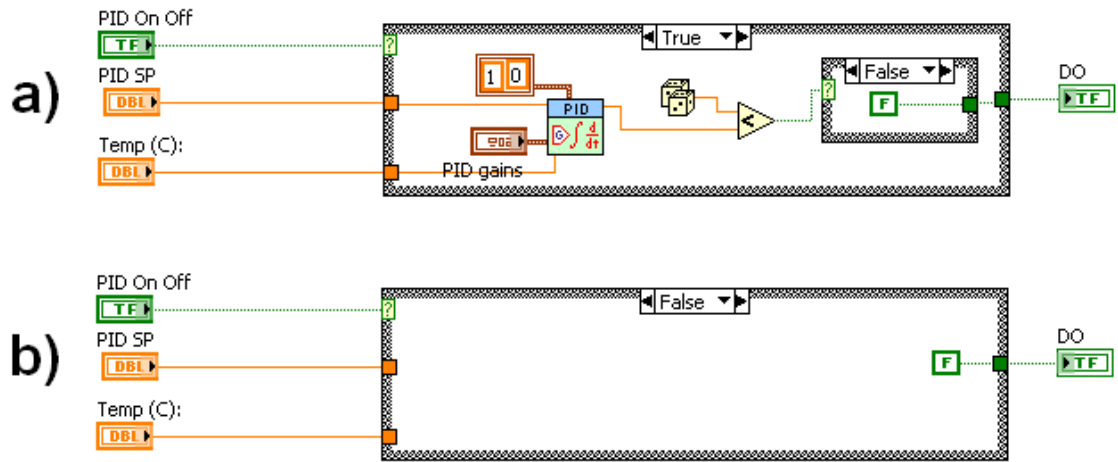
Figure C.3. The subVI used to modify the analog PID subVI such that it outputs digital logic

APPENDIX D: ESTIMATING TRANSPORT PARAMETERS

If accurate catalytic data is to be derived from the results of the studies in this thesis, it must be shown that reactions are not transport limited. Specifically it must be shown that reaction rates are not a result of mass transport limitations or "hotspots" on the catalyst surface.

To this end, a number of "back of the envelope" calculations are performed to verify potential transport imitations. In this appendix, several parameters are calculated based on the average catalyst particle size (635 micron, 30 mesh) of Mo/K/MMO-5,3 reacting at 8 % CO conversion.

C-1 Internal Mass Transport Effects (Weisz-Prater Criterion)

If reaction rate is sufficiently high or pore diffusion is sufficiently low, a reaction can become diffusion limited rather than rate limited. The Weisz-Prater criterion is a non-dimensional comparison between rate of reaction and mass diffusion inside a pore. When the Weisz-Prater number (WPN) is less than 0.25, transport limitations from pore diffusion may be assumed to be negligible. When the value is greater than 5, pore diffusion effects may be assumed to be substantial. The standard equation for the WPN is shown below.

$$WPN = \frac{R_{obs}L^2}{D_{eff}C_A}$$

R_{obs} is the observed rate of reaction of the catalyst. L is the catalyst particle radius. D_{eff} is effective pore diffusion. C_A is the reactant gas concentration at the particle surface. For the sake of simplicity and obtaining results that are reasonably close to true values.

Several approximations are be made to calculate the WPN for the catalyst studied in this appendix.

First, because particle diameter is fairly large, D_{eff} must be estimated from a combination of Knudsen and binary diffusivities. Binary diffusion is estimated from the Lennard-Jones parameters of CO and ethanol. H_2 is not used because it is assumed to diffuse faster than CO and therefore be less likely limit reaction rate. While the reaction of CO and H_2 produces far more than one product, using ethanol as a model product is sufficient for this calculation as other products will not have drastically different properties. A pore diameter of 10 nm is used to compute Knudsen diffusion. This value is within the range of a mesoporous material and is approximately the size of a pore in MMO. is com. A more thorough treatment of diffusion coefficients may be found in Chemical Engineering Kinetics.[170]

Second, reaction rate is calculated assuming CO is converted at a 1.0 to 0.9 ratio with hydrogen. This ratio results from the assumption that the WGS reaction consumes all excess oxygen by forming CO_2 (which is reasonable for a strong WGS catalyst like MoS_2) and that the average product chain length is 3 carbons. Under these conditions 8 % of CO conversion equates approximately to 7.2 % conversion of the total syngas including the internal standard. Substituting the resulting values in the the WPN equations gives:

$$WPN = \frac{R_{obs}L^2}{D_{eff}C_A} = \frac{1.4 \times 10^{-6} \frac{mol}{ml_{cat}s} \times (0.03cm)^2}{0.00179 \frac{cm^2}{g} \times 0.0018 \frac{mol}{ml}} = 0.0008$$

Given that the result is several orders of magnitude below the 0.25 threshold, reaction rate is not limited by pore diffusion.

C-2 External Heat Transfer ("Hotspots")

External heat transfer can result in localized increases in catalyst particle surface temperature, which can intern alter catalyst structure or alter reactivity. The phenomenon results from high reaction enthalpies that produce heat more quickly than can be dissipated across a reactor wall or catalyst surface. This temperature change is estimated by dividing the heat generated by the reaction over the heat transfer coefficient as shown below.

$$\Delta T = \frac{-R_{obs}L(-\Delta H_{rxn})}{h}$$

ΔH_{rxn} is the overall reaction enthalpy. h is the heat transfer coefficient. R_{obs} is the observed rate of reaction of the catalyst. L is the catalyst particle radius. R_{obs} and L are approximated in the same fashion as they were in the *WPN* equation. ΔH_{rxn} is estimated according to the reaction enthalpies of the main products formed in the reaction (methane, ethane, propane, methanol, ethanol, propanol, and butanol) that have been adjusted according to approximate selectivity of the catalyst at 8 % CO conversion. h is estimated from the Chilton-Colburn analogy which is covered in a variety of chemical engineering texts such as *Transport Phenomena*.[171] The expression may be evaluated as shown below.
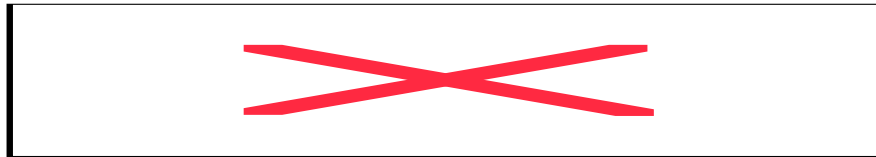
A change of 0.4 K in surface temperature of the catalyst is smaller than the fluctuations in reactor temperature ($\pm$ 2 °C) and is consequently negligible with respect to the reaction.

APPENDIX E: ADDITIONAL CONTROL EXPERIMENTS

A multitude of control experiments were carried out over the course of the studies reported in this thesis. While literature provided a strong basis for expectations concerning catalyst reactivity, topics concerning effect of sulfidation method and temperature required verification in the context of the MMO supported catalyst and the reactor. Additionally, Mo-free and K-free catalysts were tested in the reactor to provide information of the direct effects of these components on the CO hydrogenation reaction.

D-1 Reaction

D-1-1 Reactivity of ex-situ sulfided catalyst compared in-situ sulfided catalyst

The catalysts discussed in Chapters 2 – 5 were sulfided in-situ at 450 °C in 10 % H_2S/H_2, reacted immediately with syngas under the conditions listed in **Table 2.1**, passivated, and then characterized. However, for the sake of characterization before reaction but after sulfidation, a 0.5 g aliquot of a batch of Mo/K/MMO-5,3 was instead sulfided ex-situ, passivated, and then reacted without further pretreatment. This catalyst will be referred to as "Mo/K/MMO-5,3-PS450-ex-situ." A 1.0 g aliquot from the same batch was also sulfided in-situ and reacted for direct reactivity comparison. This catalyst will be referred to as "Mo/K/MMO-5,3-PS450-in-situ" and is analogous to the "Mo/K/MMO-5,3" catalysts referred to in previous chapters of this thesis. Reactivity for these two catalysts is reported in **Table 5.1**.

The catalysts have similar $C_{2+}OH$, hydrocarbon, and CO_2 selectivities, and vary most in methanol selectivity though even that variation is relatively small and within the range generally observed for the "5,3" catalysts. The catalysts also show somewhat higher total hydrocarbon selectivity than other batches of catalyst. This outcome is attributed to the age of the reactor at the time of the reactions. Over the course of the

research used in this thesis, several of the reactors produced higher amounts of hydrocarbons after approximately 6 months of use when loaded with a catalyst and were somewhat more reactive with syngas when run without catalyst under standard reaction conditions (0.1 – 0.5 % CO for aged reactors and 0.01 – 0.04 % for new reactors). The "in-situ" catalyst showed substantially lower $C_{2+}OH$ productivity than is expected. While a smaller aliquot was used for reaction (on account of insufficient material to react a full gram), that quantity should not affect productivity because it is scaled according to g of Mo in the catalyst. For that reason it is assumed that the lower productivity is a result of the catalyst being deactivated by the passivation process. Because selectivities were fairly similar, it may be assumed that structural differences between the two catalysts is minimal. The two catalysts showed identical XRD patterns (not shown). Nitrogen physisorption data was not collected for the catalysts.

D-1-2 Effect of sulfidation and sulfidation temperature.

Two other 1 g aliquots of the same batch of Mo/K/MMO-5,3 catalyst also loaded into the reactor and reacted with syngas. The first was sulfided in 10 % H_2S/H_2 at 310 °C for 2 hours ("Mo/K/MMO-5,3-PS310-In-situ") and then reacted under the standard conditions listed in Table 2.1. The second was not exposed to 10 % H_2S/H_2 at all. Instead it was heated to 450 °C in syngas for 2 hours at 5 °C /min, allowed to cool to 310 °C, and then reacted under the same conditions as the other catalysts ("Mo/K/MMO-5,3-NPS").

Reactivity results are shown in **Table 5.1**. Mo/K/MMO-5,3-PS310-In-situ showed lower alcohol selectivity and slightly higher overall activity than the catalysts sulfided at 450 °C. This outcome is expected because 310 °C is understood to yield incomplete sulfidation of Mo. However, because the catalyst was not heated to 450 °C, the possibility remains that the K loaded on the catalyst did not sufficiently migrate to maximize alcohol selectivity.

Mo/K/MMO-5,3-NPS showed surprisingly low activity but very high hydrocarbon selectivity. The best explanation is that the alkali deactivated most of the hydrocarbon forming sites on the MoO_x domains. Because there were minimal active MoS_2 sites on the catalyst, alcohol production was also minimal.

D-1-3 Effect of K promotion

To test the hypothesis that K promoted MMO supported MoO_x was fairly inactive for both hydrocarbon and alcohol production. An MMO supported Mo catalyst was tested without the addition of K_2CO_3 (Mo/MMO-5). This catalyst was pretreated in 10 % H_2S/H_2 and reacted under the conditions specified in **Table 2.1**. Reactivity results are reported in **Table 5.1**

Mo/MMO-5 was substantially more active than the other catalysts discussed in this appendix. It was also the most selective for hydrocarbons, which is expected. These results provide confirmation that while basic, MMO by itself cannot replace alkali in promoting higher alcohol and/or suppressing hydrocarbon formation. The unpromoted catalyst was highly selective for C_{2+} hydrocarbons. An interesting follow-up study would be to test an unpromoted bulk MoS_2 catalyst in the reactor and to compare chain growth probabilities accordingly. MMO could potentially promote chain growth in the form of alcohols or in hydrocarbons.

D-1-4 Effect of Mo

Reactivity results for a 1 g aliquot of MMO/K-3 are also reported **Table 5.1**. The catalyst was presulfided and reacted catalyst under the same conditions reported in **Table 2.1**. While this catalyst is from a different batch than the MMO/K-3 catalyst used in Chapter 4, the reactivity results are similar. Primarily, CO conversion was low while hydrocarbon selectivity was high. CO_2 selectivity was well over 50 %, which is statistically impossible, however because conversion is so low chromatogram peaks on the GC were also very small and consequently subject to substantially more error than what when they result from higher conversions.

Table 5.1 Reactivity data for various catalysts used in control experiments

ID	Description	WHSV (ml/g/hr)	CO Conv. (% from	CO_2 Sel. (%)	Organic Product Selectivity (Carbon % excluding CO_2)							$C_{2+}OH$ Prod. (g/g$_{Mo}$/hr)
					MeOH	EtOH	Lin $C_{3+}OH$	CH_4	C_2H_6	Total OH	Total HC	
M-21131BS-R2-03272011	Mo/K/MMO-5,3-PS450-Ex-situ	1313	6.1	45.8	6.8	21.6	18.3	16.8	14.2	48.8	49.8	0.137
M-21131AS-R1-03252011	Mo/K/MMO-5,3-PS450-In-situ	2411	6.8	46.3	3.3	20.9	19.2	18.8	16.0	45.3	52.7	0.277
M-21131A-R2-032232011	Mo/K/MMO-5,3-PS310-In-situ	2646	8.4	47.3	4.4	11.3	7.2	29.5	25.1	23.6	75.9	0.171
M-21131A-R1-03302011	Mo/K/MMO-5,3-NPS	1329	2.6	50.0	8.8	3.5	1.7	30.1	21.8	14.4	84.4	0.007
M-22121-R2-09252011	Mo/MMO-5	3600	9.0	47.1	1.4	4.0	1.8	21.8	40.7	7.4	92.5	0.079
M-22161-R1-12032011	MMO/K-3	1451	0.4	62.4	2.7	2.1	3.3	23.7	17.7	10.5	86.0	0.001

D-2 Using XANES to Monitor Mo Oxidation

XANES can be used to track the level of oxidation in a supported Mo catalyst. Using the same parameters discussed in Chapter 3, the XANES of catalysts investigated in this appendix were analyzed at BNL. Additionally, several bulk Mo standards (MoO_3, MoO_2, MoS_2, Mo foil) were also analyzed for comparison.

Normally, the absolute value of an absorption edge is estimated from the first maxima of the first derivative of the XANES data. However when relative comparisons are being made, it is more useful to normalize the absorption edges of the materials being studied, pick a defensible value (normally between 0.3 and 0.7), and compare each material at that specific point. The materials with the lowest corresponding energies are considered to be the most reduced while those with the highest energies are considered to be the most oxidized.

This data is shown in the vertical axis of Figure E.1 for the following catalysts and bulk standards:

1. Mo/K/MMO-5,3-NPS unreacted

2. Mo/K/MMO-5,3-NPS after 1 day of reaction

3. Mo/K/MMO-5,3-NPS after 3 days of reaction

4. Mo/K/MMO-53,-PS310 after 3 days of reaction

5. Mo/K/MMO-5,3-PS450-In-Situ after 3 days of reaction

6. MoO_3

7. MoO_2

8. MoS_2

9. Mo foil

The horizontal axis is reported in terms of formal oxidation state, which is used primarily because it is a well-known reference frame for transition metal compounds. Expectedly, the unreacted "NPS" catalyst is closest in energy to MoO_3. As the NPS catalyst is exposed to H_2S in the syngas (50 ppm at 1500 psig), it is slowly reduced over time to a sulfide giving it a similar oxidation level as MoO_2. The rate of reduction drops as time increases however as is seen by the drop in energy difference between the unreacted and 1 day reacted sample and the drop between the 1 day reacted and 3 day reacted sample.

Additionally, these results suggest that the NPS catalyst will never reach the same level of sulfidation as the "PS310" catalyst. The "PS450" catalyst fairly close in oxidation level as bulk MoS_2 and is also further sulfided than the "PS310" catalyst, which suggests that a treatment temperature of 450 °C is likely sufficient to fully sulfide the catalyst while 310 °C is not. Finally, this data suggests that the level to which Mo can be sulfided is dependent on both temperature and H_2S concentration.

The data shows that MoS_2 is substantially more reduced than MoO_2, which might be unexpected because both compounds have a formal oxidation state of 4. This discrepancy may be explained by considering the electronic nature of the two compounds. Namely, oxygen is more electronegative than sulfur. As such, the Mo-O bond has more ionic character than a Mo-S bond, which will has more covalent. Formal oxidation states are assigned with the assumption that a compound is completely ionic. A deeper discussion of this topic along with quantitative comparisons with DFT-computed partial charges is covered by Li et al.[172]
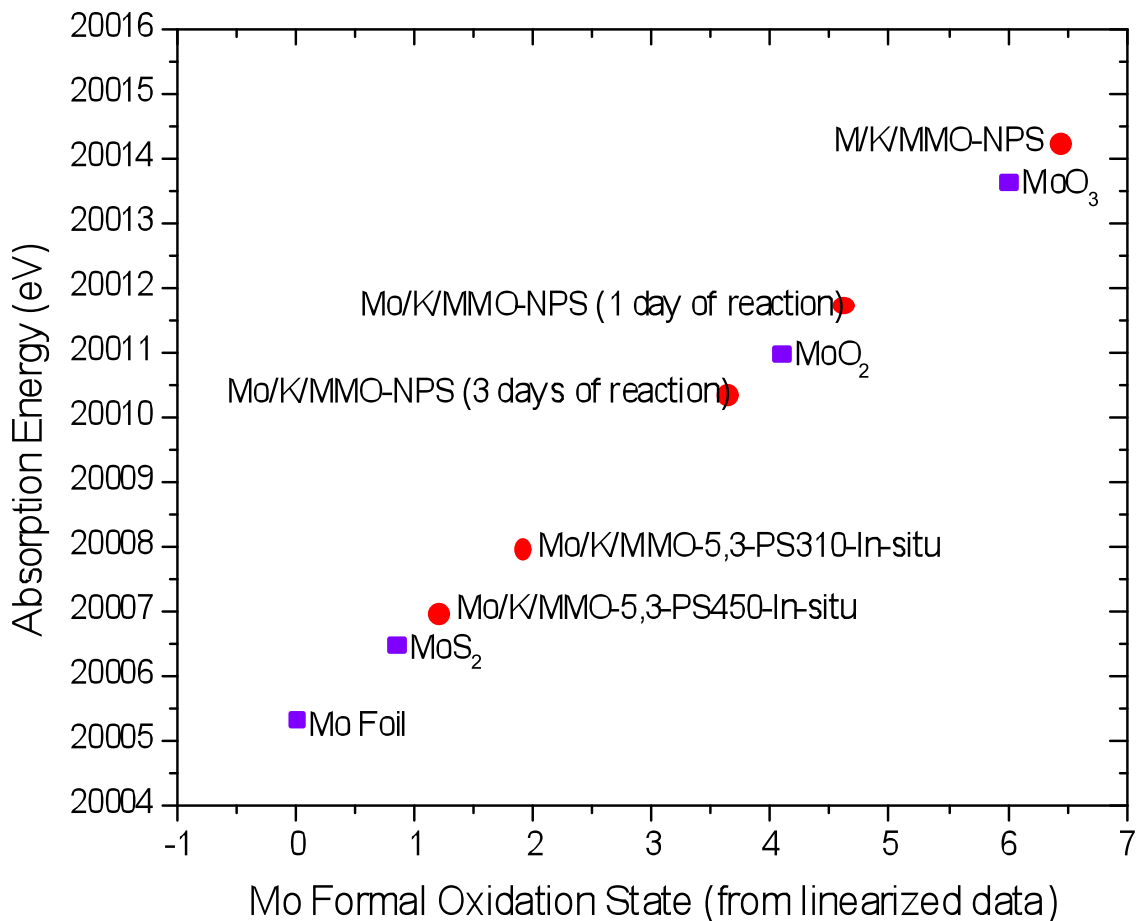
Figure E.1 The Mo *k*-edge energy of various materials at a normalized absorption of 0.5.

REFERENCES

(1)   Wilhelm, D. J.; Simbeck, D. R.; Karp, A. D.; Dickenson, R. L. *Fuel Proc. Technol.* **2001**, *71*, 139–148.

(2)   Pena, M. A.; Gomez, J. P.; Fierro, J. L. G. *Appl. Catal. A.* **1996**, *144*, 7–57.

(3)   Ponec, V. *Catal. Today.* **1992**, *12*, 227–254.

(4)   Laurendeal, N. *Prog. Energy Combust. Sci.* **1978**, *4*, 221–270.

(5)   Radovic, L. R.; Walker, P. L.; Jenkins, R. G. *Fuel* **1983**, *62*, 849–856.

(6)   Bharadwaj, S. S.; Schmidt, L. D. *Fuel Proc. Technol.* **1995**, *42*, 109–127.

(7)   Hickman, D. A.; Schmidt, L. D. *Science* **1993**, *259*, 343–346.

(8)   Bridgwater, A. V. *Fuel* **1995**, *74*, 631–653.

(9)   Sutton, D.; Kelleher, B.; Ross, J. *Fuel Proc. Technol.* **2001**, *73*, 155–173.

(10)   Fischer, F.; Tropsch, H. *Chem. Ber.* **1926**, *59*, 830–832.

(11)   Spivey, J. J.; Egbedi, A. *Chem. Soc. Rev.* **2007**, *36*, 1514–1528.

(12)   Subramani, V.; Gangwal, S. G. *Energy Fuels* **2008**, *22*, 814–839.

(13)   Surisetty, V. R.; Dalai, A. K.; Kozinski, J. *Appl. Catal. A.* **2011**, *404*, 1–11.

(14)   Natesakhawat, S.; Lekse, J. W.; Baltrus, J. P.; Ohodnicki, P. R., Jr.; Howard, B. H.; Deng, X.; Matranga, C. *ACS. Catal.* **2012**, *2*, 1667–1676.

(15)   Gupta, M.; Smith, M. L.; Spivey, J. J. *ACS. Catal.* **2011**, *1*, 641–656.

(16)   Grabow, L. C.; Mavrikakis, M. *ACS. Catal.* **2011**, *1*, 365–384.

(17)   Yang, R.; Fu, Y.; Zhang, Y.; Tsubaki, N. *J. Catal.* **2004**, *228*, 23–35.

(18)   Schwartz, V.; Campos, A.; Egbebi, A.; Spivey, J. J.; Overbury, S. H. *ACS. Catal.* **2011**, *1*, 1298–1306.

(19)   Chinchen, G. C.; Denny, P. J.; Jennings, J. R.; Spencer, M. S.; Waugh, K. C. *Appl. Catal.* **1988**, *36*, 1–65.

(20)   Shou, H.; Ferrari, D.; Barton, D. G.; Jones, C. W.; Davis, R. J. *ACS. Catal.* **2012**, *2*, 1408–1416.

(21)   Solomon, E. I.; Jones, P. M.; May, J. A. *Chem. Rev.* **1993**, *93*, 2623–2644.

(22)   Liu, X.-M.; Lu, G. Q.; Yan, Z.-F.; Beltramini, J. *Ind. Eng. Chem. Res.* **2003**, *42*, 6518–6530.

(23)   Fang, K.; Li, D.; Lin, M.; Xiang, M.; Wei, W.; Sun, Y. *Catal. Today.* **2009**, *147*, 133–138.

(24)   Yang, Y.; Wang, Y.; Liu, S.; Song, Q.; Xie, Z.; Gao, Z. *Catal. Lett.* **2009**, *127*, 448–455.

(25)   Gogate, M. R.; Davis, R. J. *ChemCatChem.* **2009**, *1*, 295–303.

(26)   Gao, J.; Mo, X.; Chien, A. C.-Y.; Torres, W.; Goodwin, J. G., Jr *J. Catal.* **2009**, *262*, 119–126.

(27)   Mazanec, T. J. *J. Catal.* **1986**, *98*, 115–125.

(28)   Lee, J. S.; Kim, S.; Lee, K. H.; Nam, I. S.; Chung, J. S.; Kim, Y. G.; Woo, H. C. *Appl. Catal. A.* **1994**, *110*, 11–25.

(29)   Inoue, M.; Miyake, T.; Takegami, Y.; Inui, T. *Appl. Catal.* **1987**, *29*, 285–294.

(30)   Stevens, R. R. Process for Producing Alcohols from Synthesis Gas. 4752622, October 19, 1988.

(31)   Tatsumi, T.; Muramatsu, A.; Tominaga, H. *Chem. Lett.* **1985**, 593–594.

(32)   Murchison, C. B.; Conway, M. M.; Stevens, R. R.; Quarderer, G. J. Calgary, 1988; Vol. 2, pp. 626–633.

(33)   Santiesteban, J. G.; Bogdan, C. E.; Herman, R. G.; Klier, K. Calgary, 1988; Vol. 2, pp. 561–568.

(34)   Nunan, J. G.; Bogdan, C. E.; Klier, K.; Smith, K. J.; Young, C. W.; Herman, R. G. *J. Catal.* **1988**, *113*, 410–433.

(35)   Nunan, J. G.; Bogdan, C. E.; Klier, K.; Smith, K. J.; Young, C.; Herman, R. G. *J. Catal.* **1989**, *116*, 195–221.

(36)   Nunan, J. G.; Herman, R. G.; Klier, K. *J. Catal.* **1989**, *116*, 222–229.

(37)   Haider, M. A.; Gogate, M. R.; Davis, R. J. *J. Catal.* **2009**, *261*, 9–16.

(38)   Arakawa, H.; Fukushima, T.; Ichikawa, M.; Natsushita, S.; Takeuchi, K.; Matsuzaki, T.; Sugi, Y. *Chem. Lett.* **1985**, *7*, 881–884.

(39)   Wu, M.; Wang, M.; Liu, J.; Huo, H. *Biotechnol. Prog.* **2008**, *24*, 1–11.

(40)   Dernotte, J.; Mounaim-Rousselle, C.; Halter, F.; Seers, P. *Oil Gas Sci .Technol.* **2010**, *65*, 345–351.

(41)   Balat, M.; Balat, H. *Appl. Energ.* **2009**, *86*, 2273–2282.

(42)   Chen, Y.; Dong, M.; Wang, J.; Jioa, H. *J. Phys. Chem. B.* **2010**, *114*, 16660–16676.

(43)   Li, D.; Yang, C.; Qi, H.; Zhang, H.; Li, W.; Sun, Y.; Zhong, B. *Catal. Commun.* **2004**, *5*.

(44)   Li, D.; Yang, C.; Li, W.; Sun, Y.; Zhong, B. *Top. Catal.* **2005**, *32*, 233–239.

(45)   Li, D.; Yang, C.; Zhao, N.; Qi, H.; Li, W.; Yuhan, S.; Zhong, B. *Fuel Proc. Technol.* **2007**, *88*, 125–127.

(46)   Pecoraro, T. A.; Chianelli, R. *J. Catal.* **1981**, 430–445.

(47)   Schrader, G. L.; Angelici, R. J.; Beson, J. W. *Abstr. Pap. Am. Chem. S.* **1994**, *208*, 36–46.

(48)   Dungey, K.; Curtis, M.; Penner-Hahn, J. *J. Catal.* **1998**, *{175}*, {129–134}.

(49)   Alonso, G.; Berhault, G.; Aguilar, A.; Collins, V.; Ornelas, C.; Fuentes, S.; Chianelli, R. *J. Catal.* **2002**, *{208}*, {359–369}.

(50)   Bachelier, J.; Tilliette, M. J.; Duchet, J. C.; Cornet, D. *J. Catal.* **1982**, *76*, 300–315.

(51)   Kantshewa, M.; Delannay, F.; Jeziorowski, H.; Delgado, E.; Eder, S.; Ertl, G.; Knozinger, H. *J. Catal.* **1984**, *87*, 482–496.

(52)   Liang, K. S.; Chianelli, R.; Chien, F. Z.; Moss, S. C. *J. Non-Cryst. Solids* **1986**, *79*, 251–273.

(53)   Petkov, V.; Billinge, S. J. L.; Larson, P.; Mahanti, S. D.; Vogt, T.; Rangan, K. K.; Kanatzidis, M. G. *Phys. Rev. B* **2002**, *65*, 092105.

(54)   Semiletov, S. A. *Kristallografiya* **1961**, *6*, 536–540.

(55)   Daage, M.; Chianelli, R. *J. Catal.* **1994**, *149*, 414–427.

(56)   Tatsumi, T.; Muramatsu, A.; Tominaga, H. *Appl. Catal.* **1986**, *27*, 69–82.

(57)   Takashi, T.; Muramatsu, A.; Tominaga, H. *Chem. Lett.* **1984**, *13*, 685–688.

(58)   Woo, H. C.; Park, K. Y.; Kim, Y. G.; Nam, I.-S.; Chung, J. S.; Lee, J. S. *Appl. Catal.* **1991**, *75*, 267–280.

(59)   Woo, H. C.; Nam, I.-S.; Chung, J. S. L. A. J. S.; Kim, Y. G. *J. Catal.* **1993**, *142*, 672–690.

(60)   Christensen, J. M.; Jensen, P. A.; Schiødt, N. C.; Jensen, A. D. *ChemCatChem.*

2010, *2*, 523–526.

(61)   Tatsumi, T.; Muramatsu, A.; Tominaga, H. *Appl. Catal.* **1987**, *34*, 77–88.

(62)   Concha, B. E.; Bartholomew, G. L.; Bartholomew, C. H. *J. Catal.* **1984**, *89*, 536–541.

(63)   Tatsumi, T.; Muramatsu, A.; Yokota, K.; Tominaga, H. *J. Catal.* **1989**, *115*, 388–398.

(64)   Tatsumi, T.; Muramatsu, A.; Yokota, K.; Tominaga, H. *J. Mol. Catal.* **1987**, *41*, 385–389.

(65)   Li, X.; Feng, L.; Zhang, L.; Dadyburjor, D. B.; Kugler, E. L. *Molecules* **2003**, *8*, 13–30.

(66)   Li, X.; Feng, L.; Lui, Z.; Zhong, B.; Dadyburjor, D. B.; Kugler, E. L. *Ind. Eng. Chem. Res.* **1998**, *37*, 3853–3863.

(67)   Li, Z.-R.; Jiang, M.; Hu, T.-D.; Lui, T.; Xie, Y.-N. *J. Catal.* **2001**, *199*, 155–161.

(68)   Iranmahboob, J.; Hill, D. O. *Catal. Lett.* **2002**, *78*, 49–55.

(69)   Gang, L.; Chengfang, Z.; Yanqing, C.; Zhibin, Z.; Yianhui, N.; Linjun, C.; Fong, Y. *Appl. Catal. A.* **1997**, *150*, 243–252.

(70)   Duchet, J. C.; Van Oers, E. M.; De Beer, H. J.; Pruins, R. *J. Catal.* **1983**, *89*, 386–402.

(71)   Ma, X.; Lin, G.; Zhange, H. *Catal. Lett.* **2006**, *111*, 141–151.

(72)   Ma, X.; Goudong, L.; Hongbin, Z. *Chin. J. Catal.* **2006**, *27*, 1019–1027.

(73)   Ma, C.-H.; Li, H.-Y.; Lin, G.-D. *Catal. Lett.* **2010**.

(74)   Surisetty, V. R.; Tavasoli, A.; Dalai, A. K. *Appl. Catal. A.* **2009**, *365*, 243–251.

(75)   Surisetty, V. R.; Dalai, A. K.; Kozinski, J. *Ind. Eng. Chem. Res.* **2010**, *49*, 6956–6963.

(76)   Surisetty, V. R.; Dalai, A. K.; Kozinski, J. *Appl. Catal. A.* **2010**, *385*, 153–162.

(77)   Surisetty, V. R.; Dalai, A. K.; Kozinski, J. *Appl. Catal. A.* **2010**, *381*, 282–288.

(78)   Surisetty, V. R.; Dalai, A. K.; Kozinski, J. *Energy Fuels* **2010**, *24*, 4130–4137.

(79)   Surisetty, V. R.; Dalai, A. K.; Kozinski, J. *Appl. Catal. A.* **2011**, *393*, 50–58.

(80)   Surisetty, V. R.; Dalai, A. K.; Kozinski, J. *Energy Fuels* **2011**, *25*, 580–590.

(81)   Surisetty, V. R.; Kozinski, J.; Dalai, A. K. *Int. J. Chem. React. Eng.* **2011**, *9*, 1–18.

(82)   Surisetty, V. R.; Eswaramoorthi, I.; Dalai, A. K. *Fuel* **2012**, *96*, 77–84.

(83)   Surisetty, V. R.; Epelde, E.; Dalai, A. K.; Trepanier, M.; Kozinski, J. *Int. J. Chem. React. Eng.* **2012**, *10*, 1–15.

(84)   Li, Z.-R.; Fu, Y.-L.; Jiang, M. *Appl. Catal. A.* **1999**, *187*, 187–198.

(85)   Li, Z.; Fu, Y.-L.; Jiang, M.; Meng, M.; Xie, Y.-N.; Hu, T.-D.; Lui, T. *Catal. Lett.* **2000**, *65*, 43–48.

(86)   Fu, Y.; Fujimoto, K.; Lin, P.; Omata, K.; Yu, Y. *Appl. Catal. A.* **1995**, *126*, 273–285.

(87)   Bian, G.; Fu, Y.; Ma, Y. *Catal. Today.* **1999**, *51*, 187–193.

(88)   Jiang, M.; Bian, G.-Z.; Fu, Y.-L. *J. Catal.* **1994**, *146*, 144–154.

(89)   Bian, G.-Z.; Fu, Y.-L.; Yamada, M. *Appl. Catal. A.* **1996**, *144*, 79–91.

(90)   Jalowiecki-Duhamel, L.; Grimblot, J.; Bonnelle, J. P. *J. Catal.* **1991**, *129*, 511–518.

(91)   Morrill, M. R.; Thao, N. T.; Agrawal, P. K.; Jones, C. W.; Davis, R. J.; Shou,

H.; Barton, D. G.; Ferrari, D. *Catal. Lett.* **2012**, *142*, 875–881.

(92)   Valente, J. *J. Catal.* **2000**, *189*, 370–381.

(93)   Fishel, C. T.; Davis, R. J. *Catal. Lett.* **1994**, *25*, 87–95.

(94)   Bezen, M. C. I.; Breitkopf, C.; Lercher, J. A. *ACS. Catal.* **2011**, *1*, 1384–1393.

(95)   Kasztelan, S.; Toulhoat, H.; Grimblot, J.; Bonnelle, J. P. *Appl. Catal.* **1984**, *13*, 127–159.

(96)   Bian, G.-Z.; Fan, L.; Fu, Y.-L.; Fujimoto, K. *Appl. Catal. A.* **1998**, *170*, 255–268.

(97)   Arai, H.; Take, J.; Saito, Y.; Yoneda, Y. *J. Catal.* **1967**, *9*, 146–153.

(98)   Golay, S.; Doepper, R.; Renken, A. *Appl. Catal. A.* **1998**, *172*, 97–106.

(99)   Bautista, F. M.; Delmon, B. *Appl. Catal. A.* **1995**, *1995*, 47–65.

(100)   Bian, G.-Z.; Fan, L.; Fu, Y.-L.; Fujimoto, K. *Ind. Eng. Chem. Res.* **1998**, *37*, 1736–1743.

(101)   Gines, M. J. L.; Iglesia, E. *J. Catal.* **1998**, *176*, 155–172.

(102)   Rao, K. K.; Gravelle, M.; Valente, J. S.; Figueras, F. *J. Catal.* **1998**, *173*, 115–121.

(103)   Cosimo, J. I. D.; Apesteguia, C. R.; Gines, M. J. L.; Iglesia, E. *J. Catal.* **2000**, *190*, 261–275.

(104)   Smith, K. J.; Anderson, R. B. *J. Catal.* **1984**, *85*, 428–436.

(105)   Pratt, E. F.; Kubler, D. G. *J. Am. Chem. Soc.* **1953**, *76*, 52–56.

(106)   Veibel, S.; Nielsen, J. I. *Tetrahedron* **1967**, *23*, 1723–1733.

(107)   Burk, P. L.; Pruett, R. L.; Campo, K. S. *J. Mol. Catal.* **1985**, *33*, 1–14.

(108)   Burk, P. L.; Pruett, R. L.; Campo, K. S. *J. Mol. Catal.* **1985**, *33*, 15–21.

(109)   Carlini, C.; Di Girolamo, M.; Marchionna, M.; Noviello, M.; Galletti, A. M. R.; Sbrana, G. *J. Mol. Catal. A* **2002**, *184*, 273–280.

(110)   Carlini, C.; Di Girolamo, M.; Macinai, A.; Marchionna, M.; Noviello, M.; Galletti, A. M. R.; Sbrana, G. *J. Mol. Catal. A* **2003**, *200*, 137–146.

(111)   Carlini, C.; Macinai, A.; Marchionna, M.; Noviello, M.; Galletti, A. M. R.; Sbrana, G. *J. Mol. Catal. A* **2003**, *206*, 409–418.

(112)   Carlini, C.; Di Girolamo, M.; Macinai, A.; Marchionna, M.; Noviello, M.; Galletti, A. M. R.; Sbrana, G. *J. Mol. Catal. A* **2003**, *204-205*, 721–728.

(113)   Ueda, W.; Kuwabara, T.; Ohshida, T.; Morikawa, Y. *J. Chem. Soc. Chem. Commun.* **1990**, 1558.

(114)   Carlini, C.; Flego, C.; Marchionna, M.; Noviello, M.; Galletti, A. M. R.; Sbrana, G.; Basile, F.; Vaccari, A. *J. Mol. Catal. A* **2004**, *220*, 215–220.

(115)   Carlini, C.; Marchionna, M.; Noviello, M.; Galletti, A. M. R.; Sbrana, G.; Basile, F.; Vaccari, A. *J. Mol. Catal. A* **2005**, *232*, 13–20.

(116)   Hsiao, T. C.; Lin, S. D. *Catal. Lett.* **2007**, *119*, 72–78.

(117)   Lei, X.; Zhang, F.; Yang, L.; Guo, X.; Yuanyuan, T.; Fu, S.; Li, F.; Evans, D. G.; Duan, X. *AICHE* **2007**, *54*, 932–940.

(118)   Meloni, D.; Monaci, R.; Solinas, V.; Auroux, A.; Dumitriu, E. *Appl. Catal. A.* **2008**, *350*, 86–95.

(119)   Prinetto, F.; Ghiotti, G.; Graffin, P.; Tichit, D. *Micropor. Mesopor. Mat.* **2000**, *39*, 229–247.

(120)   Takehira, K. *Catal. Commun.* **2004**, *5*, 209–213.

(121)   Perez-Ramirez, J.; Abello, S.; van der Pers, N. M. *Chem. Eur. J.* **2007**, *13*, 870–

878.

(122) Iranmahboob, J.; Toghiani, H.; Hill, D. O. *Appl. Catal. A.* **2003**, *247*, 207–218.

(123) Muller, A.; Weber, T. *Appl. Catal.* **1991**, *77*, 243–250.

(124) Christensen, J. M.; Mortensen, P. M.; Trane, R.; Jensen, P. A.; Jensen, A. D. *Appl. Catal. A.* **2009**, *366*, 29–43.

(125) Polyakov, M.; Poisot, M.; Berg, der, M. W. E. V.; Drescher, T.; Lotnyk, A.; Kienle, L.; Bensch, W.; Muhler, M.; Grunert, W. *Catal. Commun.* **2010**, *12*, 231–237.

(126) Nam, I.-S.; Park, T. Y.; Kim, Y. G. *Ind. Eng. Chem. Res.* **1997**, *36*, 5246–5257.

(127) Christensen, J. M.; Jensen, P. A.; Jensen, A. D. *Ind. Eng. Chem. Res.* **2011**, *50*, 7949–7963.

(128) Qi, H. *Catal. Commun.* **2003**, *4*, 339–342.

(129) Bowker, M.; Houghton, H.; Waugh, K. C. *J. Chem. Soc. Farad T 1* **1981**, *77*, 3023.

(130) Tsoncheva, T.; Ivanova, L.; Minchev, C.; Froba, M. *J. Colloid Interf. Sci.* **2009**, *333*, 277–284.

(131) Goodarznia, S.; Smith, K. J. *J. Mol. Catal. A* **2010**, *320*, 1–13.

(132) Zhang, J. Y.; Wang, Y. J.; Chang, L. *Appl. Catal. A.* **1995**, *126*, 1205–1218.

(133) Calverley, E. M.; Smith, K. J. *J. Catal.* **1991**, *130*, 616–626.

(134) Ravel, B.; Newville, M. *J. Synch. Rad.* **2005**, *12*, 537–541.

(135) Zabinsky, S. I.; Rehr, J. J.; Ankudinov, A.; Albers, R. C.; Eller, M. J. *Phys. Rev. B* **1995**, *52*, 2995–3009.

(136) Ressler, T. *J. Catal.* **2002**, *210*, 67–83.

(137) Lee, E. L.; Wachs, I. E. *J. Phys. Chem. C* **2007**, *111*, 14410–14425.

(138) Wachs, I. E.; Roberts, C. A. *Chem. Soc. Rev.* **2010**, *39*, 5002.

(139) Tian, H.; Roberts, C. A.; Wachs, I. E. *J. Phys. Chem. C* **2010**, *114*, 14110–14120.

(140) Weber *J. Catal.* **1995**, *151*, 470–474.

(141) Gao, X. *J. Catal.* **2002**, *209*, 43–50.

(142) Wilke, M.; Partzsch, G. M.; Bernhardt, R.; Lattard, D. *Chem. Geo.* **2004**, *213*, 71–87.

(143) Wilke, M.; Farges, F.; Petit, P.; Brown, G. E.; Martin, F. *Am. Mineral.* **2001**, *86*, 714–730.

(144) Millet, J. M. M.; Baca, M.; Pigamo, A.; Vitry, D.; Ueda, W.; Dubois, J. L. *Appl. Catal. A.* **2003**, *244*, 359–370.

(145) Mountjoy, G.; Pickup, D. M.; Wallidge, G. W.; Adnerson, R.; Cole, J. M.; Newport, R. J.; Smith, M. E. *Chem. Mater.* **1999**, *11*, 1253–1258.

(146) Farges, F.; Brown, G. E.; Rehr, J. J. *Phys. Rev. B* **1997**, *56*, 1809–1819.

(147) Chisholm, M. H.; Folting, K.; Huffman, J. C.; Kirkpatrick, C. C. *Inorg. Chem.* **1984**, *23*, 1021–1037.

(148) Delporte, P.; Huu-Pham, C.; Ledoux, M. J. *Appl. Catal. A.* **1997**, *149*, 151–180.

(149) Hou, P.; Meeker, D.; Wise, H. *J. Catal.* **1983**, *80*, 280–285.

(150) Laniecki, M.; Zmierczak, W. *Proceedings of the 10th Int. Cong. Catal.* **1992**, *10*, 2569–2572.

(151) Laniecki, M.; Malecka-Grycz, M.; Domka, F. *Appl. Catal. A.* **2000**, *196*, 292–303.

(152)   Shi, X.-R.; Wang, S.; Hu, J.; Wang, H.; Chen, Y.; Qin, Z.; Wang, J. *Appl. Catal. A.* **2009**, *365*, 62–70.

(153)   Bao, J.; sun, Z.-H.; Fu, Y.-L.; Bian, G.-Z.; Zhang, Y.; Tsubaki, N. *Top. Catal.* **2009**, *52*, 789–794.

(154)   Nickolov, R. N.; Edreva-Kardjieva, R.; Kafedjiysky, V. J.; Nikolova, D. A.; Stankova, N. B.; Mechandjiev, D. R. *Appl. Catal. A.* **2000**, *190*, 191–196.

(155)   Raybaud, P.; Hafner, J.; Kresse, G.; Kasztelan, S.; Toulhoat, H. *J. Catal.* **2000**, *189*, 129–146.

(156)   Wambeke, L. A.; Jalowiecki, S.; Kasztelan, S.; Grimblot, J.; Bonnelle, J. P. *J. Catal.* **1988**, *109*, 320–328.

(157)   Dumeignil, F.; Paul, J.; Veilly, E.; Qian, E.; Ishihara, A.; Payen, E.; Kabe, T. *Appl. Catal. A.* **2005**, *{289}*, {51–58}.

(158)   Fan, Y.; Shi, G.; Liu, H.; Bao, X. *Appl. Catal. B.* **2009**, *91*, 73–82.

(159)   Sun, M.; Adjaye, J.; Nelson, A. E. *Appl. Catal. A.* **2004**, *263*, 131–143.

(160)   Cristol, S.; Paul, J. F.; Payen, E.; Bougeard, D.; Clémendot, S.; Hutschka, F. *J. Phys. Chem. B.* **2002**, *106*, 5659–5667.

(161)   Fischer, E.; Speler, A. *Chem. Ber.* **1895**, *28*, 3252–3258.

(162)   Forster, D. *J. Am. Chem. Soc.* **1976**, *98*, 846–848.

(163)   Maitlis, P. M.; Haynes, A.; Sunley, G. J.; Howard, M. J. *J. Chem. Soc., Dalton Trans.* **1996**, 2187.

(164)   Robinson, K. K.; Hershman, A.; Craddock, J. H.; Roth, J. F. *J. Catal.* **1972**, *27*, 389–396.

(165)   Knifton, J. F. *J. Catal.* **1985**, *96*, 439–453.

(166)   Berk, S. C.; A, K. K.; Buchwald, S. L. *J. Am. Chem. Soc.* **1991**, *113*, 5093–5095.

(167)   Ohta, T.; Kamiya, M.; Kusui, K.; Michibata, T.; Nobutomo, M.; Furukawa, I. *Tetrahedron Lett* **1999**, *40*, 6963–6966.

(168)   Knifton, J. F. *J. Mol. Catal.* **1981**, *11*, 91–106.

(169)   Perry, R. H.; Green, D. W. *Perry"s Chemical Engineer"s Handbook*; 6 ed. McGraw-Hill Co., 1984.

(170)   Smith, J. M. *Chemical Engineering Kinetics*; McGraw-Hill Co., 1970; pp. 402–406.

(171)   Bird, B. R.; Stewart, W. E.; Lightfoot, E. N. *Transport Phenomena*; 2nd ed. John Wiley & Sons, Inc., 2002.

(172)   Li, L.; Morrill, M. R.; Shou, H.; Barton, D. G.; Ferrari, D.; Davis, R. J.; Agrawal, P. K.; Jones, C. W.; Sholl, D. S. *J. Phys. Chem. C.* **2013**, *117*, 2769–2773.

VITA

MICHAEL R. MORRILL

Morrill was born in Kingsport, Tennessee. He attended public schools in Green and Sullivan counties, received a B.S. in Chemistry from Brigham Young University in 2006 and an M.S. in Chemical Engineering from the University of Utah in 2008 before attending Georgia Tech to pursue a doctorate in Chemical Engineering.